The polarity and specificity of SARS-CoV2 -specific T lymphocyte responses determine disease susceptibility

Jean-Eudes FAHRNER[1,2,3,4], Agathe CARRIER[*2,3], Lyon COVID study group[*5-8], Eric DE SOUSA[*13], Damien DRUBAY[*2,12], Agathe DUBUISSON[*2,3], Arthur GERAUD[*2,9,10], Anne-Gaëlle GOUBET[*1,2,3], Gladys FERRERE[*2,3], Yacine HADDAD[*2,3], Imran LAHMAR[*1,2,3], Marine MAZZENGA[*2,3], Cléa MELENOTTE[*2,3,11], Marion PICARD[*2,3], Cassandra THELEMAQUE[*2,3], Luigi CERBONE[2,9], Joana R. LÉRIAS[13], Ariane LAPARRA[2,9,10], Alice BERNARD[2,9,10], Benoît KLOECKNER[2,3], Marianne GAZZANO[2,3], François-Xavier DANLOS[1,2,3], Safae TERRISSE[2,3], Carolina ALVES COSTA SILVA[1,2,3], Eugenie PIZZATO[2,3], Caroline FLAMENT[2,3], Pierre LY[2,3], Eric TARTOUR[14,15], Lydia MEZIANI[2], Abdelhakim AHMED-BELKACEM[16], Makoto MIYARA[17], Guy GOROCHOV[17], Fabrice BARLESI[2,9,18], Caroline PRADON[2,19,20], Emmanuelle GALLOIS[2,21], Fanny POMMERET[2,22], Emeline COLOMBA[2,9], Pernelle LAVAUD[2,9], Eric DEUTSCH[1,2,23,24], Bertrand GACHOT[2,25], Jean-Philippe SPANO[26], Mansouria MERAD[2,27], Florian SCOTTE[2,22], Aurélien MARABELLE[1,2,3,9,10,28], Frank GRISCELLI[2,21,29,30,31], Jean-Yves BLAY[32,33,34], Jean-Charles SORIA[1,2], Fabrice ANDRE[1,2,9,35], Mathieu CHEVALIER[36], Sophie CAILLAT-ZUCMAN[37], Florence FENOLLAR[38], Bernard LA SCOLA[38], Guido KROEMER[39,40,41,42,43,44], Markus MAEURER[**13,45,46,47], Lisa DEROSA[**1,2,3,9], and Laurence ZITVOGEL[**1,2,3,28].

[*]Co-second authors, listed in alphabetical order, have equally contributed to this work.
**Co-last authors have equally contributed to this work.

[1]Université Paris-Saclay, Faculté de Médecine, Le Kremlin-Bicêtre, France.
[2]Gustave Roussy, Villejuif, France
[3]Institut National de la Santé et de la Recherche Médicale, UMR1015, Gustave Roussy, Villejuif, France.
[4]Transgene S.A., Illkirch-Graffenstaden, France
[5]Open Innovation & Partnerships (OIP), bioMérieux S.A., Marcy l'Etoile, France. R&D – Immunoassay, bioMérieux S.A., Marcy l'Etoile, France.
[6]Joint Research Unit Hospices Civils de Lyon-bioMérieux, Civils Hospices of Lyon, Lyon Sud Hospital, Pierre-Bénite, France.
[7]International Center of Research in Infectiology, Lyon University, INSERM U1111, CNRS UMR 5308, ENS, UCBL, Lyon, France.
[8]Hospices Civils de Lyon, Lyon Sud Hospital, Pierre-Bénite, France.
[9]Département d'Oncologie Médicale, Gustave Roussy, Villejuif, France.
[10]Département d'Innovation Thérapeutique et d'Essais Précoces (DITEP), Gustave Roussy, Villejuif, France
[11]Aix-Marseille Université, Institut de Recherche pour le Développement, Assistance Publique – Hôpitaux de Marseille, Microbes Evolution Phylogeny and Infections, Marseille, France.
[12]Département de Biostatistique et d'Epidémiologie, Gustave Roussy, Université Paris-Saclay, Villejuif, France.
[13]ImmunoTherapy/ImmunoSurgery, Champalimaud Centre for the Unknown, Lisboa, Portugal.
[14]Department of Immunology, Hôpital Européen Georges Pompidou, AP-HP, Paris, France.
[15]PARCC, INSERM U970
[16]Univ Paris Est Creteil, INSERM U955, IMRB, Creteil, France.

[17] Sorbonne Université/Institut National de la Santé et de la Recherche Médicale, U1135, Centre d'Immunologie et des Maladies Infectieuses, Hôpital Pitié-Salpêtrière, Assistance Publique – Hôpitaux de Paris, Paris, France.
[18]Aix Marseille University, CNRS, INSERM, CRCM, Marseille, France.
[19]Centre de ressources biologiques, ET-EXTRA, Gustave Roussy, Villejuif, France.
[20]Département de Biologie Médicale et Pathologie Médicales, service de biochimie, Gustave Roussy, Villejuif, France.
[21]Département de Biologie Médicale et Pathologie Médicales, service de microbiologie, Gustave Roussy, Villejuif, France.
[22]Département Interdisciplinaire d'Organisation des Parcours Patients, Gustave Roussy, Villejuif, France.
[23]Institut National de la Santé et de la Recherche Médicale, U1030, Gustave Roussy, Villejuif, France.
[24]Département de Radiothérapie, Gustave Roussy, Villejuif, France.
[25]Service de Pathologie Infectieuse, Gustave Roussy, Villejuif, France.
[26]Department of Medical Oncology, Pitié-Salpétrière Hospital, APHP, Sorbonne Université, Paris, France
[27]Service de médecine aigue d'urgence en cancérologie, Gustave Roussy, Villejuif, France.
[28]Center of clinical investigations BIOTHERIS, INSERM CIC1428, Gustave Roussy, Villejuif, France
[29]Institut National de la Santé et de la Recherche Médicale – UMR935/UA9, Université Paris-Saclay, Villejuif, France.
[30]INGESTEM National IPSC Infrastructure, Université de Paris-Saclay, Villejuif, France.
[31]Université de Paris, Faculté des Sciences Pharmaceutiques et Biologiques, Paris, France.
[32]Centre Léon Bérard, Lyon, France.
[33]Université Claude Bernard, Lyon, France.
[34]Unicancer, Paris, France.
[35]Institut National de la Santé et de la Recherche Médicale, U981, Gustave Roussy, Villejuif, France.
[36]INSERM UMR 976, Institut de Recherche Saint-Louis, Université de Paris, Paris, France.
[37]Laboratory of Immunology, AP-HP, Hôpital Saint Louis, INSERM UMR1149, Université de Paris, Paris, France.
[38]Institut Hospitalo-Universitaire Méditerranée Infection, Marseille, France.
[39]Centre de Recherche des Cordeliers, Equipe labellisée par la Ligue contre le cancer, Université de Paris, Sorbonne Université, Inserm U1138, Institut Universitaire de France, Paris, France.
[40]Metabolomics and Cell Biology Platforms, Gustave Roussy Cancer Center, Université Paris Saclay, Villejuif, France.
[41]Pôle de Biologie, Hôpital Européen George Pompidou, Assistance Publique – Hôpitaux de Paris, Paris, France.
[42]Université de Paris, Paris, France.
[43]Department of Women's and Children's Health, Karolinska Institute, Karolinska University Hospital, Stockholm, Sweden.
[44]Suzhou Institute for Systems Biology, Chinese Academy of Medical Sciences, Suzhou, China.
[45]Medizinische Klinik, Johannes Gutenberg University Mainz, Germany.
[46]Division of Infection and Immunity, University College London, London, UK.
[47]NIHR Biomedical Research Centre, University College London Hospitals, London, UK.

Corresponding author:
Laurence ZITVOGEL, MD, PhD, Full Professor
University Paris Saclay,
Gustave Roussy Cancer Center,
114 rue Edouard Vaillant,
94805 Villejuif Cedex, France
Telephone: +33 1 42 11 50 41
E-mail: laurence.zitvogel@gustaveroussy.fr

Keywords: TH2/TH1 paradigm, cancer, COVID-19, S1-RBD, viral variants, T cell memory

Abstract

Optimal vaccination and immunotherapy against coronavirus disease COVID-19 relies on the in-depth comprehension of immune responses determining the individual susceptibility to be infected by SARS-CoV-2 and to develop severe disease. We characterized the polarity and specificity of circulating SARS-CoV-2-specific T cell responses against whole virus lysates or 186 unique peptides derived from the SARS-CoV-2 or SARS-CoV-1 ORFeome on 296 cancer-bearing and 86 cancer-free individuals who were either from the pre-COVID-19 era (67 individuals) or contemporary COVID-19-free (237 individuals) or who developed COVID-19 (78 individuals) in 2020/21. The ratio between the prototypic T helper 1 (TH1) cytokine, interleukin-2, and the prototypic T helper 2 (TH2) cytokine, interleukin-5 (IL-5), released from SARS-CoV-2-specific memory T cells measured in early 2020, among SARS-CoV-2-negative persons, was associated with the susceptibility of these individuals to develop PCR-detectable SARS-CoV-2 infection in late 2020 or 2021. Of note, T cells from individuals who recovered after SARS-CoV-2 re-infection spontaneously produced elevated levels of IL-5 and secreted the immunosuppressive TH2 cytokine interleukin-10 in response to SARS-CoV-2 lysate, suggesting that TH2 responses to SARS-CoV-2 are inadequate. Moreover, individuals susceptible to SARS-CoV-2 infection exhibited a deficit in the TH1 peptide repertoire affecting the highly mutated receptor binding domain (RBD) amino acids (331-525) of the spike protein. Finally, current vaccines successfully triggered anti-RBD specific TH1 responses in 88% healthy subjects that were negative prior to immunization. These findings indicate that COVID-19 protection relies on TH1 cell immunity against SARS-CoV-2 S1-RBD which in turn likely drives the phylogenetic escape of the virus. The next generation of COVID-19 vaccines should elicit high-avidity TH1 (rather than TH2)-like T cell responses against the RBD domain of current and emerging viral variants.

Introduction

The emergence and spread of severe acute respiratory syndrome coronavirus-2 (SARS-CoV-2), the causative agent of coronavirus disease 2019, have resulted in devastating morbidities and socioeconomic disruption. The development of community protective immunity relies on long-term B and T cell memory responses to SARS-CoV-2. This can be achieved through viral infection [1] or by vaccination [2-4]. Reports on rapidly decreasing

spike- and nucleocapsid-specific antibody titers post-COVID-19 infection [5] or reduced neutralizing capacity of vaccine-induced antibodies against viral escape variants compared to the ancestral SARS-CoV-2 strain [6, 7] have shed doubts on the importance of humoral immunity as a standalone response. In contrast, T cell immunity was identified as an important determinant of recovery and long-term protection against SARS-CoV-1, even 17 years after infection [8-11].

The TH1 versus TH2 concept suggests that modulation of the relative contribution of TH1 or TH2 cytokines regulates the balance between immune protection against microbes and immunopathology [12-14]. TH1 cells (as well as cytotoxic T cells with a similar cytokine pattern referred to as TC1 cells) produce IFNγ, IL-2, and TNFβ, promote macrophage activation, antibody-dependent cell cytotoxicity, delayed type hypersensitivity, and opsonizing and complement-fixing IgG2a antibody production [12]. Therefore, TH1/TC1 cells drive the phagocyte-dependent host response and are pivotal for antiviral responses [13, 14]. In contrast, TH2 (and TC2) cells produce IL-4, IL-5, IL-6, IL-9, IL-10, and IL-13, providing optimal help for both humoral responses and mucosal immunity, through the production of mast cell and eosinophil growth and differentiation factors, thus contributing to antiparasitic and allergic reactions. Naïve T cell differentiation to distinct TH fates is guided by inputs integrated from TCR affinity, CD25 expression, costimulatory molecules, and innate cell–derived cytokines [15].

SARS-CoV-2-specific T cell immunity plays a key role during acute COVID-19, and up to eight months after convalescence [16-20]. Indeed, functional T cell responses remain increased in both frequency and intensity up to six months post-infection [5]. They are mainly directed against spike, membrane and nucleocapsid proteins, and have been studied in greater detail by single cell sequencing in a limited number of patients. Memory TH1/TC1 T cells specific for SARS-CoV-2 and follicular T helper cells (TFH) cells have been detected in mild cases [21]. However, cases of reinfection have been reported [22] raising questions on the clinical significance of T cell polarization and peptide repertoire specificities against current viral variants. Moreover, pioneering reports suggest that, before SARS-CoV-2 became prevalent (i.e., before 2020), some individuals exhibit immune responses, mainly among $CD4^+$ T cells, against SARS-CoV-1 nucleocapsid (NC) and ORF1a/b, or common cold coronaviruses (CCC) spike and nucleocapsid proteins that are cross-reactive with SARS-CoV-2 [9, 23, 24, 80]. However, the relevance of CCC or SARS-CoV-1-specific memory T cells for effective protection against the current pandemic remains questionable [21, 25].

In the present report, we studied SARS-CoV-2 –specific T cell responses in 382 cancer-bearing or cancer-free subjects, and prospectively followed up 227 COVID-free individuals to understand which T cell polarity and peptide repertoire may convey resistance to COVID-19. We found that a SARS-CoV-2-specific IL-2/IL-5 lymphokine ratio<1 conferred susceptibility to COVID-19 infection or re-infection, coinciding with defective TH1 recognition of the receptor binding domain (RBD) of the spike protein, likely affecting viral evolution by selecting for new antigenic variants.

Results

Effector and memory T cell responses against coronaviruses during COVID-19 infection

We conducted a cross-sectional analysis of the functional T cell responses across several cohorts of healthy individuals and cancer patients enrolled in various prospective studies (Table S1-S2). First, an epidemiological observational study (Figure 1A) aimed at defining the incidence, prevalence, and severity of COVID-19 in cancer patients, opened during the first surge of the pandemic at Gustave Roussy [26]. While the majority of the 227 enrolled cancer patients stayed COVID-19-free, we could analyze T cell responses during the acute phase of SARS-COV-2 infection (n=24) or during convalescence post-COVID-19 (n=28). All the other "unexposed" (COVID-19-negative) cancer patients were analyzed anytime between mid-March and September 2020 (Table S1, Figure 1A). In parallel, we analyzed 22 cancer-free, COVID-19-free healthy volunteers (HV) from 15 distinct families at the same time as their family members were in convalescent phase for COVID-19 (n=26) (Figure 2A, Table S3). A third cohort of 67 individuals from the pre-COVID-19 era (leukocytes frozen between 1999 and 2018) were either HV from the blood bank (n=38) or cancer patients (n=29) recruited in the context of clinical trials [27-30] (Table S1, Figure 1A).

T cell responses directed against viral lysates from the historic SARS-CoV-2 strain IHUMI846 (CoV-2) isolated in early 2020 or two endemic common cold coronaviruses (CCC), OC43 and 229E, were evaluated by an *in vitro* stimulation assay (IVS). As outlined in Figure 1B, in a first step, autologous dendritic cells (DC) were differentiated from monocytes for 72hrs in GM-CSF+IFNα2b. DC were spinoculated with viral particles from heat-inactivated viral lysates and activated with LPS in a second step. Peripheral blood lymphocytes (PBL) kept in low-dose IL-2 during this first step were then stimulated for 48hrs by activated DC after removal of LPS (Figure 1B). The specific viral lysates were compared to supernatants from cell

lines permissive for viral replication (such as Vero E6 for SARS-CoV-2, HCT8 for OC43, MRC5 for 229E). Negative controls were unloaded DC/PBL cell cocultures, while positive controls were PBL stimulated with anti-CD3/anti-CD28 -coated beads. The cytokines accumulating in the supernatants were analyzed by means of a 12-plex flow cytometry-based bead assay (Figure S1A). In this cross-presentation assay, SARS-CoV-2-related IFNγ or IL-2 secretions from PBL depended on MHC class I and MHC class II molecules, as shown using specific neutralizing antibodies (Figure S1B). We calculated the ratio of cytokine release by dividing interleukin concentrations following exposure to viral lysates by those obtained with the respective control supernatants, to ascribe the specificity of the reactivity to SARS-CoV-2 or to CCC antigens for each subject.

First, we characterized the intensity and the quality of PBL responses elicited at the acute phase of SARS-CoV-2 infection (day of symptom onset and/or first positive qPCR of the oropharyngeal swab and/or serology), between mid-March and mid-May 2020 in 24 interpretable tests performed on COVID-19^{+} subjects compared to a cohort of 304 controls (Table S2). Robust SARS-CoV-2 specific IL-2 and IFNγ release, most likely caused by TH1/TC1 cells, and the secretion of IL-4, IL-5 and IL-10, most likely mediated by TH2/TC2 effector T cells, were detectable, and were dominated by IL-2 and IL-5, respectively (Figure 1C, Figure 1D). An antiviral response, characterized by type 1 IFN release, was also prevalent (Figure S1C), as previously detected by single cell transcriptomics in the subset of transitional memory CD4^{+} T cells [21]. Of note, COVID-19 infection did not reactivate CCC-specific T cell responses (Figure 1D, Figure S2A). Interestingly, the systemic T cell tone was shifted towards an inflammatory TH2 profile during the acute phase of the infection, as suggested by increased IL-5, IL-6, TNFα, and IL-17 secretion following TCR cross-linking in COVID-19 patients compared with individuals without COVID-19 (Figure 1D, Figure S1C).

We next examined the polarization of SARS-CoV-2-specific memory T cell responses between May and September 2020 in 54 convalescent COVID-19 individuals (median time lapse between PCR negative and T cell assay: 85 days, range: 13-106 days) compared with contemporary controls (Figure 1A, Figure 1C, Figure 1D, Figure S2, Table S2). A dominant SARS-CoV-2-specific memory TH1 response (resulting in the secretion of IFNγ, IL-2 and TNFα) prevailed in most convalescent subjects within the next 2-3 months after acute infection (Figure 1D). Of note, SARS-CoV-2 specific IL-2 release at recovery correlated with an increase in the frequency of circulating non-activated TFH cells (Figure S1D). In addition, SARS-CoV-2 specific IL-2 secretion was the only parameter correlating with anti-SARS-CoV-2

nucleocapsid (NC) antibody titers (reported to be stable for 8 months [5]) but not with IgG and IgA antibodies targeting the S1 domain of the SARS-CoV-2 spike protein including the RBD (Figure 1E-F and not shown).

More than 30% convalescent COVID-19 individuals displayed polyfunctional T cell responses defined by at least 2 cytokines with a secretion ratio >1.5 (Figure S2A-B). Memory TH1 (IL-2, IFNγ) responses were comparable in both healthy and cancer subsets of COVID-19 positive individuals (Figure S2B-C). As previously described [21, 23, 24, 31, 32], contemporary COVID-19 negative subjects also harbored significant SARS-CoV-2 specific-TH1/TC1 memory responses that appear to pre-exist in cancer patients and healthy individuals whose blood was drawn in the pre-COVID-19 era, including prior to outbreaks of SARS-CoV-1 and MERS (Figure S2B-C). The unsupervised hierarchical clustering considering 12 cytokines monitored in 358 subjects did not segregate pre-COVID-19 from contemporary unexposed individuals nor convalescent patients (Figure S2A).

Hence, while polyfunctional T cell responses dominated by IL-2 and IL-5 were elicited during the acute phase of COVID-19, after convalescence, recirculating memory T cells exhibited a TH1/TC1 profile in about 70% of COVID-19 patients, correlating with anti-SARS-CoV-2 NC antibody titers.

Clinical relevance of the IL-2/IL-5 ratio to predict COVID-19 infection

We next determined the clinical significance of these memory T cell responses monitored in unexposed individuals during the first surge of COVID-19 (mid-March to mid-May 2020) to decipher the nature of memory T cells contributing to susceptibility or resistance to the successive surges of this viral pandemic in fall 2020 and winter 2021. We phoned 229 patients to discover that 22 individuals had developed COVID-19 infections (diagnosed by qPCR or serology) with different degrees of severity according to WHO criteria (Table S1, Figure 2A, Table S4). Indeed, about one third of the initially COVID-19-free individuals became contact cases (n=70) and 29% among these contact cases were diagnosed with COVID-19 infection by specific RT-qPCR or serology (n= 22, Figure 2B, Table S4). The unsupervised hierarchical clustering of the T cell secretory profiles in these 70 individuals failed to correctly segregate resistant (contact) from susceptible (infected) cases (Figure S3A). In addition, the polyfunctionality of T cell responses failed to segregate the two categories of individuals (Figure 2C, Figure S4B). However, two lymphokines, IL-2 and IL-5, secreted by memory T cells responding to SARS-CoV-2 correlated with resistance and susceptibility to SARS-CoV-

2, respectively (Figure 2D-E). Indeed, the levels of IL-2 in the recall response and the proportions of individuals exhibiting IL-2 polarized T cell memory responses were both associated with resistance to COVID-19 (Figure 2D, p=0.01, two-sided Wilcoxon-Mann-Whitney test, Figure 2E, p=0.049, Fisher exact test). In contrast, IL-5 levels in recall responses were associated with increased susceptibility to COVID-19 (Figure 2D, p=0.057, two-sided Wilcoxon-Mann-Whitney test). Resistant individuals harbored a coordinated SARS-CoV-2 specific-TH1 response (IFNγ, TNFα) in mid-March to mid-May 2020, while subjects susceptible to COVID-19 exhibited inflammatory TH9/TH17-like networks (Figure S4C-D). These findings are reminiscent of data segregating asymptomatic or mild from severe diseases [33, 34]. For this reason, we henceforth analyzed the clinical significance of the ratio between SARS-CoV2-specific IL-2 and IL-5 release. Indeed, the IL-2/IL-5 recall response ratio was significantly higher in cancer patients who were SARS-CoV-2-resistant (Figure 2F) and in convalescent patients (Figure S4A). The vast majority (16 out of 19) of cancer patients doomed to be infected with SARS-CoV-2 harbored an IL-2/IL-5 ratio $\leq$1, with the two severe COVID-19 cases exhibiting an IL-2/IL-5 ratio <10 (Figure S4B). In contrast, CCC-specific T cell reactivities did not allow to discriminate susceptible from resistant individuals (Figure 2G), although IL-5 stood out as the strongest correlate between SARS-CoV-2 and CCC-specific T cell responses among 156 individuals with no correlation between SARS-CoV-2 and OC43-specific IL-2 secretion (Figure 2H). Reinforcing this notion, titers of IgG antibodies directed against the spike of the seasonal betacoronaviruses OC43 and HKU1 (but not the alphacoronavirus 229E and NL63) were higher in individuals susceptible to SARS-CoV2 compared to resistant individuals (Figure 2I and not shown).

The SARS-CoV2-specific IL-2/IL-5 recall response ratio was also clinically significant in the cohort of cancer-free individuals that were locked down together with their COVID-19-positive family members (Figure 2A, Table S3, Figure S4D). Individuals who did not get infected harbored IL-2/IL-5 ratios>1 reaching mean values comparable to those achieved in convalescent individuals (Figure 2F, Figure S4A) at higher frequencies than the overall population (Figure S4C).

We next compared the immunogenicity of the lysates derived from the original SARS-CoV-2 strain (IHUMI846) with that of the Danish (IHUMI2096, 20A.EU2, B.1.367, GH) and North African (IHUMI2514, 20C, B.1.160, GH) strains isolated at the end of 2020 [35]. Of note, T cells lost their capacity to produce IL-2 in response to the IHUMI2096 and IHUMI2514 viral variants while IL-17 release tended to increase (p= 0.0857, Figure S5A).

Given that 15-20% of convalescent individuals mounted a TH2/TC2 memory response to SARS-CoV-2 (Figure S2A), we wondered whether these individuals could be at higher risk to get re-infected by SARS-CoV-2 variants. Hence, we analyzed PBMCs in a series of individuals (n=12) who were diagnosed with COVID-19 during the first surge of the SARS-CoV-2 pandemic and then were re-infected with a viral variant prevailing during the later outbreak occurring in fall 2020 or winter 2021, comparing them to health care workers who were multi-exposed cases with multiple negative oropharyngeal SARS-CoV-2 -specific PCR assays (n=17) (Table S5, Figure 2J, left panel). Surprisingly, monocytes could be differentiated into dendritic cells only in 4 re-infected patients. Unstimulated PBL from re-infected and re-convalescent subjects spontaneously secreted much higher levels of IL-5 than did PBL from multi-exposed cases, reaching similar ranges as those obtained after TCR crosslinking (Figure 2J, middle panel). After specific re-stimulation with SARS-CoV-2 lysates, IL-10 was markedly increased in recall responses from re-infected but not multi-exposed cases (Figure 2J, right panel) and IL-2 was undetectable (Figure S5B). In this small cohort of multi-exposed individuals, the recognition pattern of the United Kingdom (UK) (IHUMI3076, B.1.1.7), South Africa (IHUMI3147, B.1.351) and Brazil (IHUMI3191, P.1) [35] strains were quite variable, some individuals losing the TH1/TC1 or acquiring a TH2/TC2 profile, depending on the strain (Figure S5C).

We conclude that the TH1/TC1 *versus* TH2/TC2 polarity of SARS-CoV-2 specific-memory T cell responses is associated with effective clinical protection against infection, an IL-2/IL-5 ratio >1 indicating resistance to the COVID-19.

Defects in the TH1/TC1 response against the SARS-CoV-2 RBD of spike glycoprotein in susceptible individuals

In hosts affected by viral infections or cancer, the breadth of T cell epitope recognition is a prerequisite for protective immunity [36-38]. We analyzed the diversity of SARS-CoV-2 T cell responses by single peptide mapping using 186 peptides with 9 to 51 amino acids corresponding to 146 non-overlapping or poorly overlapping epitopes of the SARS-CoV-2 ORFeome (among which 25 epitopes were shared with SARS-CoV-1), encompassing membrane, nucleocapsid, spike, ORF3a, ORF8 and ORF10 proteins, plus 41 epitopes covering the SARS-CoV-1 ORFeome of immunological relevance (among which 8 epitopes were shared with SARS-CoV-2), as well as a series of positive controls, namely epitopes from Influenza virus, Epstein Barr

virus (EBV), Cytomegalovirus (CMV), phytohemagglutinin (PHA), and anti-CD3ε (OKT3) antibody. IFNγ responses against these 186 peptides were evaluated in 164 individuals (123 unexposed individuals, 25 convalescent COVID-19-positive patients, 16 re-infected patients, see Table S6). To enable the detection of low-frequency SARS-CoV-2 peptide-specific T cells, we used an *in vitro* 7 day-long, IL-2+IL-15 enriched IVS assay in the presence of each individual peptide in duplicates (Figure 3A). We chose to monitor IFNγ, a proxy for TH1/TC1 responses, as opposed to IL-2, in the 7 day- coculture supernatants by ELISA because recombinant human IL-2 was already added to the IVS assay (Figure 3A). The overall recognition patterns of these peptides across various patient populations, and their individual frequencies are detailed in Figure 3B, and Figure S6-S7. About 10% convalescent individuals recognized more than 15% of our peptide selection within the SARS-CoV-2 ORFeome (Figure S6 inset). T cell responses in unexposed patients, in particular in the pre-COVID-19 era, covered large specificities, as suggested by previous reports [9, 21, 24] (Figure 3C, right panel and Figure S6). In accord with the literature [9, 24], the immune response of convalescent COVID-19 patients was mainly directed against spike, membrane, and nucleocapsid (NC) and, to a lower extent, against ORF3a, ORF8, and ORF10 (Figure 3B, 3D left panel). The breadth of the peptide recognition coverage was not significantly reduced in cancer patients compared with others (Figure 3B, 3C left panel). In a limited number of individuals, we measured not only IFNγ but also IL-5, IL-9 and IL-17 by ELISA. The recognition profile specific to the spike (and more specifically the RBD) as well as ORF8 was more geared toward TH1/TC1 (IFNγ) than TH9 or TH2 (IL-9 or IL-5 production respectively) (Figure S8A-C). The membrane- and NC-specific repertoire was strongly TH17 oriented (Figure S8B).

Using logistic regression analyses, we determined the TH1/TC1 peptide recognition fingerprint significantly associated with each patient category (Figure S9). The hallmark repertoire of the pre-COVID-19 era consisted in a stretch of peptides covering part of the SARS-CoV-1 genome (spike, membrane, ORF3a, NC), some peptide residues sharing high or complete homology with SARS-CoV-2, as well as numerous ORF8 sequences (Table S6). Of note, the recognition pattern of these SARS-CoV-1 epitopes highly correlated with responses directed against ORF8 peptides (not shown). In contrast, the COVID-19-associated blueprint encompassed many nucleocapsid peptides (NC_1 (residues 1-15), NC_6-7 (residues 76-105, NC_8 (residues 106-120) sharing 93% and 100% homology with OC43 and HKU1, respectively, the HLA-A2- restricted nonamer (RLNQLESKV) NC_226-234 from SARS-

CoV-1 (sharing high structural homology with the SARS-CoV2 epitope RLNQLESKM) and another SARS-CoV-1 NC nonamer peptide (NC_345-361), three peptides residing in ORF8, two epitopes belonging to the RBD region ("SPIKE29") found at high frequency across subjects (23.5%), as well as a peptide from the C terminal portion of spike ("SPIKE84", residues 1246-1260) (Figure S9A). Cancer patients tended to lack some specificities, yet with no prototypical signature (Figure S9A).

Next, we investigated the ORFeome peptide repertoire associated with SARS-CoV-2-specific IL-2 memory responses in 118 unexposed individuals by means of linear regression analysis (Figure 4A, left panel). Among the 9 peptides associated with a positive contribution to IL-2 secretion, one nonamer (KLPDDFMGCV in SARS-CoV-1 genome and KLPDDFTGCV in the SARS-CoV-2 genome) resided in the RBD region that constitutes the binding site for its cellular receptor angiotensin-converting enzyme 2 (ACE2) [39] while, conversely among the 13 peptides associated with a hole in the TH1 response, 5 resided within the RBD of the spike glycoprotein. More specifically, there was a statistically significant enrichment of RBD-related peptides within this TH1/TC1 hole (Figure 4A, right panel).

In order to validate the clinical significance of the TH1/TC1 repertoire hole and the assumption that a defect in the TH1/TC1 recognition pattern of the RBD sequence could be a risk factor for COVID-19, we calculated the number of positive peptides selected from the RBD region spanning aminoacid 331-525 residues (called "SPIKE23" to "SPIKE35" in Table S6), in each of the 83 individuals who were comprehensively explored in the peptide-based IVS assay, 37 resistant (contact) individuals, 14 infected persons (susceptible) as well as 32 controls (unexposed lockdown and/or unknown) using the IFNγ ELISA (Table S1). While susceptible individuals exhibited a significant defect in the RBD-related TH1/TC1 repertoire (Figure 4B), up to 25% of the resistant individuals harbored robust TH1/TC1 responses to the 331-525 aminoacid residues of RBD (Figure 4B, p=0.049, Fisher exact test). Again, the RBD-specific TH1/TC1 responses were almost undetectable in patients who got infected twice with SARS-CoV-2 (Table S5), while they could be measured in 50% convalescent COVID-19 patients (Figure 4C, p=0.011, Fisher exact test) in accordance with a recent report highlighting the immunodominance of the S346-365 region (corresponding to our "SPIKE24" epitope) in convalescent individuals [40]. Such S1-RBD-specific TH1 responses pre-existed in the pre-COVID-19 era at the same frequency in cancer or cancer-free individuals (Figure 4D). T cell responses directed against S1-RBD peptides were evaluated for both IL-5 and IFNγ secretions in 36 patients. They almost exclusively exhibited a TH1 pattern (in 10/36 cases), with only 3/36 individuals harboring a TH2 profile (Table S7). Of note, there was a robust consistency and

concordance of the polarization status of patients between the two (cross-priming and peptide-based) IVS assays (McNemar test, p= p.val=2,2e-16 comparing SARS-CoV-2 or peptide-specific IL-2 and IFNγ release, McNemar test, p= p.val=2.2e-16 comparing SARS-CoV-2 or peptide-specific IFNγ release, p.val <1e-16).

We performed immunoinformatic-based prediction analyses of S1-RBD peptide binding affinities to MHC class I and class II molecules using the NetMHCpan algorithm. This approach revealed strong binding affinities to MHC class I HLA-A, -B and -C alleles for the RBD epitopes "SPIKE25" (residues 361_375), "SPIKE27" (residues 391-405), "SPIKE31" (residues 451-465). In contrast, "SPIKE33" (residues 481_495) was predicted to have a low or absent affinity for HLA-B and HLA-C alleles, respectively (Table S8a). Only "SPIKE24", "SPIKE25" and "SPIKE31 were predicted to bind with a high affinity to HLA-DR alleles (Table S8b) as already reported for the immunodominant S346-365 region [40].

In accordance with the immunodominance of S1-RBD, the other signatures indicated by our logistic regression analysis (Figure S9A), namely the convalescent or the pre-COVID-19 era -related blueprints were not significantly associated with COVID-19 resistance (Figure S9B-C).

Given that immunoselection may drive antigenic drift of viruses as well as the evolution of viral phylogeny, we analyzed the coincidence of hot spot mutations in the SARS-CoV-2 ORFeome [41] with T cell memory patterns of clinical significance (Table S9). Of note, significantly higher mutation frequencies were detected within the S1-RBD-specific TH1 response (62%) compared with other regions of the SARS-CoV2 orfeome (26%) (Odd Ratio = 0.21, 95% confidence interval [0.06; 0.68], p=0.01, Figure 4E).

During the course of this study, two SARS-CoV-2 mRNA vaccines were approved by FDA and EMA based on reports that they prevent COVID-19 infection with an efficacy of >90% [3]. Using a simple whole blood stimulation assay allowing the detection of IFNγ-producing anti-viral T cells following peptide stimulation within 18 hours [42], we analyzed RBD-specific T cell reactivities before and after dual vaccination with BNT162b2 mRNA (BioNTech/Pfizer) in 70 unexposed health care workers (HCW) and 14 COVID-19 convalescent HCW (Table S10). The vast majority (approximately 90%) of naive vaccinees mounted robust RBD-specific TH1/TC1 cell responses after 2 immunizations (Figure 4F).

Hence, our findings suggest that defects in the TH1 repertoire affecting the recognition of SARS-CoV-2 S1-RBD are associated with susceptibility to infection or re-infection by

SARS-CoV-2. This antigenic region appears to mutate more than other regions of the SARS-CoV-2 orfeome, perhaps as a result of an immune system-mediated evolutionary pressure.

Discussion

Here, we unravel the first *prospective* correlation between preexisting (before the first surge) SARS-CoV-2-specific TH2/TC2 immune responses and susceptibility to infection with SARS-CoV-2 or re-infection with viral variants. Both in cancer patients and cancer-free subjects, the best immunological correlate with future SARS-CoV-2 infection was undistinguishably a recall response characterized by a low ratio of TH1/TH2 lymphokines (and more precisely an IL-2/IL-5 ratio <1) secreted upon exposure to the original SARS-CoV-2 viral strain. This recall response coincided with a hole within the TH1/TC1 cell repertoire affecting the RBD of the spike protein. Moreover, in a small series of re-infected individuals, maladaptive anti-SARS-CoV-2 responses were characterized by elevated baseline TH2 responses (spontaneous IL-5 release from PBL) and IL-10-centered recall responses. Finally, vaccinees immunized with a clinically approved mRNA encoding the spike protein mounted a robust RBD-specific TH1/TC1 response, that may account for immune protection.

Reportedly, $CD4^+$ TH1 and TH2 responses are induced during the primary phase of viral infection, and both TH1 and TH2 can generate an anamnestic response upon rechallenge with the same virus [43]. Survivors from SARS-CoV-1 infection developed polyfunctional T cells producing TH1 cytokines and long-term $CD8^+$ T cell responses as late as 11 years post-infection [9]. The TH1 cytokine IL-2 (which correlated with circulating non-activated TFH cells in convalescent patients in our study) was the pivotal factor allowing us to distinguish susceptible from resistant individuals. Signaling via the high-affinity IL-2 receptor (which requires CD25/IL-2Rα expression) favors the generation of $CXCR5^-$ T effector cells, and this is associated with TH1 responses sustained by the transcription factor TBX21. Moreover, the development of IFNγ producing effector memory T cells depends upon CD25 [15]. Accordingly, upon infection with lymphocytic choriomeningitis (LCMV), CD25-deficient $CD4^+$ T cells largely fail to form IFNγ producing T effector cells in secondary lymphoid organs and to generate lung tissue resident memory T cells [44].

In contrast, increased TH2 cytokine release correlated with poor outcome in patients, a finding corroborated in mouse studies of SARS-CoV-1 [45, 46]. During SARS-CoV-2 infection, TH2-associated blood markers, such as eosinophilia and circulating IL-5, IL-33,

eotaxin-2 and eotaxin- 3 correlated with COVID-19 severity, contrasting with the fact that $CD4^+$ and $CD8^+$ T cells from COVID-19 patients secrete comparable amounts of IFNγ in moderate and severe disease [47].

What cellular cues may influence TH2 differentiation or maintenance? Distinct dendritic cell subsets could specifically induce TH2 immunity, while limiting TFH responses and humoral immunity [48-50]. Indeed, preferential trans-vasation of blood-born cDC2 ($CD1c^+$ DC) into the bronchoalveolar fluid was described for severe COVID-19 [51], and TH1/TH2 polarization is not only achieved during the priming response in lymphoid organs but is largely driven by the preferential expansion of either TH1 or TH2 cells in non-lymphoid tissues [52]. Various cell types located in peripheral tissues can impact T cell fate [53]. In the lungs of severe COVID-19 patients, a clonal expansion of IL-17A/F and GM-CSF producing TRM-like $CD4^+$ T cells persisted even after viral clearance [34]. Our findings point to some correlative links between IL-5 and GM-CSF in recall responses from individuals susceptible to COVID-19. While IL-7 secreting stromal cells may promote survival of TH2 memory cells within lung tertiary lymphoid structures [54, 55], it remains unclear to which extent local (oropharyngeal or pulmonary) cues might influence the maintenance of SARS-CoV-2 specific or cross-reactive TH2 responses.

TCR signaling plays a major role in $CD4^+$ polarization and can vary according to the TCR affinity, the amount of peptide/MHC-II complexes perceived by a TCR, or the length of time a T cell spends proofreading peptide/MHC-II complexes [15]. Of note, the RBD-specific TH1/TC1 responses against regions 361_375 and 391_405 of spike exhibited robust binding capacities across all MHC class I alleles. Several authors reported cross-reactivities between CCC and SARS-CoV2 [9, 20, 23, 24, 31, 32, 56, 57]. However, such cross-reactive T cells may turn out to be harmful with respect to clinical correlations [58-63]. Indeed, according to one report [21], preexisting CCC-specific memory $CD4^+$ T cells exhibit low TCR avidity in almost all unexposed individuals, and are strongly expanded in severe COVID-19 but not in mild cases. Moreover, CCC/SARS-CoV-2-cross-reactive T cell clones shared among convalescent and infected individuals harbored lower functional avidity than non-cross-reactive clones, suggesting antigenic imprinting of the TCR repertoire by previous exposure to CCC [25, 82]. Of note, these spike-specific cross-reactive $CD4^+$ T cells might not only re-expand during infection but also following vaccination. In line with this possibility, we detected a strong positive correlation between CCC and SARS-CoV2-specific IL-5 release by memory T cells in all unexposed individuals. Moreover, CCC-specific IgG titers were higher in susceptible compared to resistant individuals. Finally, the SARS-CoV-1 and ORF8-specific T cell

508 repertoire prevailing in the pre-COVID-19 era failed to be clinically relevant for the avoidance
509 of COVID-19 and such a repertoire was frequently detected in re-infected individuals during
510 their convalescence phase. Hence, we cannot rule out the possibility that a preexisting TH2
511 immunity, for instance directed against sequences shared by sarbecoviruses [9] could increase
512 the susceptibility to, and severity of, SARS-CoV-2 infection [45-47].
513
514 The landscape of prevalence and immunodominance of SARS-CoV-2 epitopes - supposedly
515 associated with protection during the acute phase - has been thoroughly investigated [64]. Using
516 40-mer peptide pools covering regions of membrane, nucleocapsid, ORF3a, ORF7/8, and spike
517 proteins, Tan et al. observed a statistically significant correlation between the early appearance
518 of SARS-CoV-2 peptide-reactive cells and shorter duration of infection [65]. However, viruses
519 employ numerous strategies to evade $CD8^+$ T cell immune responses [66]. Our data obtained
520 in COVID-19-free individuals who remained resistant to overt infection despite exposure to the
521 virus strongly support the immunological and clinical relevance of memory TH1/TC1
522 responses directed against the spike S1-RBD region. An immune-driven selection process of
523 viral phylogeny can occur [67]. Early (but transient) induction of ORF7/8-specific TH1 cell
524 immune responses as well as antibody responses against ORF8 have already been reported
525 during the acute phase of COVID-19 in small numbers of patients. Some arguments plead for
526 the biological significance of ORF8-specific T cell immunity in viral control. Indeed, a 382-
527 nucleotide deletion that truncates ORF7b and ORF8, culminating in the loss of ORF8
528 transcription, and conferring mild forms of infections [68] has been reported [69]. However,
529 our data do not support the clinical relevance of ORF8-specific immune responses.
530 There is growing evidence of the links between mutations within the SARS-CoV-2
531 spike protein and the evasion of neutralizing antibody responses [70, 71]. Single
532 nonsynonymous mutations in SARS-CoV-2 can theoretically subvert the immune response to
533 CTL epitopes as well [72]. These studies suggested that immune selection may shape the
534 mutational landscape of $CD8^+$ T cell epitopes. Our data fuel the theory that i) robust TH1
535 memory immune responses against RBD might be important in restraining viral infection, thus
536 exerting a selective pressure on the virus, obliging it to generate escape variants by mutation of
537 RBD, ii) preexisting TH2 antiviral responses might not only be incapable of eliminating SARS-
538 CoV-2-infected cells but actually favor (re-)infection with SARS-CoV-2, ultimately increasing
539 the viral reservoir, thus favoring the emergence of viral variants.
540

Our work may have important consequences for the design of next-generation vaccines against COVID-19. Immunization strategies should aim at triggering SARS-CoV-2 specific TH1/TC1 (rather than TH2/TC2) responses. The efficacy of cellular immune response relies on three components, (i) the antigen, (ii) the adjuvant and (iii) the dynamics of viral evolution [73]. Immunization with inactivated SARS-CoV-1 or with the whole spike (S) protein, caused eosinophilic infiltration following viral re-exposure in mice [74, 75]. In contrast, at least in the case of SARS-CoV-1, immunization with RBD induced neutralizing antibodies in the absence of a TH2/TC2 response [76]. Vaccine adjuvants can stimulate TH1/TC1-favorable innate immunity [77, 82], as this is the case for multiple viral vectors, virus-like particles and mRNA containing nanoparticles. Finally, virus adaptation to the host has to be outcompeted. One might infer from our data that the currently protective immunodominant regions generating a TH1/TC1 profile may be the focus of the future antigenic drift of SARS-CoV-2.

Community-protective immunity can affect RNA virus evolution by selecting for new antigenic variants on the scale of years, as exemplified by the need for annual evaluation of influenza vaccines [78]. It is likely that pandemic SARS-CoV-2 evolution bears similarities with human influenza A virus evolution including accumulation of adaptive changes in the receptor binding domain (RBD), in which case vaccines would have to be updated regularly [78]. Therefore, to win the race against current virus strains and emerging variants, an expedited world-wide vaccination rollout ensuring an immunization *en masse* against relevant epitopes (and in particular the entire RBD region of the variants from Brazil, India, and South Africa) with vaccine formulations ensuring TH1/TC1 (rather than TH2/TC2) responses should outwit the COVID-19 pandemic. It will be of utmost interest to monitor the polarity and specificity elicited by current COVID-19 vaccines and to correlate these recognition profiles with failed immunization, reinfection and emergence of severe disease.

SUPPLEMENTAL MATERIALS

Material and methods

Patient and cohort characteristics. All clinical studies were conducted after written informed consent in accordance with Good Clinical Practice guidelines and the provisions of the Declaration of Helsinki. Cohorts' characteristics are detailed in Table S1, Figure 1A and Figure S1. Two cohorts of cancer patients (from the pre-COVID-19 era and from the COVID-19 era) and three cohorts of healthy volunteers (from the pre- COVID-19 era and from the COVID-19 period including a cohort of vaccinees) were exploited to set up the translational research analyses. Peripheral blood mononuclear cells (PBMC) were provided by Gustave Roussy

Cancer Campus (Villejuif, France) and IHU Méditerranée Infection (Marseille, France) (see Blood analyses section).

Contemporary clinical studies (COVID-19 era): ***1/ ONCOVID clinical trial and regulatory approvals.***

Principles. The protocol is available at https://clinicaltrials.gov/ct2/show/NCT04341207. Gustave Roussy Cancer Center sponsored the trial named `ONCOVID` and collaborated with the academic authors on the trial design and on the collection, analysis, and interpretation of the data. Sanofi provided trial drugs. Protocol approval was obtained from an independent ethics committee (ethics protocol number EudraCT No: 2020-001250-21). ***Patients.*** ONCOVID eligible patients were all comer adults with advanced solid tumors or advanced hematological malignancies spontaneously presenting at Gustave Roussy between April 10th, 2020 and January 15th, 2021 (data cut-off for our analyses). ***Trial design.*** Cancer patients were screened for SARS-CoV-2 virus carriage by nasopharyngeal sampling at every hospital visit. The presence of SARS-CoV-2 RNA was detected by RT-qPCR assay in a BSL-2 laboratory. Asymptomatic and symptomatic patients (*i.e* presenting with fever (t°>38°C) and/or cough and/or shortness of breath and/or headache and/or fatigue and/or runny nose and/or sore throat, anosmia/ageusia) with a positive SARS-CoV-2 RT-qPCR test, shifted to the interventional phase (tailored experimental approach with Hydroxychloroquine and Azithromycin therapy in symptomatic SARS-CoV-2 positive subjects). Asymptomatic or symptomatic patients with negative SARS-CoV-2 RT-qPCR tests continued their standard of care anti-cancer treatments. Repeated RT-qPCR for SARS-CoV-2 on nasopharyngeal swabs and blood samples were performed to monitor the status for SARS-CoV-2 and the immune response, respectively, in COVID-19 positive and negative patients. The COVID-19 severity was defined based on oxygen, imaging and hospitalization criteria (WHO criteria). Unexposed and exposed individuals included in the ONCOVID trial during the first surge were followed-up by telephone interview at 12-months in order to record documented COVID-19 infections and degree of severity (WHO criteria) during the successive surges. ***Samples for translational research.*** PMBCs were isolated less than 8 hours after the blood collection (at patient inclusion and at every hospital visit) and kept frozen at-80°C. ***2/ PROTECT-Cov clinical trial and regulatory approvals. Principles.*** IHU Méditerranée Infection sponsored the trial named `PROTECT-Cov` and collaborated with the academic authors on the trial design and on the collection, analysis, and interpretation of the data. Protocol approval was obtained from an independent ethics committee (ethics protocol number ANSM No: 2020-A01546-33). The trial was conducted in accordance with Good Clinical Practice guidelines and the provisions of the Declaration of Helsinki. All patients provided written informed consent. ***Subjects.*** PROTECT-Cov eligible subjects were members of the same family/home composed of two or more people and selected from the microbiology laboratory register on SARS-Cov-2 tests performed between March 23 and April 10, 2020. ***Trial design.*** Members of the same family/home who had at least one (a)symptomatic COVID-19 + case (RT-qPCR <35 Ct values for SARS-CoV-2 on nasopharyngeal swabs) and at least one member with negative RT-qPCR for SARS-CoV-2 (≥35 Ct) were screened. A telephone interview was conducted in order to confirm and complete the list of family circles in connection with the positive case. The compliant subjects finally selected were invited to come back to the IHU Méditerranée Infections hospital where they

were included in the trial and had a blood test. ***3/ COVID-SER clinical trial and regulatory approvals. Principles.*** At the "Hospices Civils de Lyon", France was conducted the trial named COVID-SER. Protocol approval was obtained from an independent ethics committee (the national review board for biomedical research, Comité de Protection des Personnes Sud Méditerranée, ID-RCB-2020-A00932-37). The clinical study was registered on ClinicalTrial.gov (NCT04341142). Written informed consent was obtained from all participants and the study. ***Subjects. COVID-SER*** eligible subjects were health care workers who received the Pfizer–BioNTech mRNA COVID-19 vaccine BNT162b2. All subjects with a positive SARS-CoV-2 RT-PCR prior vaccination and/or a positive serological result with Wantaï Ab total kit at the pre-vaccination visit were considered as convalescent. Blood sampling was performed before vaccination and 4 weeks after receiving 1 or 2 doses of vaccine for naive and convalescent health care workers respectively. According to French procedures, a written non-opposition to the use of donated blood for research purposes was obtained from healthy volunteers. The donors' personal data were anonymized before transfer to our research laboratory. We obtained approval from the local ethical committee and the French ministry of research (DC-2008-64) for handling and conservation of these samples. Human biological samples and associated data were obtained from NeuroBioTec (CRB HCL, Lyon France, Biobank BB-0033-00046) and Virginie Pitiot.

Clinical studies from the Pre-COVID-19 era: ***1/ Series of patients with cancer:*** This cohort is composed of different IGR clinical trials. Patients were included and blood was collected and banked between 1999 and 2018 (Pre-COVID-19 era). ***Clinical studies:*** *1/* Patients with acute myeloid leukemia admitted in the Hematology Department of IGR in Villejuif, France, between March 2008 and March 2009 were included. The study was approved by the local ethics committee (Comité de Protection des Personnes (CPP) Hopital Bicêtre –CALEX protocol, n1 ID RCB 2007-A01074-49, date 29 February 2008). The main clinical and biological characteristics of the patients are summarized in [30] PMBC were isolated less than 8 hours after the blood collection (before chemotherapy) and were kept frozen at -80°C. *2/* Phase II vaccine trial immunizing cancer patients (diagnosed with inoperable Non-small cell lung cancer after induction with four cycles of platinum-based chemotherapy) with autologous DC-derived exosomes and cyclophosphamide (CTX) (Study code « Dex2 »: NCT01159288, date 19 December 2005) [28]. Eligible patients required at least stabilization of their disease prior to being on maintenance immunotherapy with sc injections of IFNγ- dendritic cell derived-exosomes loaded with MHC class I and class II-restricted cancer antigens. PBMCs were collected at baseline after the 4th cycle of platinum-based chemotherapy, before metronomic CTX followed by exosome injections and were kept frozen at -80°C. *3/* Phase I/II study of intradermal and subcutaneous immunization with the recombinant MAGE-3 protein in patients with MAGE-3 positive, measurable non visceral metastatic melanoma. The study was approved by the local ethics committee (Study code « LUD 99 003 »: N-CSET : 99/090/752, date 1 December 1999). Patients were required to have cutaneous melanoma with detectable cutaneous and/or lymph node metastasis, but no visceral metastasis (AJCC 1997 stage III or IVM1a). No chemotherapy, radiotherapy, or immunotherapy was allowed in the 4-week period before the first vaccination. PBMCs were collected at baseline before the first vaccination and

were kept frozen at -80°C. 4/Adult patients with metastatic or locally advanced solid malignancy, measurable or evaluable disease who were refractory to standard therapy were eligible for the study (Phase I IMAIL-2 trial approved by the Kremlin Bicêtre Hospital Ethics Committee [no 07–019] and the Agence Française de Sécurité Sanitaire des Produits de Santé [no A70385–27; EudraCT N°:2007–001699–35 in 2007) [79]. They received Imatinib mesylate (IM) combined with increasing doses of IL-2. PMBCs were isolated less than 8 hours after the blood collection (at baseline before treatment) and were kept frozen at -80C. ***2/ Series of patients without cancer :*** Peripheral blood was obtained from healthy volunteers at the *Etablissement Français du Sang* (EFS, Paris France, n 18EFS031 date 24 September 2018).

Blood analyses. Blood samples (for serum and PBL) were drawn from patients enrolled in the different cohorts presented in the cohort description section above. Whole human peripheral blood was collected into sterile vacutainer tubes. ***Anti-SARS-CoV-2 immunoglobulins measurements.*** Serum was collected from whole blood after centrifugation at 600 g for 10 min at room temperature and transferred to -80°C freezer to await analysis. Serological analysis SARS-CoV-2 specific IgA, IgM and IgG antibodies were measured in 119 serum samples from 87 patients (Supplementary Material Figure 1) with The Maverick ™ SARS-CoV-2 Multi-Antigen Serology Panel (Genalyte Inc. USA) according to the manufacturer's instructions. The Maverick™ SARS-CoV-2 Multi-Antigen Serology Panel (Genalyte Inc) is designed to detect antibodies to five SARS-CoV-2 antigens: nucleocapsid, Spike S1 RBD, Spike S1S2, Spike S2 and Spike S1 or seasonal HCoV -NL-63 nucleocapsid, -OC-43, -229E and -HK-U1 Spike in a multiplex format based on photonic ring resonance technology. This system detects and measures with good reproducibility changes in resonance when antibodies bind to their respective antigens in the chip. The instrument automates the assay. Briefly, 10µl of each serum samples were added in a sample well plate array containing required diluents and buffers. The plate and chip are loaded in the instrument. First the chip is equilibrated with the diluent buffer to get baseline resonance. Serum sample is then charged over the chip to bind specific antibodies to antigens present on the chip. Next, chip is washed to remove low affinity binders. Finally, specific antibodies of patients are detected with anti-IgG or -IgA or -IgM secondary antibodies. ***Isolation of peripheral blood mononuclear cells (PBMCs) from fresh blood sampling.*** Venous blood samples (10ml to 30ml) were collected in heparinized tubes (BD Vacutainer® LH 170 U.I., Dutscher, UK). On the same day, blood was processed in a biosafety level 2 laboratory at Gustave Roussy Institute, Villejuif, France, or in IHU Méditerranée Infection, Marseille, France. Peripheral blood mononuclear cells (PBMCs) were freshly isolated by LSM, Lymphocyte Separation Medium (Eurobio Scientific, France) density gradient centrifugation according to manufacturer's instructions. (Leucosep tubes, Greiner; Biocoll, Bio&SELL). PBMCs were then collected, washed once with phosphate-buffered saline solution (PBS) and aliquoted in 1ml of cryopreservation medium (CryoStor®, STEMCELLS Technologies, USA) in cryovials (two cryovials per patient). Cryovials (Cryotube™vials ThermoFisher Scientific, Denmark) were conserved for 24h at -80°C in a cryo-freezing container (Mr.Frosty™,Thermo Fisher Scientific) before storage in liquid nitrogen.

Viral studies. ***Biosafety levels for in vitro experiments.*** Frozen PBMCs from patients with a confirmed negative RT-qPCR for SARS-CoV-2 genome at the time of blood drawing were processed in a biosafety level 2 laboratory at Gustave Roussy Institute, Villejuif, France. All samples from patients with positive RT-qPCR were processed in a biosafety level 3 laboratory

at Henri Mondor Hospital, Créteil, France. When a patient was sampled at different timepoints, samples were processed together in the same laboratory. ***RT-qPCR analysis.*** SARS-CoV-2 diagnostic testing of clinical nasopharyngeal swabs or other samples by RT-qPCR was conducted from 14 March to 23 March 2020 at an outside facility using the Charité protocol. From the 23th March 2020 testing was performed internally at the Gustave Roussy. The cycle thresholds were collected only for assays performed at Gustave Roussy. Nasopharyngeal swab samples were collected using flocked swabs (Sigma Virocult) and placed in viral transport media. SARS-CoV-2 RNA was detected using one of two available techniques at Gustave Roussy: the GeneFinder COVID-19 Plus Real*Amp* kit (ELITech Group) targeting three regions (*RdRp* gene, nucleocapsid and envelope genes) on the ELITe InGenius (ELITech Group) or the multiplex real-time RT-PCR diagnostic kit (the Applied Biosystems TaqPath COVID-19 CE-IVD RT-PCR Kit) targeting three regions (ORF1ab, nucleocapsid and spike genes) with the following modifications. Nucleic acids were extracted from specimens using automated Maxwell instruments following the manufacturer's instructions (Maxwell RSC simplyRNA Blood Kit; AS1380; Promega). Real-time RT-PCR was performed on the QuantiStudio 5 Dx Real-Time PCR System (Thermo Fisher Scientific) in a final reaction volume of 20 µl, including 5 µl of extracted nucleic acids according to the manufacturer instruction. ***Viral lysates and their production.*** SARS-CoV-2 IHUMI2, IHUMI845, IHUMI846, IHUMI847 (early 2020 episode), IHUMI2096 (20A.EU2, B.1.160) and IHUMI2514 (20C, B.1.367) [80] IHUMI3076 (20I/501Y.V1, B.1.1.7), IHUMI3147 (20H/501Y.V2, B.1.351) and IHUMI3191 (20J/501Y.V3, P.1) strains were isolated from human nasopharyngeal swab as previously described [35] and grown in Vero E6 cells (ATCC CRL-1586) in Minimum Essential Medium culture medium (MEM) with 4% fetal calf serum (FCS) and 1% L-glutamine. Influenza strains H1N1 (0022641132) and H3N2 (8091056304) were isolated then produced from human nasopharyngeal swab in MDCK cells (ATCC CCL-34) in MEM with 10% FCS and 1% L-glutamine. All these clinical isolates were characterized by whole viral genome sequencing from culture supernatants. Coronavirus OC43 (ATCC vr-1558) was grown in HCT8 cells (ATCC CCL-244) in RPMI with 10% FCS. Coronavirus 229E (ATCC vr-740) was grown in MRC5 cells (ATCC CCL-171) in MEM with 10% FCS. All reagents for culture were from ThermoFisher Scientific and all cultures were incubated at 37°C under 5% CO_2 without antibiotics. All viral strains were produced in 125 cm^2 cell culture flasks. When destruction of cell monolayer reached approximately 80%, between 2 to 7 days according to cell line and viral strain, culture supernatant was harvested. After low speed centrifugation to remove cells and debris (700 x g for 10 min.) supernatants were filtered through 0.45 then 0.22 µm pore-sized filters. These viral suspensions were then inactivated for 1 hour at 65°C before use. Batches of scrapped control uninfected cells were rinsed twice in PBS, and then finally resuspended in 5 ml of PBS at 5.10^5 cells/ml. All cells and antigens were tested negative for Mycoplasma before use.

In vitro stimulation assays. ***Cross-presentation assay or peripheral blood lymphocyte stimulation with autologous monocyte derived- dendritic cells (DC).*** Frozen PBMCs were thawed, washed and resuspended in RPMI 1640 media (GIBCO). Viability and count were evaluated using a Vi-Cell XR Cell Counter (Beckman Coulter, Brea). PBMC were then cultured in RPMI 1640 supplemented with 10% human AB serum, 1mM Glutamine, 1% sodium pyruvate, 1% HEPES, 1% penicillin/streptomycin at a cell density of 0.5M cells/cm^2 for 2 hours at 37°C, 5% CO_2 and separated into adherent and non-adherent cell populations. Non-adherent cells, containing Peripheral Blood Lymphocytes (PBL), were collected and cultured 4 days at 37°C, 5% CO_2 in IMDM medium (Sigma-Aldrich, UK), supplemented with 10% human AB serum (Institut de Biotechnologies Jacques Boy, France), 1mM Glutamine

(GIBCO/ThermoFisher Scientific, UK) 1% Sodium Pyruvate (GIBCO/ThermoFisher Scientific, UK), 1% HEPES (GIBCO/ThermoFisher Scientific, UK), 1% penicillin/streptomycin (GIBCO/ThermoFisher Scientific, UK) and 200 UI/mL rhIL-2 (Miltenyi, Germany). The adherent cell population was cultured for 3 days, at 37°C, 5% CO_2, in a mo-DC differentiating media containing RPMI 1640 supplemented with 10% human AB serum, 1mM Glutamine, 1% sodium pyruvate, 1% HEPES, 1% penicillin /streptomycin, 1000UI/mL rhGM-CSF (Miltenyi) and 250UI/mL human IFNα-2b (Introna, MSD France). At day 3, adherent cells were slowly detached by pipetting after 20 minutes of incubation at 4°C and 20.000 cells were seeded in 96 well round bottom plate and were pulsed, or not (control condition), overnight, at 37°C, 5% CO_2, with 1/10 heat inactivated viral lysates, or their respective control (see viral lysates production section). Spinoculation (800g for 2h, Centrifuge 5810R, Eppendorf, Germany) was next performed to ensure synchronized capture of the viral particles by mo-DCs. For activation and maturation, adherent cells were stimulated with LPS (10 ng/mL, Thermofisher) and GM-CSF (1000UI/mL). After 6h, mo-DCs were washed twice to remove LPS from the media and 100 000 PBL/well were seeded onto mature mo-DCs. PBL alone served as negative control, and PBL stimulated with anti-CD3 and anti-CD28 microbeads (1µL/mL, Dynabeads T-Activator, InVitrogen) as a positive control. moDC-PBL co-culture was incubated at 37°C, 5% CO_2 for 48h and supernatants were harvested and stored at -20°C.

Multiplex Cytokine Analysis* or *bead-based multiplex assays. moDC-PBL co-culture supernatants were analyzed using bead-based multiplex kit assays (MACSplex cytokine 12 human, Miltenyi) according to the manufacturer protocol. Briefly, 50uL of supernatant were used with a MACSPLEX Cytokine12 Capture Beads (Miltenyi, France) to measure the concentration of 12 cytokines (GM-CSF, IFN-α, IFN-γ, IL-10, IL-12, IL-17A, IL-2, IL-4, IL-5, IL-6, IL-9, TNF-a). Bead fluorescence was acquired on a CytoFLEX flow cytometer (Beckman Coulter) for samples processed at Gustave Roussy Institute and on a FACSAria Fusion (Becton Dickinson) for samples processed in the biosafety level 3 laboratory at Henri Mondor Hospital. FlowJo (Treestar, Ashland, OR, USA) software was used for analysis.

Peptide-based assay. Lyophilized peptides were dissolved in sterile water and used at 2µg/mL in RPMI 1640 glutamax media (GIBCO) supplemented with 1% penicillin/streptomycin (GIBCO). 185 single peptides were plated in duplicates in 96 well round bottom TPP treated culture plates. Peptide plates were then stored at -80°C until use. The day of the experiment, peptide plates were thawed at room temperature. Frozen PBMCs were thawed, washed and resuspended in RPMI 1640 media (GIBCO). Viability and count were evaluated using a Vi-Cell XR Cell Counter (Beckman Coulter, Brea). PBMCs were then plated in RPMI 1640 glutamax media (GIBCO) supplemented with 1% penicillin/streptomycin (GIBCO), with 200UI/mL rhIL-2 (Miltenyi) and 200UI/mL rhIL-15 (Miltenyi) at a cell density of $10x10^3$ cells and incubated with each peptide at 37°C, 5% CO_2. PBMCs were stimulated with 60 ng/mL OKT-3 antibody (ThermoFisher Scientific, clone OKT3) or with 10µg/mL phytohemagglutinin as positive controls and PBMCs alone served as negative controls. After 6 hours, 20µL of human AB serum was added to each well and plates were incubated at 37°C, 5% CO_2 for 6 additional days. On day 7, supernatants were harvested and frozen at -80°C. Concentration of

IFNγ, IL-9, IL-5 and IL-17A in the culture supernatant was determined using a commercial ELISA kit (ELISA Max Deluxe set human IFN-γ, Biolegend).

Positivity threshold determination for cytokine concentration using multiplex assays and commercial ELISA assays. For multiplex assays (or ELISA), a 4 parameter logistic regression was fitted for each cytokine based on the APC mean fluorescent intensity(or Optical Density) of standard dilution samples using nlpr(v0.1-7). This model was then used to calculate the concentration of each sample of unknown concentration. For multiplex assays, a ratio was computed for each cytokine using the cytokine concentration measured in response to each virus (SARS-CoV-2, HCoV-229E, HCoV-OC43) divided by the median concentration of their respective biological controls (Vero 81, MRC5, HCT8). A positivity threshold was set up based on the ratio for each cytokine. A ratio of above 1.5 minimum was requested to consider the supernatant "positive" for a cytokine. When necessary, a higher threshold was set up as such, median cytokine concentration of the biological controls + 2 times the standard deviation of the biological control concentrations divided by the median concentration. For ELISA assays, a ratio was computed as the concentration of the sample divided by the mean concentration of the negative controls.

COVID IGRA Biomérieux assay utilized for the COVID-SER clinical trial vaccinees [42]. Fresh blood collected in heparanized tubes was stimulated for 22 hours at 37°C under 5% of CO2 with peptide pools targeting RBD (46 peptides) (bioMérieux,France) diluted in IFA solution (bioMérieux, France). The IFA solution was used as a negative control and a mitogen was used as a positive control. The peptides (15-mer) encompassed the whole RBD protein sequence and overlapped by 5-residues. The concentration of IFNγ in the supernatant was measured using the VIDAS automated platform (VIDAS® IFNγ RUO, bioMérieux). The positivity range was 0.08 -8 IU/mL and IFA positivity thresholds were defined at 0.08 IU/mL. The IFNγ response was defined as positive when the IFNγ concentration of the test was above threshold and the negative control was below threshold or when the IFNγ concentration of the test minus IFNγ concentration of the negative control was above threshold. All positive controls were ≥8 IU/mL.

Reagents: culture media, cytokines, ELISA and multiplex assays. ***PBMC isolation.*** Blood samples were collected in heparinized tubes BD Vacutainer® LH 170 U.I., from Dutscher (catalog reference: 367526), diluted in PBS 1X purchased from Eurobio Scientific (catalog reference: CS3PBS01-01) and transferred in Leucosep™ - 50mL purchased from Greiner Bio-One (catalog reference: 227290). Blood was centrifuged using MF48-R Centrifuge from AWEL Industries (catalog reference: 20023001). PBMC were collected in Centrifuge tube 50mL TPP from Dutscher (catalog reference: 91050), washed with PBS 1X, resuspended in CryoStor® CS10 purchased from STEMCELL™ technologies (catalog reference: 5100-0001) and transferred in Cryotube™ vials from ThermoFisher Scientific (catalog reference: 377267). Samples were finally conserved for 24h at -80°C in a cryo-freezing container Mr.Frosty™ from Thermo Fisher Scientific before storage in liquid nitrogen. ***Cross-presentation assay or peripheral blood lymphocyte stimulation with autologous monocyte derived- dendritic cells (DC).*** Frozen PBMCs were thawed, washed and resuspended in RPMI Medium 1640 (1X) purchased from GIBCO (catalog reference: 31870-025). Counting and viability were evaluated

using Vi-CELL™ XR Cell Viability Analyzer from Beckman Coulter (catalog reference: AV13289).To separate adherent and non-adherent cell populations, PBMC were transferred in 6 or 24 well flat bottom Sterile tissue culture testplate TPP purchased from Dutscher (catalog reference: 92006 / 92024) and cultured in complex medium (Complex Medium 1) containing human AB serum (catalog reference: 201021334), purchased from Institut de Biotechnologies Jacques Boy France), RPMI Medium 1640 (1X) (catalog reference: 31870-025), Sodium Pyruvate (catalog reference: 11360-039), Penicillin /Streptomycin (catalog reference: 15140-122), L-Glutamine (200mM) (catalog reference: 25030-024) HEPES Buffer Solution (catalog reference: 15630-056), MEM NEAA (catalog reference: 1140-035), purchased from GIBCO/ThermoFisher Scientific. The Non-adherent fraction was cultured in another complex medium (Complex Medium 2) containing human AB serum, Iscove's Modified Dulbecco's Medium (catalog reference: I3390), from Sigma-Aldrich, Sodium Pyruvate (catalog reference: 11360-039), Penicillin/Streptomycin (catalog reference: 15140-122), L-Glutamine (200mM) (catalog reference: 25030-024) HEPES Buffer Solution (catalog reference: 15630-056), MEM NEAA (catalog reference: 1140-035) from GIBCO/ThermoFisher Scientific and Recombinant Human IL-2 (PHAR000306) from Gustave Roussy Institute pharmacy. The adherent fraction was differentiated into monocyte derived- dendritic cells (mo-DC) in a mo-DC differentiating media constituted with Complex Medium 1 supplemented with Recombinant Human GM-CSF Premium purchased from Miltenyi (catalog reference: 130-093-867) and human IFNα-2b (Introna) purchased from MSD (France) (catalog reference: PHAR008943). For activation and maturation, DCs were stimulated with LPS purchased from Invivogen (catalog reference:) and GM-CSF purchased from Miltenyi Biotec (catalog reference: 130-093-867). PBL and mo-DC were finally co-cultured into 96 well V bottom Sterile Nunc™ plate, VWR purchased from Dutscher (catalog reference: 92097). For positive control, PBL were stimulated with Dynabeads™ Human T-Activator CD3/CD28 purchased from GIBCO / ThermoFisher Scientific (catalog reference: 11131D). All cell cultures were performed at 37°C, 5% CO_2 into Heraus® incubator purchased from Kendro Laboratory Products, ThermoFisher Scientific (catalog reference: BB 6220) And supernatants were transferred into 96 well V bottom Sterile Nunc™ plate, VWR purchased from Dutscher (catalog reference: 734-0491) and frozen. ***Peptide-based assay.*** 96 well V bottom Sterile Nunc™ plate were coated with peptides at 2µg/mL in RPMI Medium 1640 (1X) (catalog reference: 31870-025) supplemented with 1% Penicillin/Streptomycin (catalog reference: 15140-122) and conserved at -80°C. PBMCs were then thawed and plated in plate containing peptides in RPMI Medium 1640 (1X) (catalog reference: 31870-025) supplemented with 1% Penicillin/Streptomycin (catalog reference: 15140-122) supplemented with Recombinant Human IL-15 Premium grade from Miltenyi biotec (catalog reference: 130-095-765) and Recombinant Human IL-2 (PHAR000306) from Gustave Roussy Hospital. For positive, PBMC were stimulated with functional grade CD3, OKT3 purchased from ThermoFisher Scientific (catalog reference: 16-0037-85). Cell cultures were then supplemented with human AB serum (catalog reference: 201021334) purchased from Institut de Biotechnologies Jacques Boy (France) and cultured at 37°C, 5% CO_2. ***Cytokines monitoring.*** Supernatants from cultured cells from Cross-presentation assay were monitored using the MACSPlex Cytokine 12 Kit human purchased from Miltenyi Biotec (catalog reference: 130-099-169). Acquisitions and analyses were performed on CytoFLEX S purchased from Beckman Coulter (catalog reference: B75442)/FACSAria Fusion purchased from

BDbiosciences and FlowJo Software from Treestar respectively. Whereas Supernatants from cultured cells from peptide-based assay were monitored using ELISA tests purchased from BioLegend: ELISA MAX™ Deluxe Set Human IFN-γ (catalog reference: 430104) ELISA MAX™ Deluxe Set Human IL-17 (catalog reference: 433914) and ELISA MAX™ Deluxe Set Human IL-9 (catalog reference: 434705).

Rationale of peptide selection and peptide synthesis (Refers to Table S6). Peptide selection and synthesis: the peptides from the spike and nucleocapsid proteins were selected by dividing the sequences of the SARS-CoV-2 spike protein (RefSeq ID QHD43416.1) and of the nucleocapsin protein (RefSeq ID QHD43423.2) in non-overlapping 15 amino acid segments. The peptides from the membrane protein were selecting by dividing the sequence of 2 potential immunogenic regions of the SARS-CoV-2 (RefSeq QHD43422.1) membrane protein in overlapping 15 amino acid segments. The peptides from the ORF8 and ORF10 proteins were selected by dividing the sequences of the SARS-CoV-2 ORF8 protein (RefSeq ID QHD43422.1) and of the ORF10 protein (RefSeq ID QHI42199.1) in overlapping 15 amino acid segments. The peptides from ORF3 and some for ORF8 were selected based on a previous study [81]. The SARS-CoV-1peptides were peptides found to be immunogenic in previous reported studies. The peptides were synthesized by peptides&elephants GmbH (Berlin, Germany). The peptide pools for the controls for Influenza, EBV and CMV were acquired from peptides&elephants GmbH (Berlin, Germany) order numbers LB01774, LB01361 and LB01232 respectively.

Statistical analysis. All calculations, statistical tests, and data visualization were performed using R v4.0.3. All analyses were performed on independent samples, excepting when the presence of replicates is mentioned. The associations between continuous variables were evaluated using Spearman correlation. Group comparisons were performed using non-parametric test with the wilcox.test R function: the Wilcoxon-Mann-Whitney test for independent samples, and the Wilcoxon signed rank test for paired samples. The comparison of categorical data was performed using the Fisher exact test with the fisher.test R function. Hierarchical clustering was performed with the package hclust, using the euclidean distance. Linear and logistic regressions were performed with respectively the lm and the glm R base functions. A peptide set enrichment analysis was performed with the R package fgsea (version 1.14.0), using as statistic the t-value of the coefficient of univariable linear regressions of the logarithm-normalized IL-2 secretion on the different peptides. All hypothesis tests (including those of regression coefficients) were two-sided and considered as statistically significant when $p<0.05$. Graphical illustrations were drawn using the standard R packages dedicated to the data visualization (ggplot2, ggpubr, corrplot, complexheatmap, circlize, and Hmisc).

Acknowledgments: We thank the ET-EXTRA team (Biological Resource Center (NF 96-600) and the microbiology team for technical help. We thank the staff from health and safety of Gustave Roussy Cancer Campus for helping to set up the translational research studies. We are thankful to the Genalyte for their supportive help. We are thankful to Jeanne Magnan and Alexandre Trubert for their supportive help. Lyon COVID Study GROUP and authors thank the Hospices Civils de Lyon and by Fondation des Hospices Civils de Lyon and all the personnel of the occupational health and medicine department of Hospices Civils de Lyon who contributed to the samples collection.

Contributions: L.D., L.Z., A.M. and F.B. conceived and designed the clinical trial. L.Z. conceived and designed the translational research, interpreted the data and formulated figure design. A.G., F-X.D., S.T., C.M., L.A., B.B., A.St., B.G., M.Mer., F.S., A.M., L.D. included patients in the clinical trial. J-E.F, I.L., A.C., M.Maz., C.T., Y.H., M.Pi., M.G., B.K., G.F., A.D., C.F., A.T. and J.M. carried out all the experiments. J-E.F., and D.D. performed all the statistical analyses. L.D., A.G. C.A-C-S. and G.M collected the clinical data. Sophie Assan provided the information from the HCL series with the contribution of BioMérieux. C.M , B.L.S., S.G. and S.C. analyzed and provided the clinical data from the IHU. E.C. and F.G. performed the RT-qPCR. A-G.G., C. A-C-S., M.Maz. and LD collected the biological data (ALC and Ct values). C.P. collected the samples. M.Maz., Y.H., E.P., C.F., G.F., C.T., A-G.G., B.K., A.T., and P.L. prepared the biological samples and provided some help for the experiments. B.L.S performed the viral cultures and provided viral lysates. A-A.B. helped with experiments performed in a BSL-3 confined environment. M.Mi. and G.G. performed the dosages of antibodies. E.d.S, MM and J.R.L designed the epitopes and prepared the peptides. All the authors advised for the interpretation of the data. L.Z. wrote the manuscript, with all authors contributing to writing and providing feedback.

Funding: L.D. has received support by the Philanthropia Fondation Gustave Roussy. The Gustave Roussy sponsored clinical study on COVID-19 (ONCOVID; NCT NCT04341207 has been supported by the Fondation Gustave Roussy, the Dassault family, Malakoff Humanis, Agnès b., Izipizi, andRalph Lauren. A-G.G. and I.L. were supported by Fondation pour la Recherche Médicale (FRM). Lyon COVID study GROUP are Biomerieux employees or received grant from Bioméireux to perform experiments. L.Z. and G.K. were supported by RHU Torino Lumière (ANR-16-RHUS-0008), ONCOBIOME H2020 network, the SEERAVE Foundation, the Ligue contre le Cancer (équipe labelisée); Agence Nationale de la Recherche – Projets blancs; ANR under the frame of E-Rare-2, the ERA-Net for Research on Rare Diseases; Association pour la recherche sur le cancer (ARC); Cancéropôle Ile-de-France; FRM; a donation by Elior; the European Research Council (ERC); Fondation Carrefour; High-end Foreign Expert Program in China (GDW20171100085 and GDW20181100051), Institut National du Cancer (INCa); Inserm (HTE); Institut Universitaire de France; LeDucq Foundation; the LabEx Immuno-Oncology; the SIRIC Stratified Oncology Cell DNA Repair and Tumor Immune Elimination (SOCRATE); CARE network (directed by Prof. Mariette, Kremlin Bicêtre AP-HP), and the SIRIC Cancer Research and Personalized Medicine (CARPEM).

G.I. and M.P. were supported by Italian Ministry of Health (grants Ricerca CorrenteLinea 1, 1 'Infezioni Emergenti e Riemergenti', projects COVID-2020-12371675 and COVID-2020-12371817). M.Mi and G.G. were supported by ANR Flash COVID-19 program and ARS-CoV-2 Program of the Faculty of Medicine from Sorbonne University ICOViD programs (PI: G.G.). M.Mer. is a member of the Gates Foundation's innate immunity advisory group and his work is supported by the Champalimaud Foundation through funds from grants UIDB/04443/2020, LISBOA-01-0145-FEDER-022231 and LISBOA-01-0246-FEDER-000007. Over the last 5 years: AM has been a Principal Investigator of Clinical Trials from the following companies: Roche/Genentech, BMS, Merck (MSD), Pfizer, Lytix pharma, Eisai, Astra Zeneca/Medimmune, Tesaro, Chugai, OSE immunotherapeutics, SOTIO, Molecular Partners, IMCheck, Pierre Fabre, Adlai Nortye. A.M. has been a Member of Clinical Trial Steering Committees for NCT02528357 (GSK), NCT03334617 (AZ) and a Member of Data Safety and Monitoring Board: NCT02423863 (Sponsor: Oncovir), NCT03818685 (Sponsor: Centre Léon Bérard). A.M. has been a compensated member of the following Scientific Advisory Boards : Merck Serono, eTheRNA, Lytix pharma, Kyowa Kirin Pharma, Novartis, BMS, Symphogen, Genmab, Amgen, Biothera, Nektar, Tesaro/GSK, Oncosec, Pfizer, Seattle Genetics, Astra Zeneca/Medimmune, Servier, Gritstone, Molecular Partners, Bayer, Partner Therapeutics, Sanofi, Pierre Fabre, RedX pharma, OSE Immunotherapeutics, Medicxi, HiFiBio, IMCheck, MSD, iTeos, Innate Pharma, Shattuck Labs, Medincell, Tessa Therapeutics, Deka Biosciences. A.M. has provided compensated Teaching/Speaker activities for Roche/Genentech, BMS, Merck (MSD), Merck Serono, Astra Zeneca/Medimmune, Amgen, Sanofi, Servier. AM has provided compensated Scientific & Medical Consulting for Roche, Pierre Fabre, Onxeo, EISAI, Bayer, Genticel, Rigontec, Daichii Sankyo, Imaxio, Sanofi/BioNTech, Molecular Partners, Pillar Partners, BPI, Faron, Applied Materials. AM has benefited of Non-Financial Support (travel expenses) from Astra Zeneca, BMS, Merck (MSD), Roche. A.M. is a shareholder of Pegascy SAS, Centessa Pharmaceuticals, HiFiBio, Shattuck Labs. A.M. has received pre-clinical and clinical research grants (Institutional Funding) from Merus, BMS, Boehringer Ingelheim, Transgene, Fondation MSD Avenir, Sanofi and Astra Zeneca. BLS has received founding from the French Government under the "Investments for the Future" programme managed by the National Agency for Research (ANR), Méditerranée-Infection 10-IAHU. E.D. reports grants and personal fees from ROCHE GENENTECH, grants from SERVIER, grants from ASTRAZENECA, grants and personal fees from MERCK SERONO, grants from BMS, grants from MSD, grant and personal fees from Boehringer and was supported by INCa 2018-1-PL BIO-06-1 outside the submitted work. J-P.S was supported by MSD Avenir and has received and personal fees from Roche, MSD, BMS, Lilly, AstraZeneca, Daiichi-Sankyo, Mylan, Novartis, Pfizer, PFO, LeoPharma and Gilead outside the submitted work.

The authors declare the following competing interests: L.Z. and G.K. are cofounders of everImmune, a biotech company devoted to the use of commensal microbes for the treatment of cancers. A.G., A.B.T. and A.M. as part of the Drug Development Department (DITEP) are Principal/sub-Investigator of Clinical Trials for Abbvie, Adaptimmune, Aduro Biotech, Agios Pharmaceuticals, Amgen, Argen-X Bvba, Arno Therapeutics, Astex Pharmaceuticals, Astra Zeneca, Astra Zeneca Ab, Aveo, Bayer Healthcare Ag, Bbb Technologies Bv, Beigene, Bioalliance Pharma, Biontech Ag, Blueprint Medicines, Boehringer Ingelheim, Boston Pharmaceuticals, Bristol Myers Squibb, Bristol-Myers Squibb International Corporation, Ca, Celgene Corporation, Cephalon, Chugai Pharmaceutical Co., Clovis Oncology, Cullinan-Apollo, Daiichi Sankyo, Debiopharm S.A., Eisai, Eisai Limited, Eli Lilly, Exelixis, Forma Tharapeutics, Gamamabs, Genentech, Gilead Sciences, Glaxosmithkline, Glenmark Pharmaceuticals, H3 Biomedicine, Hoffmann La Roche Ag, Incyte Corporation, Innate Pharma, Institut De

Recherche Pierre Fabre, Iris Servier, Janssen Cilag, Janssen Research Foundation, Kura Oncology, Kyowa Kirin Pharm. Dev., Lilly France, Loxo Oncology, Lytix Biopharma As, Medimmune, Menarini Ricerche, Merck Kgaa, Merck Sharp & Dohme Chibret, Merrimack Pharmaceuticals, Merus, Millennium Pharmaceuticals, Molecular Partners Ag, Nanobiotix, Nektar Therapeutics, Nerviano Medical Sciences, Novartis Pharma, Octimet Oncology Nv, Oncoethix, Oncomed, Oncopeptides, Onyx Therapeutics, Orion Pharma, Oryzon Genomics, Ose Pharma, Pfizer, Pharma Mar, Philogen S.P.A., Pierre Fabre Medicament, Plexxikon, Rigontec Gmbh, Roche, Sanofi Aventis, Sierra Oncology, Sotio A.S, Syros Pharmaceuticals, Taiho Pharma, Tesaro, Tioma Therapeutics, Wyeth Pharmaceuticals France, Xencor, Y's Therapeutics, Research Grants from Astrazeneca, BMS, Boehringer Ingelheim, Janssen Cilag, Merck, Novartis, Pfizer, Roche, Sanofi. Non-financial support (drug supplied) from Astrazeneca, Bayer, BMS, Boringher Ingelheim, Johnson & Johnson, Lilly, Medimmune, Merck, NH TherAGuiX, Pfizer, Roche. N.L. reports to be a Speaker at Jazz Pharmaceutical. Lyon COVID study GROUP are Biomerieux employees or received grant from Bioméireux to perform experiments. F.S. reports consulting fees from Pfizer, BMS, MSD, Roche, Pierre Fabre Oncology, Leo Pharma, Bayer, Mylan/Viatris, Mundi Pharma, Vifor Pharma, Biogaran, Helsinn. D.D. reports consulting fees from Chugai and Roche. E.D. reports grants and personal fees from ROCHE GENENTECH, grants from SERVIER, grants from ASTRAZENECA, grants and personal fees from MERCK SERONO, grants from BMS, grants from MSD, grant and personal fees from Boehringer outside the submitted work. F.B. reports personal fees from Astra-Zeneca, Bayer, Bristol-Myers Squibb, Boehringer–Ingelheim, Eli Lilly Oncology, Hoffmann–La Roche Ltd, Novartis, Merck, MSD, Pierre Fabre, Pfizer and Takeda, outside the submitted work. J-C.S. was a full-time employee of AstraZeneca between September 2017 and December 2019. J-C.S. reports consultancy: Relay Therapeutics, Gritstone Oncology and shares: Gritstone, AstraZeneca, Daiichi-Sankyo, outside the submitted work. G.G. is a member of the scientific board of Luxia Scientific and reports consultancy for Pileje and Luxia Scientific, outside the submitted work.

Figure Legends

Figure 1. SARS-CoV-2 TH1/TC1 responses in COVID-19 and unexposed individuals.

A. Graphical representation of the prospective patient cohorts used for the study (refer to Table S1 and Table S2). **B.** First experimental in vitro stimulation assay of peripheral blood lymphocytes (PBL) using cross-presentation of viral lysates by autologous dendritic cells (DC). Twelve plex flow cytometric assay to monitor cytokine release in replicates. **C.** Mean fold changes (Log2, F.C) between SARS-CoV-2-specific cytokine secretions of acute COVID-19 patients or convalescent COVID-19 individuals and controls (also refer to S1C). **D.** Ratios of cytokine secretion between PBL stimulated with DC pulsed with SARS-CoV-2 (or the other CCC lysates) *versus* VeroE6 (or versus CCC respective control cell lines), at the acute or convalescent phases of COVID-19. One typical example is outlined in Figure S1A. Each dot represents the mean of replicate wells for one patient (Controls, n=304; Convalescent COVID-19, n=54; Acute COVID-19, n=24). Asterisks indicate statistically significant differences in comparison to the control group determined using two-sided Wilcoxon-Mann-Whitney test

(*p<0.05, **p<0.01, ***p<0.001, ****p<0.0001). **E.** Spearman correlations between SARS-CoV-2-specific IL-2 (left panel) or IL-5 (right panel) release and anti-NC IgG antibody titers (Controls, n=63; Convalescent, n =16).

Figure 2. Unexposed individuals susceptible to COVID-19 exhibited a SARS-CoV-2 specific TH2 profile during the first surge of the pandemic.

A-B. Upper scheme: Outline of the prospective collection of blood samples used to identify COVID-19 resistant (yellow) *versus* susceptible (red) cancer patients (A, upper panel, Table S1, Table S4) and pie chart indicating the absolute numbers (and %) of patients reported as contact (resistant) or infected (susceptible) or unexposed (green) during one-year follow-up (B). Lower scheme: Outline of the prospective collection of blood samples used for the comparison of T cell responses in the cohort of cancer-free individuals who lived in the same household with family members tested positive for COVID-19 during the 2020 lock down (Table S3). **C.** Number of positive cytokines released by SARS-CoV-2-specific PBL during the cross-presentation assay (Figure 1B) in each group (Unexposed, n=159; Resistant, n=48; Susceptible, n=22). **D-E.** SARS-CoV-2-specific IL-2 (left panel) and IL-5 (right panel) secretion contrasting resistant (yellow) *versus* infected (red) cases. Each dot represents the ratio (D) of the replicate wells in one individual and the box plots indicate medians, 25th and 75th percentiles for each patient subset. The bar plots (E) represent the percentage of positive patients (resist., n=41; suscept., n=19). Fisher exact test to compare the number of cytokine positive patients across groups (*p<0.05). **F.** SARS-CoV-2-specific IL-2/IL-5 ratios (means±SEM) in the different subsets presented in panel A. Refer to Figure S4 for the waterfall plots to visualize variations in the percentages of individuals with IL-2/IL-5 ratios > or < 1 according to subject category. **G**. CCC (OC43 and 229E)-specific IL-2 ratio (left panel) or IL-5 secretion ratio (right panel) contrasting contact (resistant, yellow dots, n=34) *versus* infected (susceptible, red dots, n=11) cases. **H.** Spearman correlations between OC43 *and* SARS-CoV-2-specific IL-2 (left panel) and IL-5 (right panel) secretions in 156 controls. **I.** Anti-spike IgG titers (means±SEM) specific of seasonal betacoronaviruses in contact (resist., yellow dots, n=34) *versus* infected (suscept., red dots, n=11) cases. **J**. Scheme detailing the two groups of cancer-free individuals from the same hospital with opposite clinical phenotypes (multi-exposed individuals (n=12) versus patients re-infected with SARS-CoV-2 (n=17) patients) (J, left panel). Results of the cross-presentation assay against SARS-CoV-2 for IL-10 (J, right panel) and IL-2 (refer to Figure S5B). IL-5 levels at baseline and after TCR cross-linking are depicted in the middle panel. Each dot represents the mean of two replicates for one patient.

All group comparisons were performed using two-sided Wilcoxon-Mann-Whitney test and asterisks indicate statistically significant differences (*p<0.05, **p<0.01, ***p<0.001, ****p<0.0001).

Figure 3. Peptide recognition patterns in all distinct subsets of individuals: repertoire breadth of peptide does not predict resistance to COVID-19.

A. Experimental setting for the 186 peptide-based *in vitro* stimulation assays. **B.** Bicolor map of peptide recognition (positive in salmon, negative in purple, not determined in grey). Patients (n=164) were ordered in columns by unsupervised hierarchical clustering and peptides were ordered on rows according to recognition frequency. The left column details clinical information and the upper line indicates the peptide frequency and the names of the proteins. **C-D.** Percentages of positive peptides in individuals from the pre-COVID19 era (n=23) *versus* contemporary controls (n=100) (C, right panel) and in cancer (n=112) *versus* cancer free contemporary individuals (n=13) (C, left panel) and in uninfected (control, n=123) *versus* convalescent (recovery, n=25) (D, left panel) and resistant individuals (non-infected contact cases (n=45) *versus* susceptible (infected, n=18) individuals (D, right panel). Group comparisons were performed using two-sided Wilcoxon-Mann-Whitney test and asterisks indicate statistically significant differences (*p<0.05, **p<0.01, ***p<0.001, ****p<0.0001).

Figure 4. Receptor Binding Domain (RBD)-directed TH1/TC1 recall responses predict resistance to COVID-19.

A. Linear regression analysis of the relative contribution (t-value corresponding to the regression coefficient) of each peptide to SARS-CoV-2-specific TH1/TC1 responses (measured as IL-2 secretion in responses to whole virus lysate in Fig. 1), as determined in the peptide-specific IFNγ secretion assay in 123 COVID-19 negative individuals. Statistically significant peptides (p<0.05) are annotated with asterisks (A, left panel). Peptides colored in blue reportedly harbor at least one mutation within SARS-CoV-2 variants (Table S7). Peptide set enrichment analysis plot (A, right panel). The contribution of each peptide to the SARS-CoV-2-specific IL-2 secretion was used to rank 164 peptides. The enrichment score of S1-RBD peptides suggested that this peptide set presented lower t-values than randomly expected (p=0.048) (A, right panel). **B-C**. Percentages of patients recognizing at least one S1-RBD peptide in the IFNγ ELISA of the peptide IVS assay across patients' groups described in Figure 2A (B) or convalescent versus re-infected patients (C). **D.** Percentages of patients recognizing at least one S1-RBD peptide in the IFNγ ELISA of the peptide IVS assay in cancer and cancer

free patients from the pre-COVID19 era. **E.** Percentages and absolute numbers of mutations contained in our S1-RBD peptide list reported in the current SARS-CoV-2 variants (refer to Table S7). The difference of the probability of mutation in S1-RBD region and in other regions was evaluated using logistic regression (Odd Ratio=0.21, 95% confidence interval [0.06; 0.68], p=0.01). **F.** IFNγ levels in whole blood samples from a cohort of COVID-19 negative or positive (convalescent) HCW (refer to Table S10) drawn pre- and post- vaccines, that were measured after a 22-hour stimulation with mitogens using a pool of overlapping RBD peptides (BioMérieux assay). Group comparisons were performed using two-sided paired Wilcoxon-Mann-Whitney test and asterisks indicate statistically significant differences (*p<0.05, **p<0.01, ***p<0.001, ****p<0.0001).

References:

1. Chen, Z. & John Wherry, E. T cell responses in patients with COVID-19. *Nat Rev Immunol* **20**, 529–536 (2020).
2. Baden, L. R. *et al*. Efficacy and Safety of the mRNA-1273 SARS-CoV-2 Vaccine. *N Engl J Med* **384**, 403–416 (2021).
3. Polack, F. P. *et al*. Safety and Efficacy of the BNT162b2 mRNA Covid-19 Vaccine. *N Engl J Med* **383**, 2603–2615 (2020).
4. Walsh, E. E. *et al*. Safety and Immunogenicity of Two RNA-Based Covid-19 Vaccine Candidates. *N Engl J Med* **383**, 2439–2450 (2020).
5. Bilich, T. *et al*. T cell and antibody kinetics delineate SARS-CoV-2 peptides mediating long-term immune responses in COVID-19 convalescent individuals. *Sci. Transl. Med.* **13**, eabf7517 (2021).
6. Garcia-Beltran, W. F. *et al*. *Multiple SARS-CoV-2 variants escape neutralization by vaccine-induced humoral immunity*. http://medrxiv.org/lookup/doi/10.1101/2021.02.14.21251704 (2021) doi:10.1101/2021.02.14.21251704.
7. Moore, J. P. Approaches for Optimal Use of Different COVID-19 Vaccines: Issues of Viral Variants and Vaccine Efficacy. *JAMA* **325**, 1251 (2021).
8. Channappanavar, R., Fett, C., Zhao, J., Meyerholz, D. K. & Perlman, S. Virus-Specific Memory CD8 T Cells Provide Substantial Protection from Lethal Severe Acute Respiratory Syndrome Coronavirus Infection. *Journal of Virology* **88**, 11034–11044 (2014).
9. Le Bert, N. *et al*. SARS-CoV-2-specific T cell immunity in cases of COVID-19 and SARS,and uninfected controls. *Nature* **584**, 457–462 (2020). 1.
10. Ng, O.-W. *et al*. Memory T cell responses targeting the SARS coronavirus persist up to 11 years post-infection. *Vaccine* **34**, 2008–2014 (2016).
11. Zhao, J. *et al*. Airway Memory CD4 + T Cells Mediate Protective Immunity against Emerging Respiratory Coronaviruses. *Immunity* **44**, 1379–1391 (2016).
12. Mosmann, T. R. & Coffman, R. L. TH1 and TH2 Cells: Different Patterns of Lymphokine Secretion Lead to Different Functional Properties. *Annu. Rev. Immunol.* **7**, 145–173 (1989).

13. Romagnani, S. Biology of human TH1 and TH2 cells. *J Clin Immunol* **15**, 121–129 (1995).
14. Romagnani, S. & Maggi, E. Th1 versus Th2 responses in AIDS. *Current Opinion in Immunology* **6**, 616–622 (1994).
15. Ruterbusch, M., Pruner, K. B., Shehata, L. & Pepper, M. In Vivo CD4 $^{+}$ T Cell Differentiation and Function: Revisiting the Th1/Th2 Paradigm. *Annu. Rev. Immunol.* **38**, 705–725 (2020).
16. Dan, J. M. *et al*. Immunological memory to SARS-CoV-2 assessed for up to 8 months after infection. *Science* **371**, eabf4063 (2021).
17. Habel, J. R. *et al*. Suboptimal SARS−CoV−2−specific CD8 $^{+}$ T cell response associated with the prominent HLA-A*02:01 phenotype. *Proc Natl Acad Sci USA* **117**, 24384–24391 (2020).
18. Oxford Immunology Network Covid-19 Response T cell Consortium *et al*. Broad and strong memory CD4+ and CD8+ T cells induced by SARS-CoV-2 in UK convalescent individuals following COVID-19. *Nat Immunol* **21**, 1336–1345 (2020).
19. Rodda, L. B. *et al*. Functional SARS-CoV-2-Specific Immune Memory Persists after Mild COVID-19. *Cell* **184**, 169-183.e17 (2021).
20. Sekine, T. *et al*. Robust T Cell Immunity in Convalescent Individuals with Asymptomatic or Mild COVID-19. *Cell* **183**, 158-168.e14 (2020).
21. Bacher, P. *et al*. Low-Avidity CD4+ T Cell Responses to SARS-CoV-2 in Unexposed Individuals and Humans with Severe COVID-19. *Immunity* **53**, 1258-1271.e5 (2020).
22. Lee, J.-S. *et al*. Evidence of Severe Acute Respiratory Syndrome Coronavirus 2 Reinfection After Recovery from Mild Coronavirus Disease 2019. *Clinical Infectious Diseases* ciaa1421 (2020) doi:10.1093/cid/ciaa1421.
23. Braun, J. *et al*. SARS-CoV-2-reactive T cells in healthy donors and patients with COVID-19. *Nature* **587**, 270–274 (2020).
24. Grifoni, A. *et al*. Targets of T Cell Responses to SARS-CoV-2 Coronavirus in Humans with COVID-19 Disease and Unexposed Individuals. *Cell* **181**, 1489-1501.e15 (2020).
25. Dykema, A. G. *et al*. Functional characterization of CD4+ T cell receptors crossreactive for SARS-CoV-2 and endemic coronaviruses. *Journal of Clinical Investigation* **131**, e146922 (2021).
26. Goubet, A.-G. *et al*. *Prolonged SARS-CoV-2 RNA virus shedding and lymphopenia are hallmarks of COVID-19 in cancer patients with poor prognosis*. http://medrxiv.org/lookup/doi/10.1101/2021.04.26.21250357 (2021) doi:10.1101/2021.04.26.21250357.
27. Andre, F. *et al*. Malignant effusions and immunogenic tumour-derived exosomes. *The Lancet* **360**, 295–305 (2002).
28. Besse, B. *et al*. Dendritic cell-derived exosomes as maintenance immunotherapy after first line chemotherapy in NSCLC. *OncoImmunology* **5**, e1071008 (2016).
29. Borg, C. *et al*. Novel mode of action of c-kit tyrosine kinase inhibitors leading to NK cell–dependent antitumor effects. *J. Clin. Invest.* **114**, 379–388 (2004).
30. Wemeau, M. *et al*. Calreticulin exposure on malignant blasts predicts a cellular anticancer immune response in patients with acute myeloid leukemia. *Cell Death Dis* **1**, e104–e104 (2010).
31. Mateus, J. *et al*. Selective and cross-reactive SARS-CoV-2 T cell epitopes in unexposed humans. *Science* **370**, 89–94 (2020).
32. Nelde, A. *et al*. SARS-CoV-2-derived peptides define heterologous and COVID-19-induced T cell recognition. *Nat Immunol* **22**, 74–85 (2021).

33. Le Bert, N. *et al*. Highly functional virus-specific cellular immune response in asymptomatic SARS-CoV-2 infection. *Journal of Experimental Medicine* **218**, e20202617 (2021).
34. Zhao, Y. *et al*. Clonal expansion and activation of tissue-resident memory-like T H 17 cells expressing GM-CSF in the lungs of patients with severe COVID-19. *Sci. Immunol.* **6**, eabf6692 (2021).
35. Fournier, P.-E. *et al*. Emergence and outcomes of the SARS-CoV-2 'Marseille-4' variant. *International Journal of Infectious Diseases* **106**, 228–236 (2021).
36. Cha, E. *et al*. Improved Survival with T Cell Clonotype Stability After Anti-CTLA-4 Treatment in Cancer Patients. *Science Translational Medicine* **6**, 238ra70-238ra70 (2014).
37. Scheper, W. *et al*. Low and variable tumor reactivity of the intratumoral TCR repertoire in human cancers. *Nat Med* **25**, 89–94 (2019).
38. Yager, E. J. *et al*. Age-associated decline in T cell repertoire diversity leads to holes in the repertoire and impaired immunity to influenza virus. *Journal of Experimental Medicine* **205**, 711–723 (2008).
39. Shang, J. *et al*. Structural basis of receptor recognition by SARS-CoV-2. *Nature* **581**, 221–224 (2020).
40. Low, J. S. *et al*. Clonal analysis of immunodominance and cross-reactivity of the CD4 T cell response to SARS-CoV-2. *Science* eabg8985 (2021)
41. Gaebler, C. *et al*. Evolution of antibody immunity to SARS-CoV-2. *Nature* **591**, 639–644 (2021).
42. Mouton, W. *et al*. *A novel whole-blood stimulation assay to detect and quantify memory T-cells in COVID-19 patients*. http://medrxiv.org/lookup/doi/10.1101/2021.03.11.21253202 (2021) doi:10.1101/2021.03.11.21253202.
43. Whitmire, J. K., Asano, M. S., Murali-Krishna, K., Suresh, M. & Ahmed, R. Long-Term CD4 Th1 and Th2 Memory following Acute Lymphocytic Choriomeningitis Virus Infection. *J Virol* **72**, 8281–8288 (1998).
44. Hondowicz, B. D., Kim, K. S., Ruterbusch, M. J., Keitany, G. J. & Pepper, M. IL-2 is required for the generation of viral-specific CD4 + Th1 tissue-resident memory cells and B cells are essential for maintenance in the lung. *Eur. J. Immunol.* **48**, 80–86 (2018).
45. Li, C. K. *et al*. T Cell Responses to Whole SARS Coronavirus in Humans. *J Immunol* **181**, 5490–5500 (2008).
46. Page, C. *et al*. Induction of Alternatively Activated Macrophages Enhances Pathogenesis during Severe Acute Respiratory Syndrome Coronavirus Infection. *Journal of Virology* **86**, 13334–13349 (2012).
47. Yale IMPACT Team *et al*. Longitudinal analyses reveal immunological misfiring in severe COVID-19. *Nature* **584**, 463–469 (2020).
48. Kumamoto, Y. *et al*. CD301b+ Dermal Dendritic Cells Drive T Helper 2 Cell-Mediated Immunity. *Immunity* **39**, 733–743 (2013).
49. Sokol, C. L., Camire, R. B., Jones, M. C. & Luster, A. D. The Chemokine Receptor CCR8 Promotes the Migration of Dendritic Cells into the Lymph Node Parenchyma to Initiate the Allergic Immune Response. *Immunity* **49**, 449-463.e6 (2018).
50. Van Dyken, S. J. *et al*. A tissue checkpoint regulates type 2 immunity. *Nat Immunol* **17**, 1381–1387 (2016).
51. Sánchez-Cerrillo, I. *et al*. COVID-19 severity associates with pulmonary redistribution of CD1c+ DCs and inflammatory transitional and nonclassical monocytes. *Journal of Clinical Investigation* **130**, 6290–6300 (2020).

52. Becattini, S. *et al*. Functional heterogeneity of human memory CD4+ T cell clones primed by pathogens or vaccines. *Science* **347**, 400–406 (2015).
53. Honda, T. *et al*. Tuning of Antigen Sensitivity by T Cell Receptor-Dependent Negative Feedback Controls T Cell Effector Function in Inflamed Tissues. *Immunity* **40**, 235–247 (2014).
54. Shinoda, K. *et al*. Thy1 $^{+}$ IL-7 $^{+}$ lymphatic endothelial cells in iBALT provide a survival niche for memory T-helper cells in allergic airway inflammation. *Proceedings of the National Academy of Sciences* **113**, E2842–E2851 (2016).
55. Yeon, S. *et al*. IL-7 plays a critical role for the homeostasis of allergen-specific memory CD4 T cells in the lung and airways. *Scientific Reports* **7**, (2017).
56. Meckiff, B. J. *et al*. Imbalance of Regulatory and Cytotoxic SARS-CoV-2-Reactive CD4+ T Cells in COVID-19. *Cell* **183**, 1340-1353.e16 (2020).
57. Weiskopf, D. *et al*. Phenotype and kinetics of SARS-CoV-2-specific T cells in COVID-19 patients with acute respiratory distress syndrome. *Science Immunology* **5**, eabd2071 (2020).
58. Bacher, P. *et al*. Human Anti-fungal Th17 Immunity and Pathology Rely on Cross-Reactivity against Candida albicans. *Cell* **176**, 1340-1355.e15 (2019).
59. Greiling, T. M. *et al*. Commensal orthologs of the human autoantigen Ro60 as triggers of autoimmunity in lupus. *Science Translational Medicine* **10**, eaan2306 (2018).
60. Koutsakos, M. *et al*. Human CD8+ T cell cross-reactivity across influenza A, B and C viruses. *Nature Immunology* **20**, 613–625 (2019).
61. Sridhar, S. *et al*. Cellular immune correlates of protection against symptomatic pandemic influenza. *Nature Medicine* **19**, 1305–1312 (2013).
62. Welsh, R. M., Che, J. W., Brehm, M. A. & Selin, L. K. Heterologous immunity between viruses: Heterologous immunity between viruses. *Immunological Reviews* **235**, 244–266 (2010).
63. Woodland, D. L. & Blackman, M. A. Immunity and age: living in the past? *Trends in Immunology* **27**, 303–307 (2006).
64. Tarke, A. *et al*. Comprehensive analysis of T cell immunodominance and immunoprevalence of SARS-CoV-2 epitopes in COVID-19 cases. *Cell Reports Medicine* **2**, 100204 (2021).
65. Tan, A. T. *et al*. Early induction of functional SARS-CoV-2-specific T cells associates with rapid viral clearance and mild disease in COVID-19 patients. *Cell Reports* **34**, 108728 (2021).
66. Hansen, T. H. & Bouvier, M. MHC class I antigen presentation: learning from viral evasion strategies. *Nature Reviews Immunology* **9**, 503–513 (2009).
67. Hachim, A. *et al*. ORF8 and ORF3b antibodies are accurate serological markers of early and late SARS-CoV-2 infection. *Nature Immunology* **21**, 1293–1301 (2020).
68. Young, B. E. *et al*. Effects of a major deletion in the SARS-CoV-2 genome on the severity of infection and the inflammatory response: an observational cohort study. *The Lancet* **396**, 603–611 (2020).
69. Su, Y. C. F. *et al*. Discovery and Genomic Characterization of a 382-Nucleotide Deletion in ORF7b and ORF8 during the Early Evolution of SARS-CoV-2. *mBio* **11**, (2020).
70. Greaney, A. J. *et al*. Complete Mapping of Mutations to the SARS-CoV-2 Spike Receptor-Binding Domain that Escape Antibody Recognition. *Cell Host & Microbe* **29**, 44-57.e9 (2021).
71. Koenig, P.-A. *et al*. Structure-guided multivalent nanobodies block SARS-CoV-2 infection and suppress mutational escape. *Science* **371**, eabe6230 (2021).

72. Agerer, B. *et al*. SARS-CoV-2 mutations in MHC-I-restricted epitopes evade CD8 $^{+}$ T cell responses. *Science Immunology* **6**, eabg6461 (2021).
73. Iwasaki, A. & Omer, S. B. Why and How Vaccines Work. *Cell* **183**, 290–295 (2020).
74. Bolles, M. *et al*. A Double-Inactivated Severe Acute Respiratory Syndrome Coronavirus Vaccine Provides Incomplete Protection in Mice and Induces Increased Eosinophilic Proinflammatory Pulmonary Response upon Challenge. *Journal of Virology* **85**, 12201–12215 (2011).
75. Tseng, C.-T. *et al*. Immunization with SARS Coronavirus Vaccines Leads to Pulmonary Immunopathology on Challenge with the SARS Virus. *PLoS ONE* **7**, e35421 (2012).
76. Jiang, S. *et al*. Roadmap to developing a recombinant coronavirus S protein receptor-binding domain vaccine for severe acute respiratory syndrome. *Expert Review of Vaccines* **11**, 1405–1413 (2012).
77. Martins, K. A., Bavari, S. & Salazar, A. M. Vaccine adjuvant uses of poly-IC and derivatives. *Expert Review of Vaccines* **14**, 447–459 (2015).
78. Jo, W. K., Drosten, C. & Drexler, J. F. The evolutionary dynamics of endemic human coronaviruses. *Virus Evolution* **7**, (2021).
79. Chaput, N. *et al*. Phase I clinical trial combining imatinib mesylate and IL-2: HLA-DR $^{+}$ NK cell levels correlate with disease outcome. *OncoImmunology* **2**, e23080 (2013).
80. Fournier, P.-E. *et al*. Emergence and outcomes of the SARS-CoV-2 'Marseille-4' variant. *International Journal of Infectious Diseases* **106**, 228–236 (2021).
81. Sahin, U. *et al*. BNT162b2 vaccine induces neutralizing antibodies and poly-specific T cells in humans. *Nature* (2021) doi:10.1038/s41586-021-03653-6.
82. Saini, S. K. *et al*. SARS-CoV-2 genome-wide T cell epitope mapping reveals immunodominance and substantial CD8 $^{+}$ T cell activation in COVID-19 patients. *Science Immunology* **6**, eabf7550 (2021).
83. Shomuradova, A. S. *et al*. SARS-CoV-2 Epitopes Are Recognized by a Public and Diverse Repertoire of Human T Cell Receptors. *Immunity* **53**, 1245-1257.e5 (2020).

Supplementary materials

Figure S1. Cross-presentation *in vitro* assay at the acute and convalescent phase of COVID-19.

A. Prototypical example of the result of the assay detailed in Figure 1B and M&M for one COVID-19 negative cancer patient. Each box plot represents the absolute values of cytokine secretion of two replicate wells in the 12 plex flow cytometric assay, in the 48hr supernatants of PBL stimulated with DC pulsed with SARS-CoV-2 versus Vero E6 (negative control) and the other common cold coronaviruses and their respective control cell line (negative controls). Each dot represents each replicate well for each stimulatory condition for one patient. Positive control: PBL stimulated with anti-CD3 and anti-CD28 antibody coated beads. **B.** MHC class I and class II neutralization experiments. Neutralizing anti-HLA-ABC and HLA-DR, DP, DQ antibodies (W6/32 & Tu39) were used to block the specific PBL reactivities in the above assay. **C.** Idem as in Figure 1D showing the other 6 cytokine ratios. **D**. Spearman correlation between SARS-CoV-2-specific IL-2 release and non-activated TFH. Group comparisons were

performed using two-sided Wilcoxon-Mann-Whitney test and the asterisks indicate statistically significant differences (*p<0.05, **p<0.01, ***p<0.001, ****p<0.0001).

Figure S2. Detailed SARS-CoV-2 and CCC-specific cytokine release for convalescent COVID-19 patients compared with unexposed individuals.

A. Non supervised hierarchical clustering of SARS-CoV-2 and CCC- specific cytokine release in all patients. Heatmap of cytokine release for SARS-CoV-2 or CCC in the cross-presentation assay performed at the convalescent phase of COVID-19 (n=54) and in unexposed individuals (n=304), aligning all 12 cytokines and all subject categories. **B.** Polyfunctional T cell responses among subjects from various cohorts. Individuals who exhibited SARS-CoV-2-specific release of one or several cytokines are enumerated in each bar. Each bar indicates a category of patients or subjects as described in Figure 1A. **C.** Percentage and number of patients in each cohort (Pre-COVID19 era (yes (+)/no(-)), Cancer (yes (+)/no(-) and COVID-19 (yes (+)/no(-)) who had a SARS-CoV-2-specific cytokine release (for the 5 statistically significant cytokines at the convalescent phase) compared with VeroE6 (Control, n=304; Convalescent, n=54). Asterisks indicate statistically significant differences of SARS-CoV-2-specific cytokine release proportions between two groups determined using Fisher exact test (*p<0.05).

Figure S3. TH1/TC1 differentiation patterns in susceptible *versus* resistant individuals.

A-B. Unsupervised hierarchical clustering of SARS-CoV-2-specific cytokine release. Heatmap of cytokine release in the cross-presentation assay performed during the first surge of the pandemic in unexposed individuals (n=60), aligning cytokines in the two subject categories, susceptible (persons who got infected during the second or the third surge of the pandemic) *versus* resistant (contact) individuals. Group comparisons were performed using a two-sided Wilcoxon-Mann-Whitney test. **C-D.** Spearman correlation matrices between cytokine levels in susceptible (n=19, C) *versus* resistant (n=41, D) individuals, respectively. The asterisks indicate statistically significant differences (p<0.05). **E**. Dynamic study of the stability of the TH1/TH2 profile in individuals that were followed up at two time points. Ratio of cytokine release at the acute and convalescent phase (left panel) and corresponding IL-2/IL-5 ratio (right panel) in 5 cancer patients. Two-sided Wilcoxon-Mann-Whitney test did not reveal significant difference between both time points.

Figure S4. Waterfall plots indicating the IL-2/IL-5 ratio in all patient or individual groups.

Waterfall plot between IL-2 and IL-5 ratio of cytokine release in the Figure 1B IVS assay in all patients during the first surge of the pandemic depicting cancer (green) versus cancer free (blue) COVID-19+ convalescent patients (A), resistant (orange) versus susceptible (red) (B), locked down (or unknown) subjects (dark green, n=301) and healthy individuals in contact with their COVID-19+ family members (light green) (D). Each bar represents one patient. Proportion of patients exhibiting an IL-2/IL-5 ratio superior or inferior to 1 is indicated in each panel. Clinical conditions are annotated as 0, +, ++, +++ for asymptomatic, mild, moderate, and severe COVID-19 severity, respectively. Refer to Figure 2F where percentages are compared inbetween groups.

Figure S5. Cross-presentation assays using viral variants.

A. Cytokine ratio in the cross-presentation assay detailed in Figure 1B, using the original strain IHUMI846 (early 2020 episode) (CoV-2 in (A)), versus the Danish mink (B.1.160, 20A.EU2, GH) and North African (B1.367, 20C, GH) strains in 25 control individuals. Statistical comparisons were performed using paired two-sided Wilcoxon-Mann-Whitney test and the asterisks indicate statistically significant differences (*p<0.05, **p<0.01, ***p<0.001, ****p<0.0001). **B.** Percentage and number of patients in Fig2J right panel who had a SARS-CoV-2-specific IL-2 release. Of note, only 4 re-infected patients could be tested because DC could not be differentiated into monocytes in the others to allow the cross-presentation assay. **C**. Similar experimental setting as in Figure 1B but loading lysates from various SARS-CoV-2 strains (original one IHUMI846 (early 2020 episode), as well as IHUMI3076 (UK variant, B.1.1.7), IHUMI3147 (South African variant, B.1.351) and IHUMI3191 (Brazilian variant, P.1) strains isolated from human nasopharyngeal swab as previously described [35]. Heatmap of the intensity of the ratios between means of cytokine levels (of experimental replicates) obtained from PBL in coculture with DC+ IHUMI846 *versus* DC+ each variant.

Figure S6. Percentages of patients reacting to each peptide and of peptides recognized by each individual in various groups or cohorts.

Bar plot of the percentage of patients recognizing a given peptide. Blue and green lines represent the frequency of peptide recognition in control versus convalescent individuals respectively. Inset. Bar plot of the percentage of positive peptides in the IFNγ ELISA per patient. The color code indicates patient category (blue for control, green for convalescent COVID-19, purple for re-infected patients).

Figure S7. Peptide recognition mapping in various categories of individuals.

Mean frequencies of IFNγ ELISA positivity in the peptide IVS assay (described in Figure 3A) for each indicated protein of the ORFeome in each subject category, for each individual peptide (each line corresponding to one peptide) in 159 subjects.

Figure S8. Correlation of secretory profiles for each peptide in the IVS assay.

Scatter plot of peptides according to the percentage of patients reacting in IFNγ or IL-9 secretion (n=43, A) IL-17 (n=23, B) or IL-5 (n=64, C). The distance to the diagonal is indicated by a gradient of color.

Figure S9. Logistic regression analyses identifying cohort -specific fingerprints of T cell repertoires.

A. Statistically significant peptide signatures in the peptide-based IVS assay (Figure 3A) using a multivariable logistic regression analysis adjusted for period (pre-COVID-19 era or contemporary patients), COVID-19 history and cancer (refer to Table S2). The left column shows variables, and the x axis indicates the significant peptides (pval<0.05). The magnitude of the log (Odd Ratio) is indicated in the red/blue color code while that of the p-value is represented by the circle size. **B-C.** Percentages of patients recognizing at least one peptide from the pre-COVID-19 (B) or convalescent (C) signature identified in the logistic regression analyses of panel A in the IFNγ ELISA in the peptide IVS assay. Fisher's exact test to compare the number of patients positive for each signature between groups (*p<0.05, **p<0.01).

Supplemental Tables

Table S1. Consort diagram. Flow diagram showing the enrollment of subjects, their allocation to different cohorts and how they are analyzed in the trial.

Table S2. Characteristics of cancer patients and healthy volunteers.

Table S3. Characteristics of family members during the 2020 lock down.

Table S4. Characteristics of contact (resistant) and infected (susceptible) cancer patients and corresponding swimmer plot for the outcome of the susceptible cases.

Individual swimmer plots for each susceptible individual (*i.e.* who got infected during the second or the third surge of the pandemic) depicting patients still alive (blue), patients dead from cancer, and patients dead from COVID-19 (red) after infection indicated with an arrow.

Table S5. Characteristics of multi-exposed cases and re-infected cancer -free individuals.

Table S6. SARS-CoV-1 and CoV-2 orfeome peptide list: sequences and positions.

Table S7. Peptide-specific T cell polarization determined by IL-5 or IFNγ quantification.

Table S8. HLA binding affinities of the S1-RBD peptides using the NetMHCpan algorithm

Table S9. Mutational hotspots in the peptide residues.

Table S10. Characteristics of vaccinated healthcare workers.

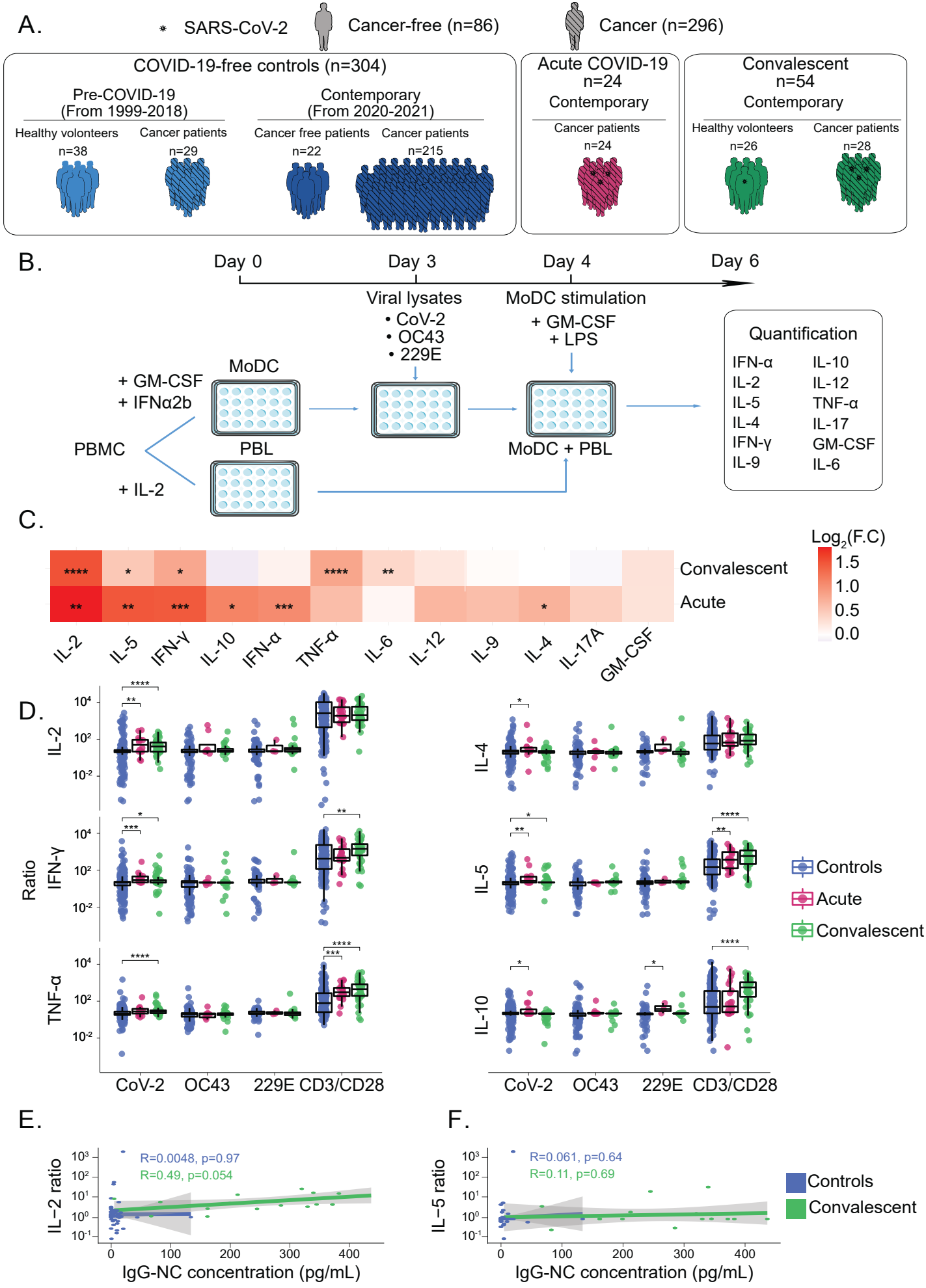
A.
SARS-CoV-2
Cancer-free (n=86)
Cancer (n=296)
COVID-19-free controls (n=304)
Pre-COVID-19 (From 1999-2018)
Healthy volonteers
n=38
Cancer patients
n=29
Contemporary (From 2020-2021)
Cancer free patients
n=22
Cancer patients
n=215
Acute COVID-19 n=24
Contemporary
Cancer patients
n=24
Convalescent n=54
Contemporary
Healthy volonteers
n=26
Cancer patients
n=28
B.
Day 0
Day 3
Day 4
Day 6
Viral lysates
• CoV-2
• OC43
• 229E
MoDC stimulation
+ GM-CSF
+ LPS
+ GM-CSF
+ IFNα2b
MoDC
PBMC
PBL
+ IL-2
MoDC + PBL
Quantification
IFN-α
IL-2
IL-5
IL-4
IFN-γ
IL-9
IL-10
IL-12
TNF-α
IL-17
GM-CSF
IL-6
C.
Log2(F.C)
1.5
1.0
0.5
0.0
Convalescent
Acute
IL-2
IL-5
IFN-γ
IL-10
IFN-α
TNF-α
IL-6
IL-12
IL-9
IL-4
IL-17A
GM-CSF
D.
Ratio
IL-2
IFN-γ
TNF-α
IL-4
IL-5
IL-10
CoV-2
OC43
229E
CD3/CD28
Controls
Acute
Convalescent
E.
IL-2 ratio
R=0.0048, p=0.97
R=0.49, p=0.054
IgG-NC concentration (pg/mL)
F.
IL-5 ratio
R=0.061, p=0.64
R=0.11, p=0.69
IgG-NC concentration (pg/mL)
Controls
Convalescent

Figure 1

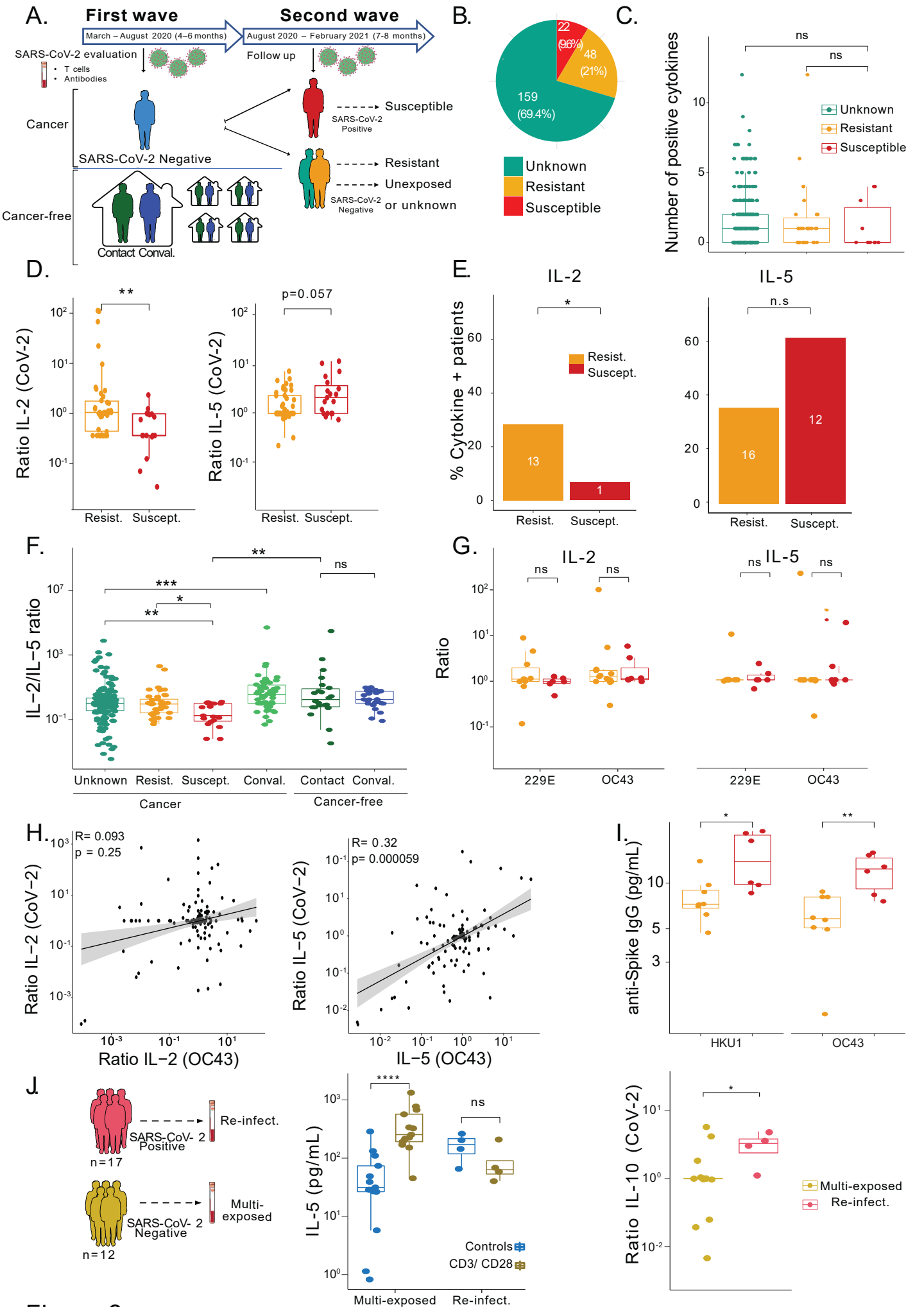
A.
First wave
Second wave
March – August 2020 (4–6 months)
August 2020 – February 2021 (7-8 months)
SARS-CoV-2 evaluation
T cells
Antibodies
Follow up
Cancer
SARS-CoV-2 Negative
Susceptible
SARS-CoV-2 Positive
Resistant
Unexposed
or unknown
SARS-CoV-2 Negative
Cancer-free
Contact
Conval.
B.
22 (96%)
48 (21%)
159 (69.4%)
Unknown
Resistant
Susceptible
C.
Number of positive cytokines
ns
ns
Unknown
Resistant
Susceptible
D.
Ratio IL-2 (CoV-2)
**
Resist.
Suscept.
Ratio IL-5 (CoV-2)
p=0.057
Resist.
Suscept.
E.
IL-2
% Cytokine + patients
*
Resist.
Suscept.
13
1
Resist.
Suscept.
IL-5
n.s
16
12
Resist.
Suscept.
F.
IL−2/IL−5 ratio
**
ns
***
*
**
Unknown
Resist.
Suscept.
Conval.
Contact
Conval.
Cancer
Cancer-free
G.
Ratio
IL-2
ns
ns
IL-5
ns
ns
229E
OC43
229E
OC43
H.
R= 0.093
p = 0.25
Ratio IL−2 (CoV−2)
Ratio IL−2 (OC43)
R= 0.32
p= 0.000059
Ratio IL−5 (CoV−2)
IL−5 (OC43)
I.
anti-Spike IgG (pg/mL)
*
**
HKU1
OC43
J.
SARS-CoV- 2 Positive
Re-infect.
n=17
SARS-CoV- 2 Negative
Multi-exposed
n=12
IL-5 (pg/mL)
****
ns
Controls
CD3/ CD28
Multi-exposed
Re-infect.
Ratio IL-10 (CoV-2)
*
Multi-exposed
Re-infect.

Figure 2

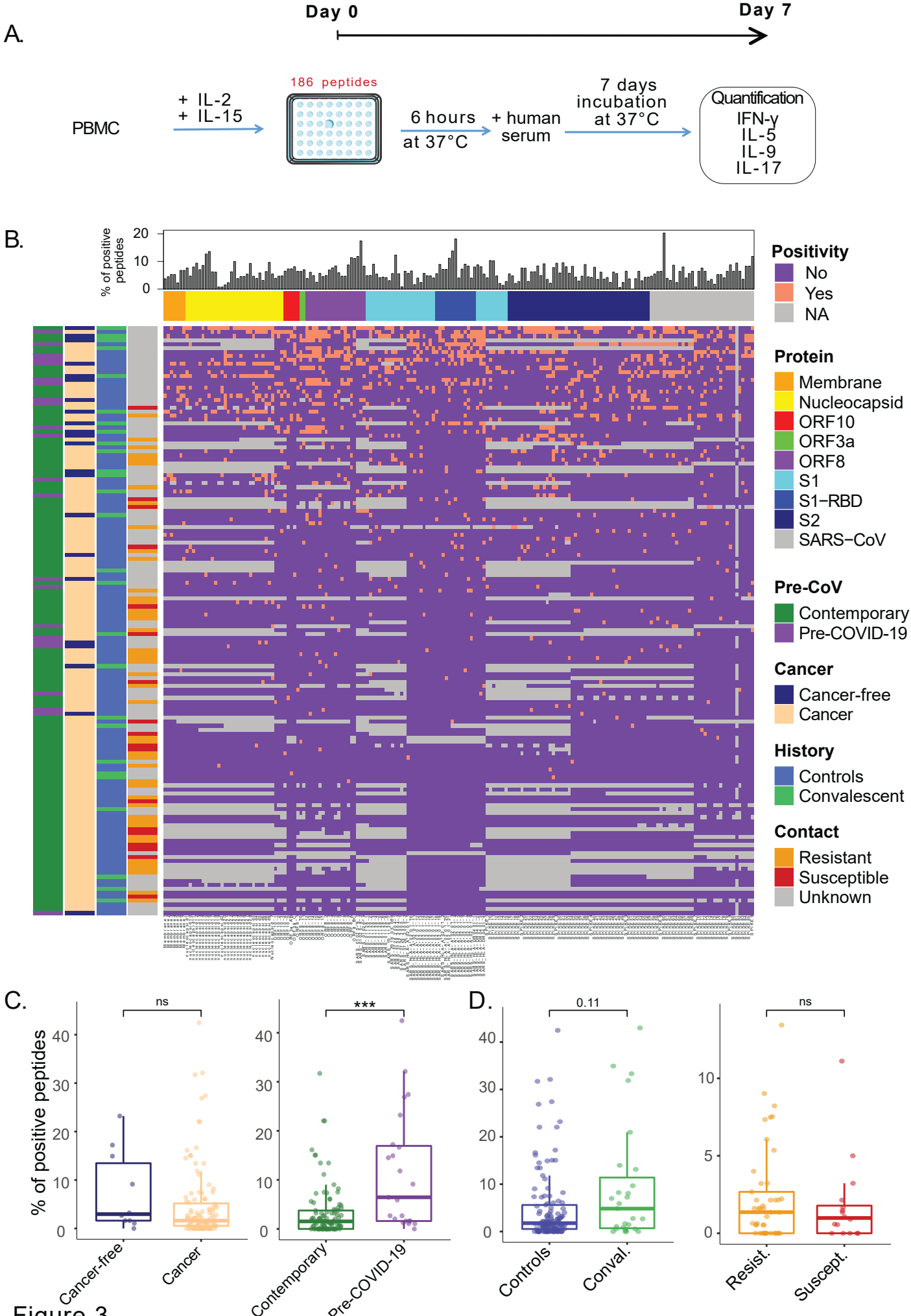
A.
Day 0
Day 7
PBMC
+ IL-2
+ IL-15
186 peptides
6 hours
at 37°C
+ human
serum
7 days
incubation
at 37°C
Quantification
IFN-γ
IL-5
IL-9
IL-17
B.
% of positive
peptides
20
10
0
Positivity
No
Yes
NA
Protein
Membrane
Nucleocapsid
ORF10
ORF3a
ORF8
S1
S1−RBD
S2
SARS−CoV
Pre-CoV
Contemporary
Pre-COVID-19
Cancer
Cancer-free
Cancer
History
Controls
Convalescent
Contact
Resistant
Susceptible
Unknown
C.
% of positive peptides
ns
***
Cancer-free
Cancer
Contemporary
Pre-COVID-19
D.
0.11
ns
Controls
Conval.
Resist.
Suscept.

Figure 3

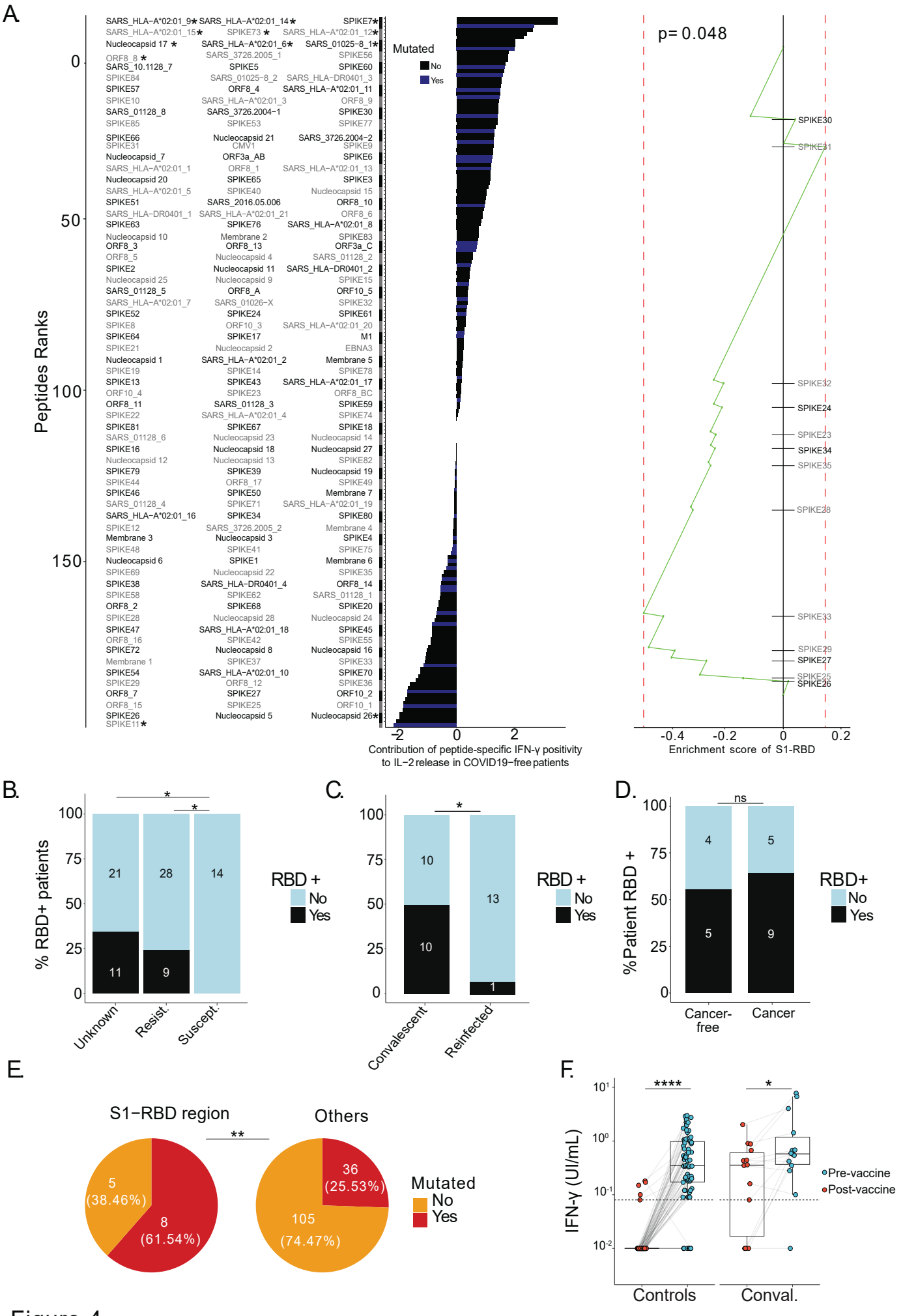
A.
Peptides Ranks
Mutated
No
Yes
Contribution of peptide-specific IFN-γ positivity to IL-2 release in COVID19-free patients
p= 0.048
Enrichment score of S1-RBD
B.
% RBD+ patients
RBD +
No
Yes
Unknown
Resist.
Suscept.
C.
Convalescent
Reinfected
D.
%Patient RBD +
ns
Cancer-free
Cancer
E.
S1-RBD region
Others
5 (38.46%)
8 (61.54%)
36 (25.53%)
105 (74.47%)
F.
IFN-γ (UI/mL)
Pre-vaccine
Post-vaccine
Controls
Conval.

Figure 4

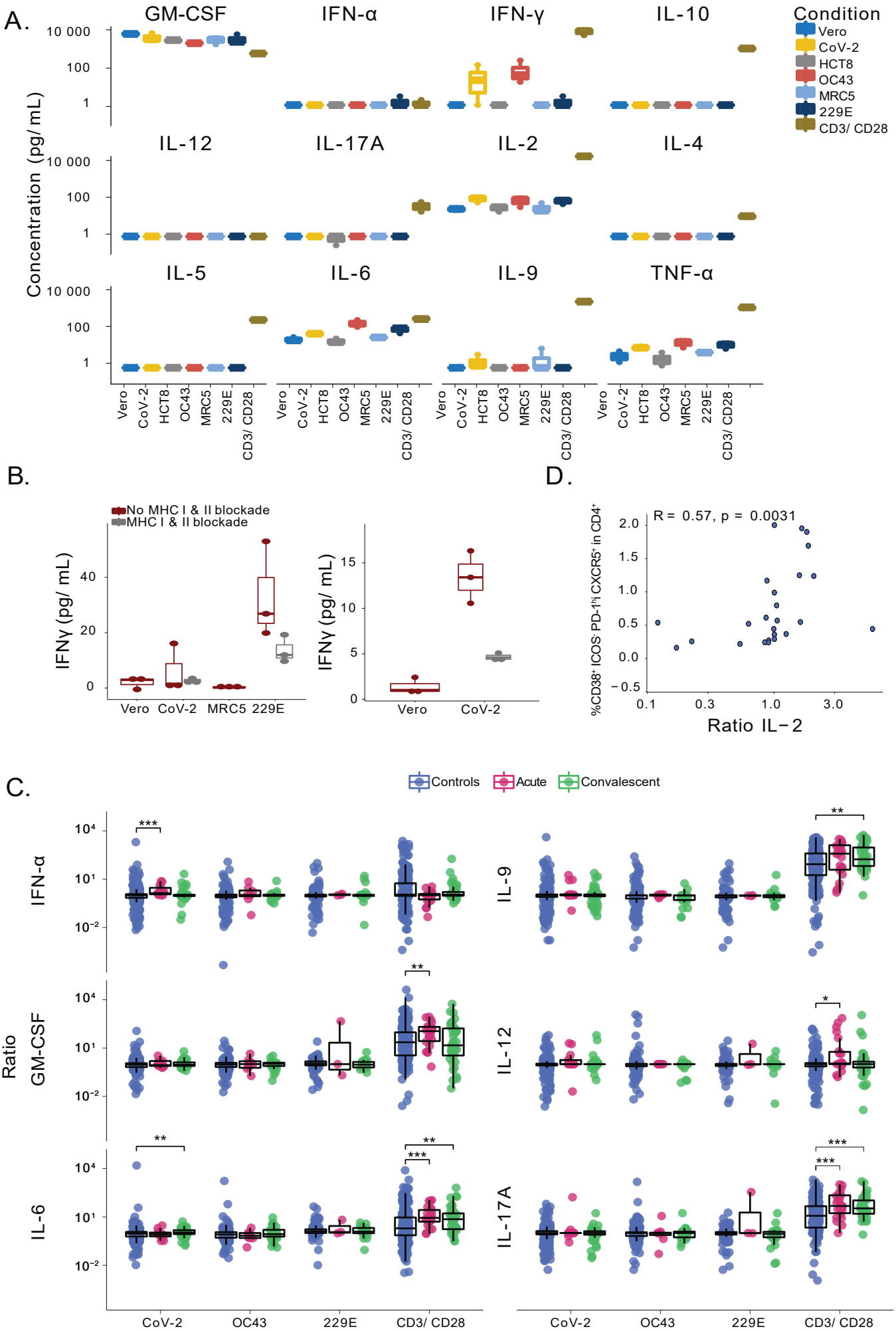
A.
GM-CSF
IFN-α
IFN-γ
IL-10
IL-12
IL-17A
IL-2
IL-4
IL-5
IL-6
IL-9
TNF-α
Concentration (pg/mL)
10 000
100
1
Vero
CoV-2
HCT8
OC43
MRC5
229E
CD3/ CD28
Condition
B.
No MHC I & II blockade
MHC I & II blockade
IFNγ (pg/ mL)
D.
R = 0.57, p = 0.0031
%CD38+ ICOS- PD-1hi CXCR5+ in CD4+
Ratio IL-2
C.
Controls
Acute
Convalescent
Ratio
IFN-α
GM-CSF
IL-6
IL-9
IL-12
IL-17A

Figure S1

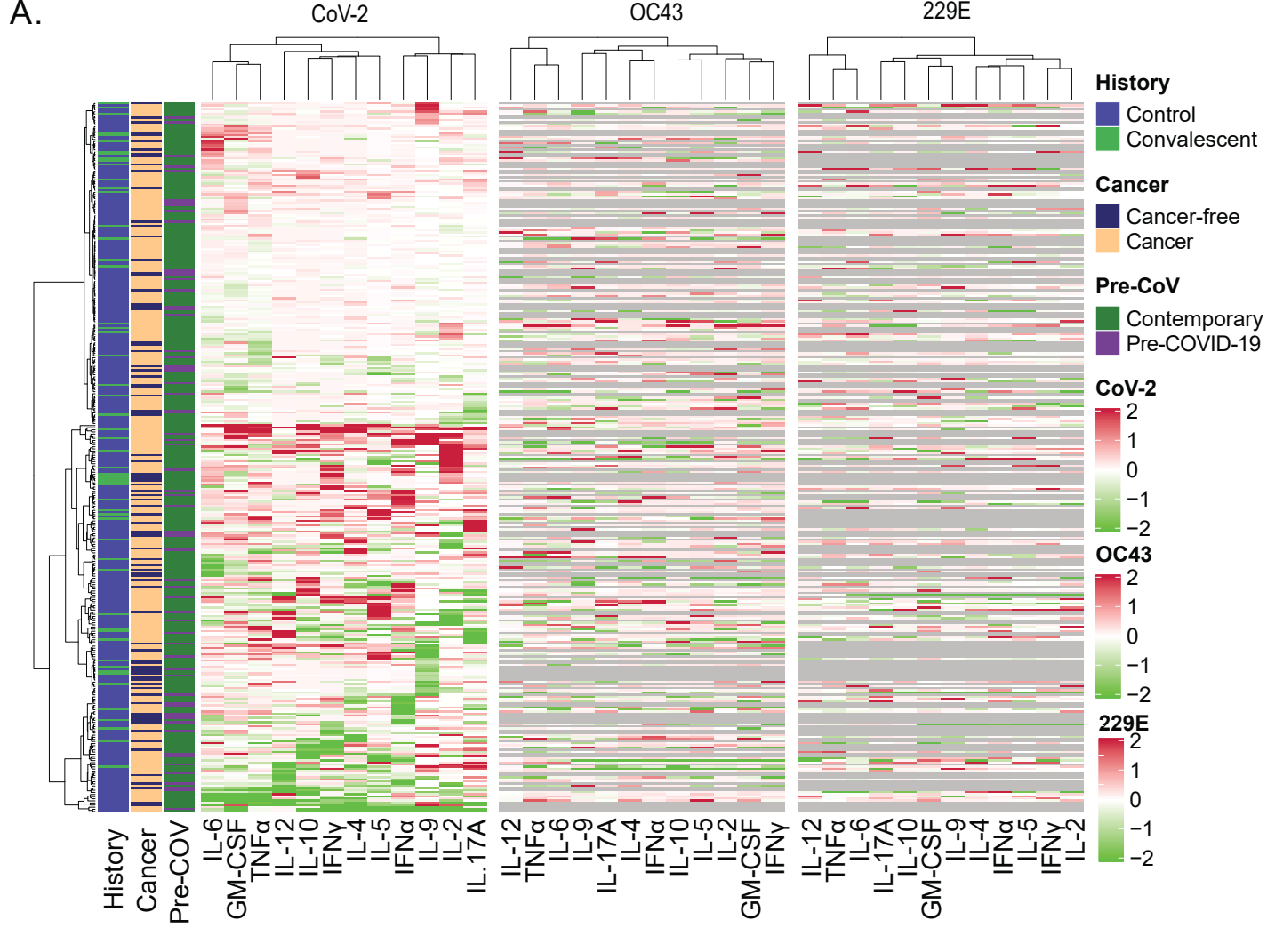
A.
CoV-2
OC43
229E
History
Control
Convalescent
Cancer
Cancer-free
Cancer
Pre-CoV
Contemporary
Pre-COVID-19
CoV-2
OC43
229E
History
Cancer
Pre-COV
IL-6
GM-CSF
TNFα
IL-12
IL-10
IFNγ
IL-4
IL-5
IFNα
IL-9
IL-2
IL.17A
IL-12
TNFα
IL-6
IL-9
IL-17A
IL-4
IFNα
IL-10
IL-5
IL-2
GM-CSF
IFNγ
IL-12
TNFα
IL-6
IL-17A
IL-10
GM-CSF
IL-9
IL-4
IFNα
IL-5
IFNγ
IL-2

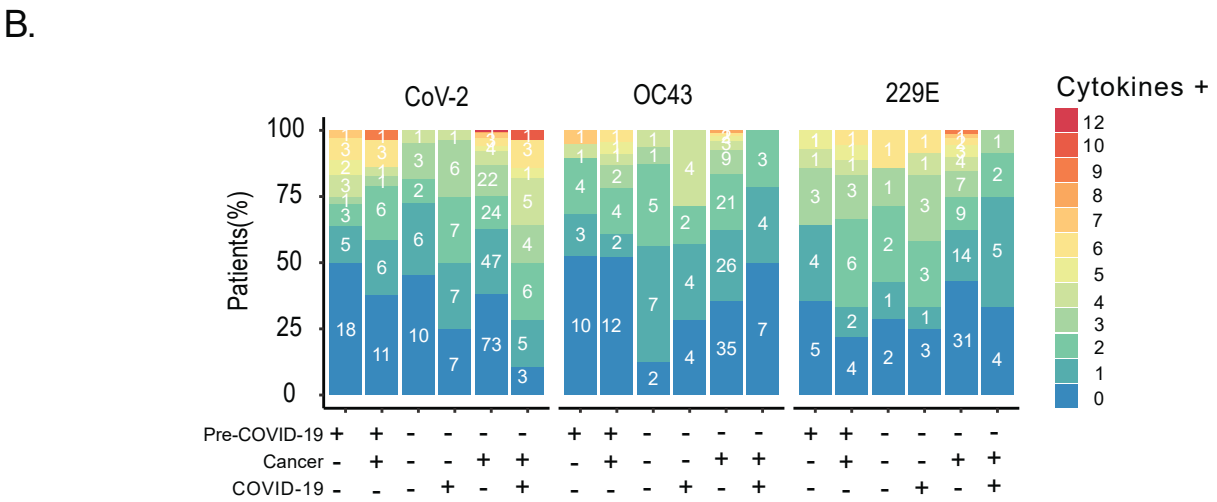
B.
CoV-2
OC43
229E
Cytokines +
Patients(%)
Pre-COVID-19
Cancer
COVID-19

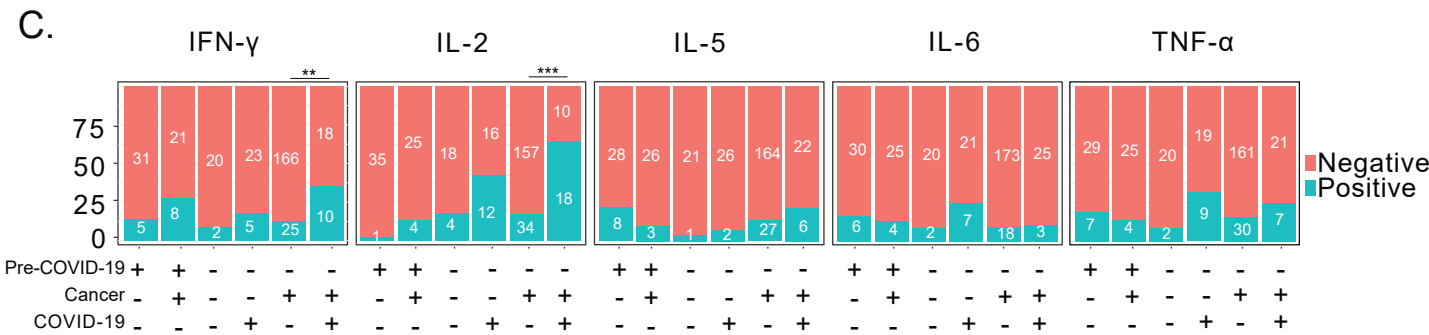
C.
IFN-γ
IL-2
IL-5
IL-6
TNF-α
Negative
Positive
Pre-COVID-19
Cancer
COVID-19

Figure S2

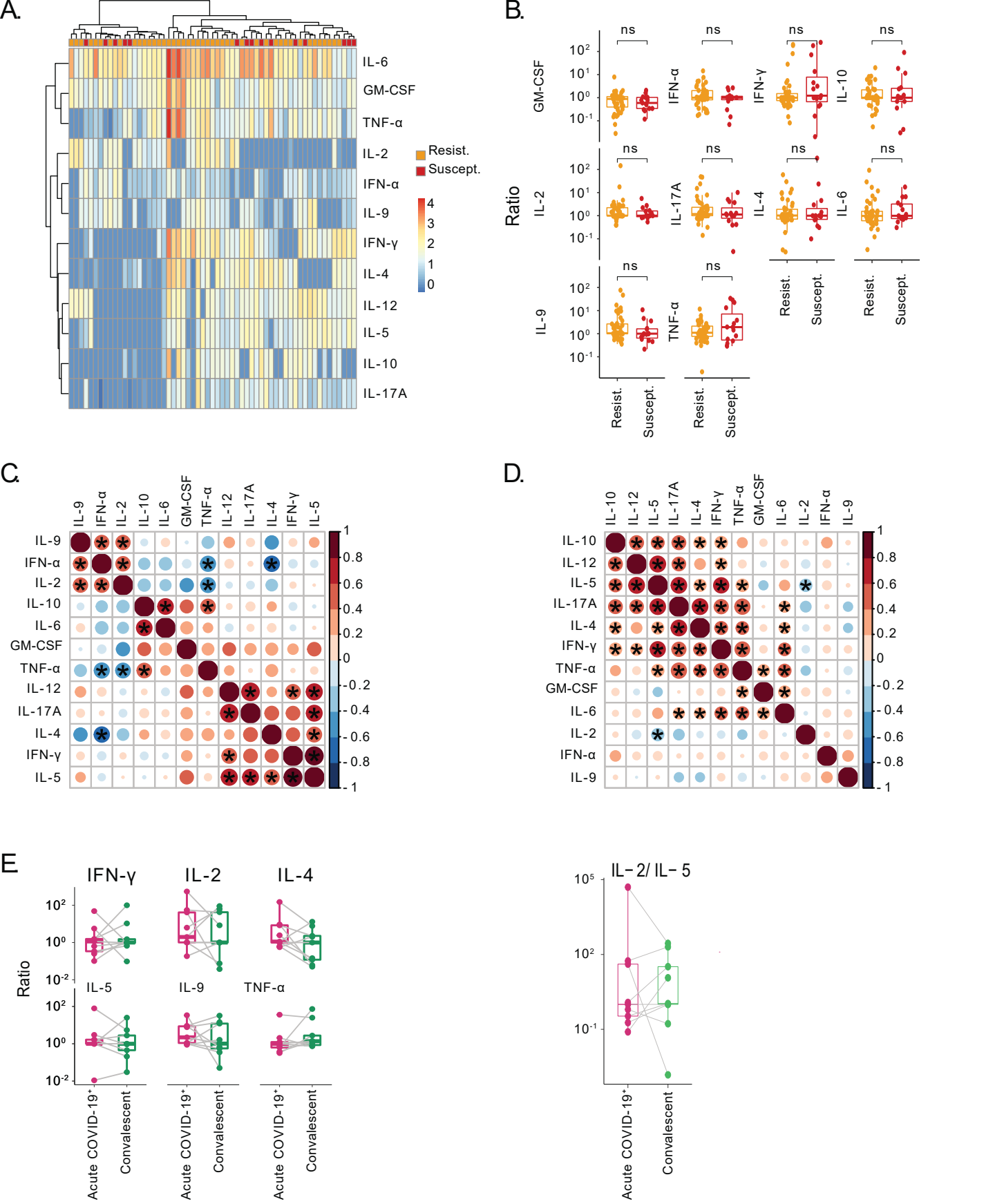
A.
IL-6
GM-CSF
TNF-α
IL-2
IFN-α
IL-9
IFN-γ
IL-4
IL-12
IL-5
IL-10
IL-17A
Resist.
Suscept.
4
3
2
1
0
B.
Ratio
GM-CSF
IFN-α
IFN-γ
IL-10
IL-2
IL-17A
IL-4
IL-6
IL-9
TNF-α
ns
Resist.
Suscept.
C.
IL-9
IFN-α
IL-2
IL-10
IL-6
GM-CSF
TNF-α
IL-12
IL-17A
IL-4
IFN-γ
IL-5
1
0.8
0.6
0.4
0.2
0
-0.2
-0.4
-0.6
-0.8
-1
D.
IL-10
IL-12
IL-5
IL-17A
IL-4
IFN-γ
TNF-α
GM-CSF
IL-6
IL-2
IFN-α
IL-9
E.
IFN-γ
IL-2
IL-4
IL-5
IL-9
TNF-α
Ratio
Acute COVID-19+
Convalescent
IL-2/ IL-5

Figure S3

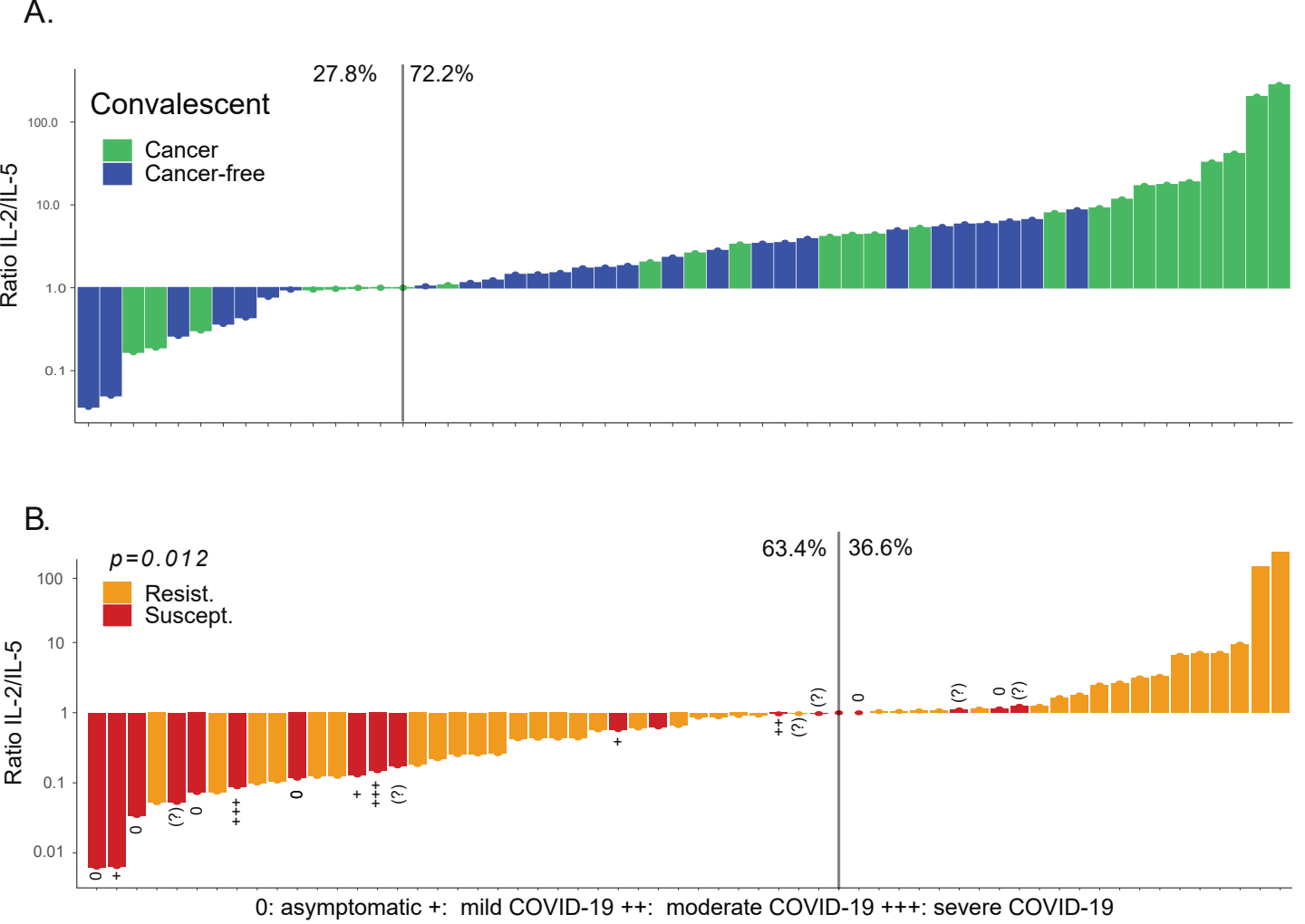
A.
27.8%
72.2%
Convalescent
Cancer
Cancer-free
Ratio IL-2/IL-5
100.0
10.0
1.0
0.1

B.
p=0.012
Resist.
Suscept.
63.4%
36.6%
Ratio IL-2/IL-5
100
10
1
0.1
0.01
0: asymptomatic +: mild COVID-19 ++: moderate COVID-19 +++: severe COVID-19

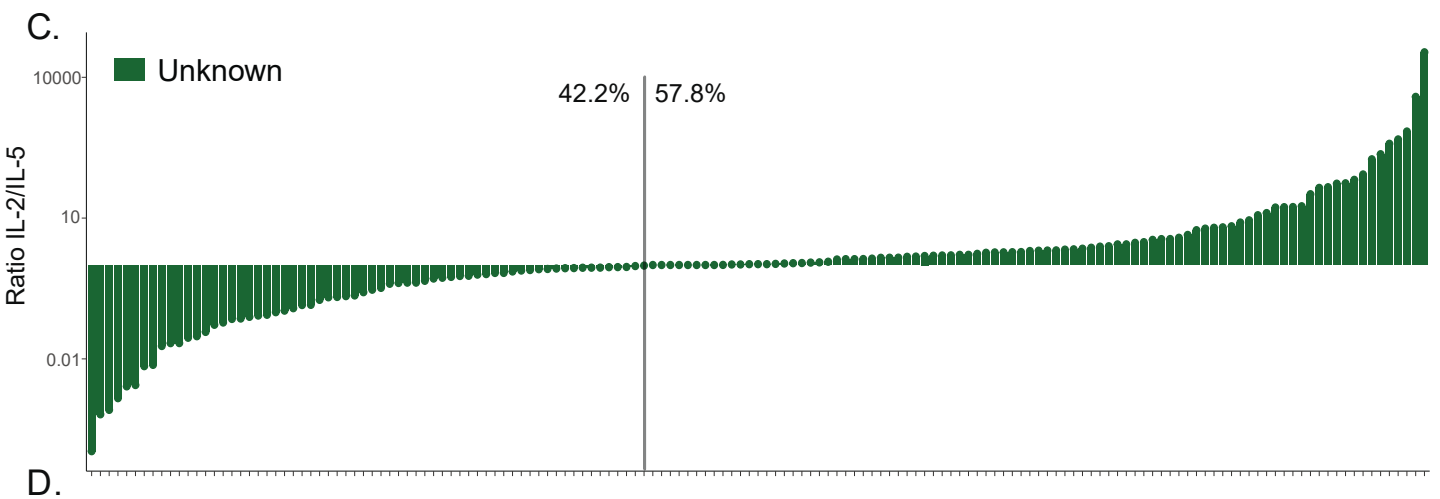
C.
Unknown
42.2%
57.8%
Ratio IL-2/IL-5
10000
10
0.01

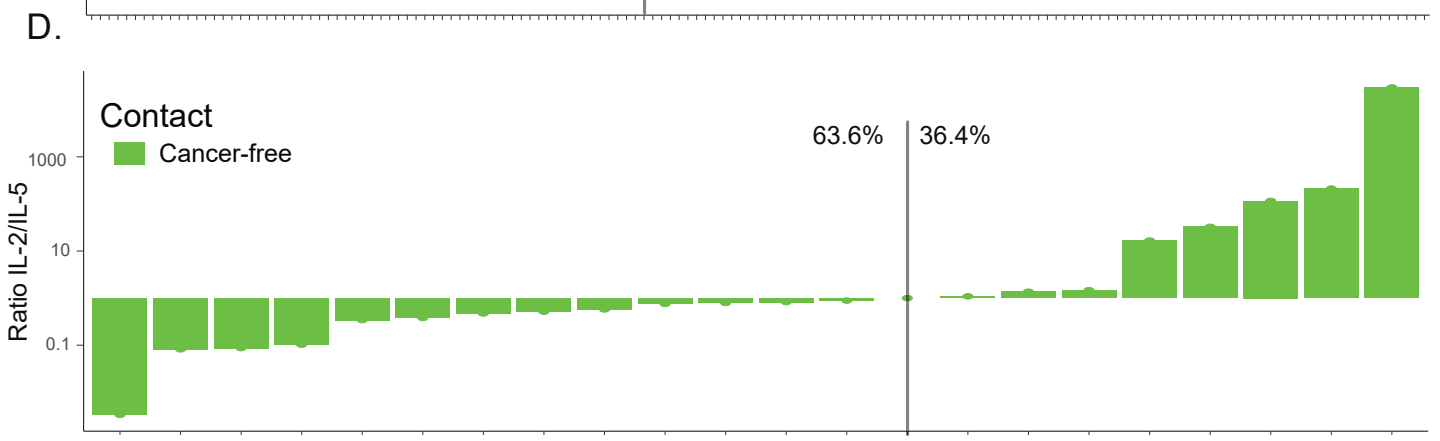
D.
Contact
Cancer-free
63.6%
36.4%
Ratio IL-2/IL-5
1000
10
0.1

Figure S4

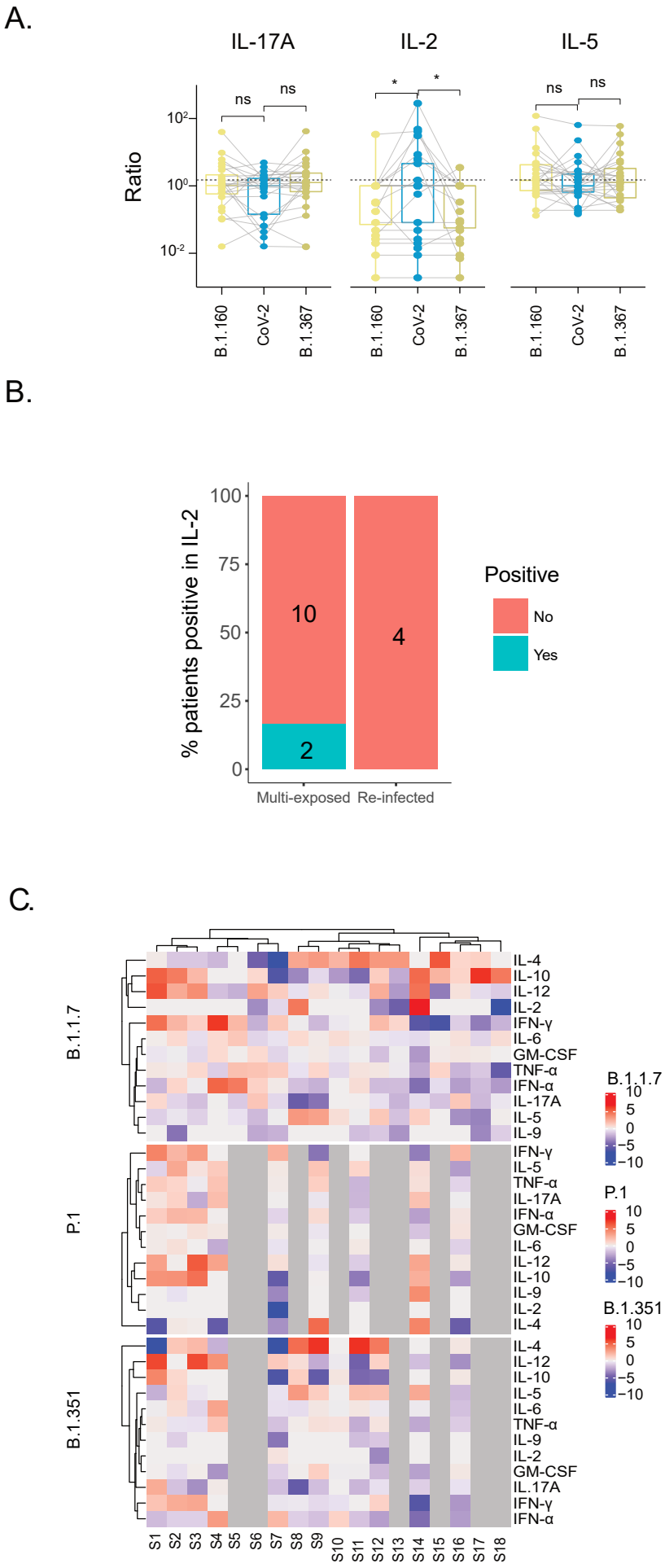
A.
IL-17A
IL-2
IL-5
Ratio
ns
*
B.1.160
CoV-2
B.1.367
B.
% patients positive in IL-2
Positive
No
Yes
10
4
2
Multi-exposed
Re-infected
C.
B.1.1.7
P.1
B.1.351
IL-4
IL-10
IL-12
IL-2
IFN-γ
IL-6
GM-CSF
TNF-α
IFN-α
IL-17A
IL-5
IL-9
IL.17A
S1
S2
S3
S4
S5
S6
S7
S8
S9
S10
S11
S12
S13
S14
S15
S16
S17
S18

Figure S5

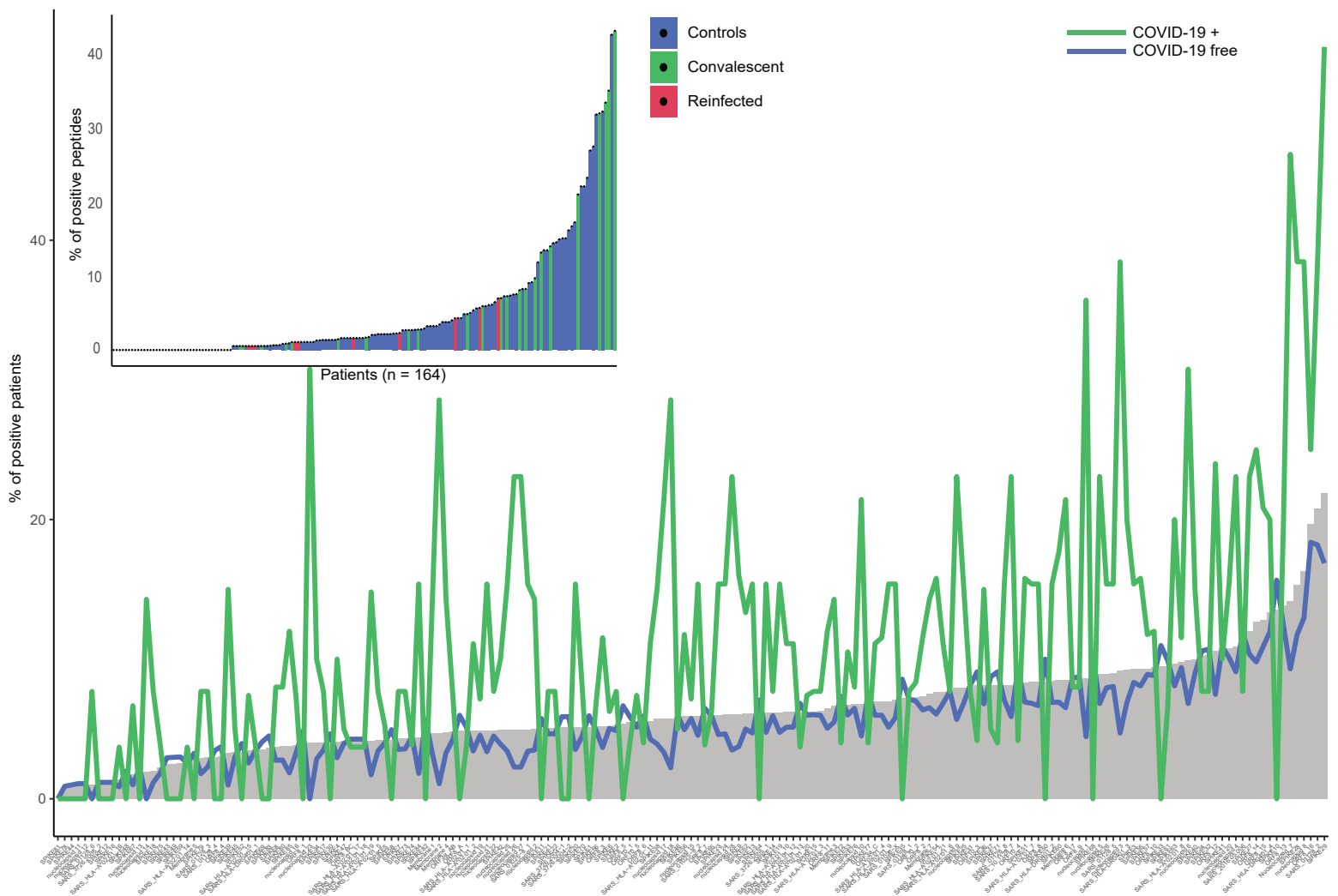
Controls
Convalescent
Reinfected
COVID-19 +
COVID-19 free
% of positive peptides
Patients (n = 164)
% of positive patients

Figure S6

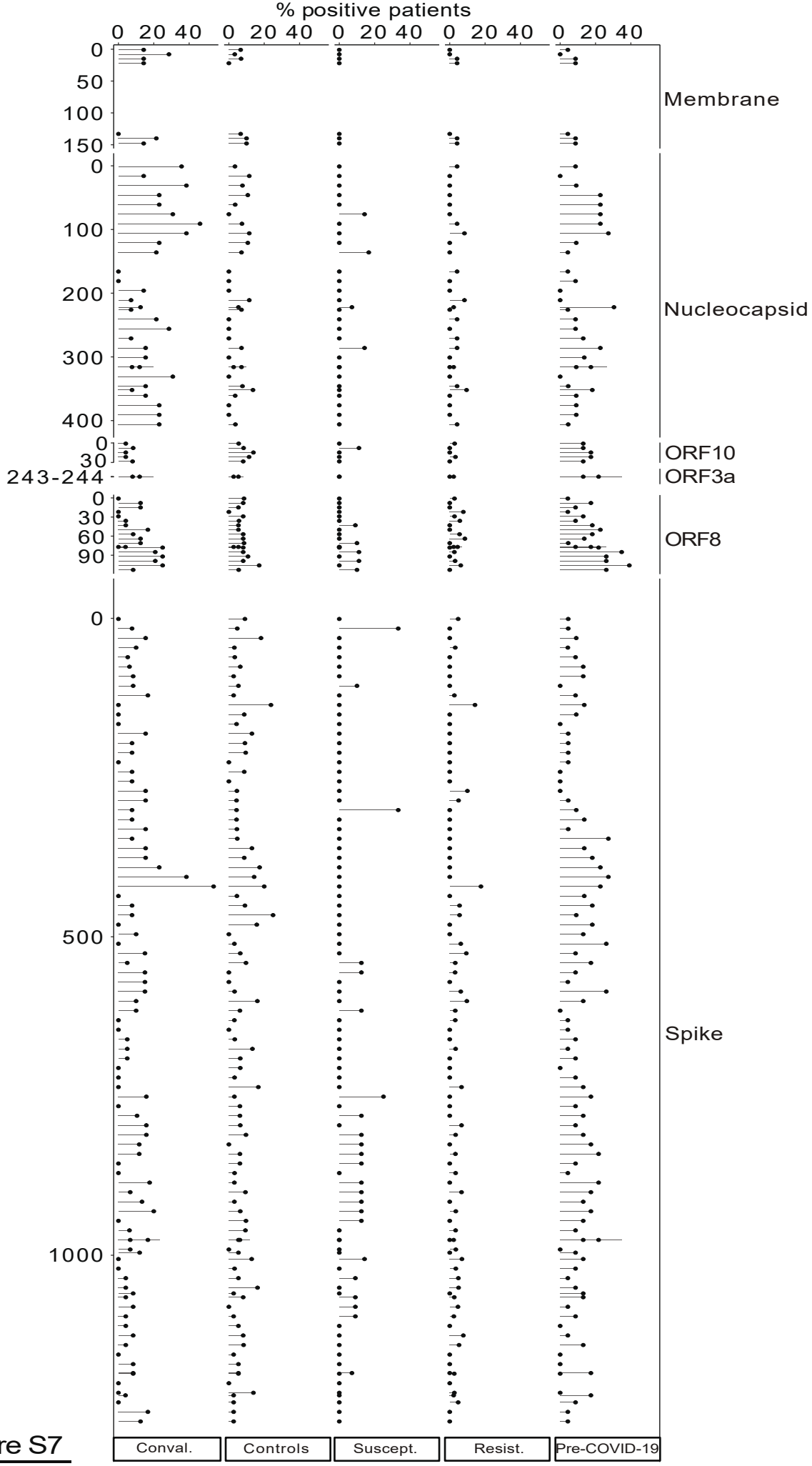
% positive patients
0 20 40
0 20 40
0 20 40
0 20 40
0 20 40
0
50
100
150
Membrane
0
100
200
300
400
Nucleocapsid
0
30
ORF10
243-244
ORF3a
0
30
60
90
ORF8
0
500
1000
Spike
Conval.
Controls
Suscept.
Resist.
Pre-COVID-19

Figure S7

A.

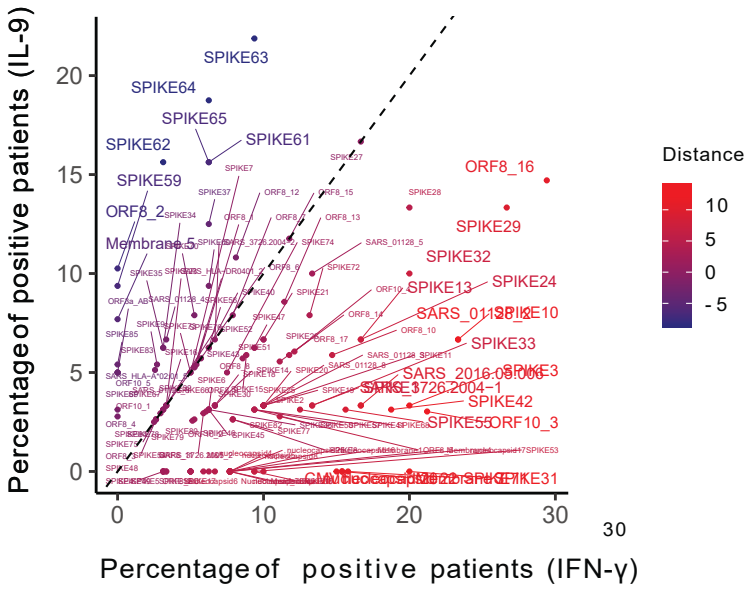

B.

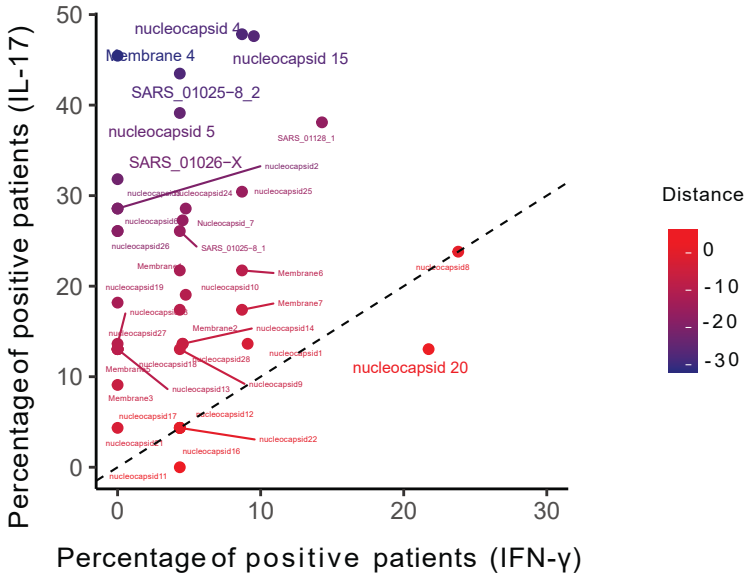

C.

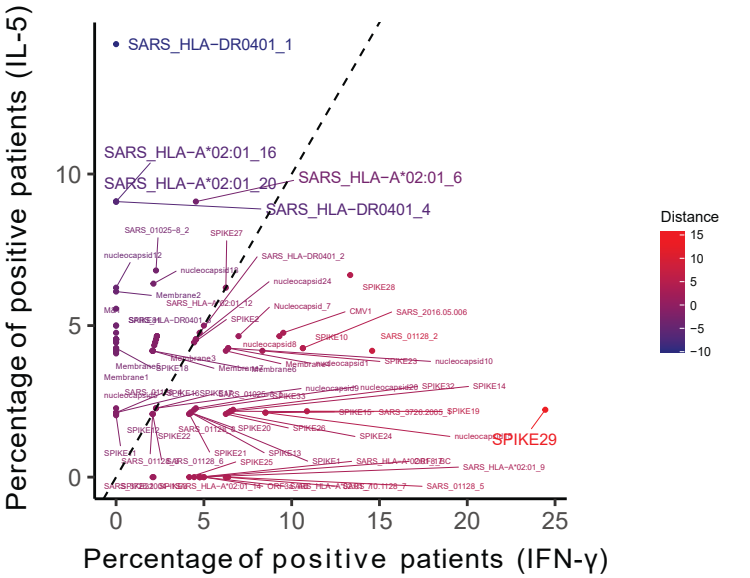

Figure S8

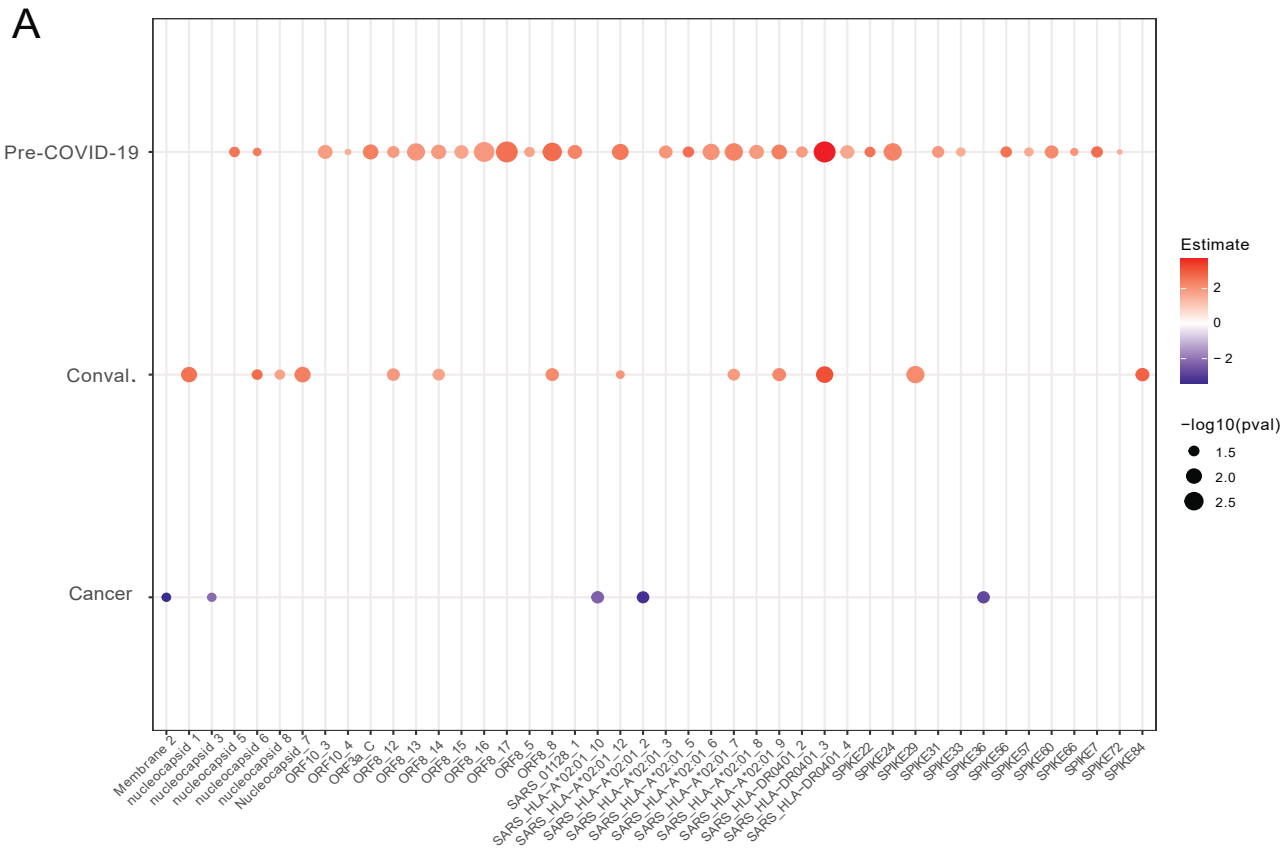
A
Pre-COVID-19
Conval.
Cancer
Estimate
2
0
−2
−log10(pval)
1.5
2.0
2.5
Membrane_2
nucleocapsid_1
nucleocapsid_3
nucleocapsid_5
nucleocapsid_6
Nucleocapsid_8
nucleocapsid_7
ORF10_3
ORF10_4
ORF3a_C
ORF8_12
ORF8_13
ORF8_14
ORF8_15
ORF8_16
ORF8_17
ORF8_5
ORF8_8
SARS_01128_1
SARS_HLA-A*02:01_10
SARS_HLA-A*02:01_12
SARS_HLA-A*02:01_2
SARS_HLA-A*02:01_3
SARS_HLA-A*02:01_5
SARS_HLA-A*02:01_6
SARS_HLA-A*02:01_7
SARS_HLA-A*02:01_8
SARS_HLA-A*02:01_9
SARS_HLA-DR0401_2
SARS_HLA-DR0401_3
SARS_HLA-DR0401_4
SPIKE22
SPIKE24
SPIKE29
SPIKE31
SPIKE33
SPIKE36
SPIKE56
SPIKE57
SPIKE60
SPIKE66
SPIKE7
SPIKE72
SPIKE84

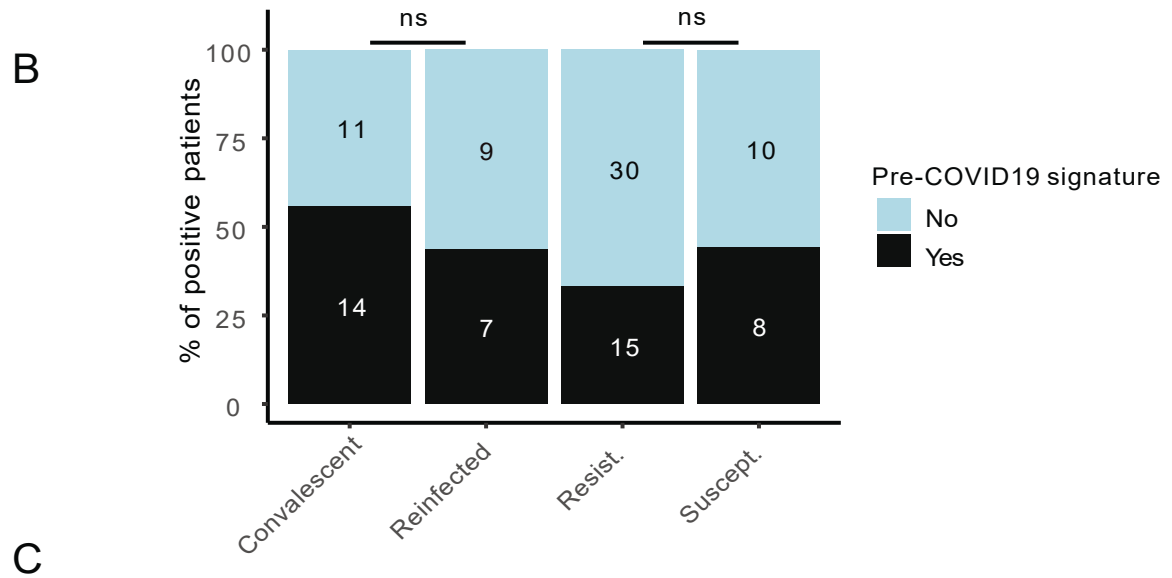
B
ns
ns
100
75
50
25
0
% of positive patients
11
9
30
10
14
7
15
8
Convalescent
Reinfected
Resist.
Suscept.
Pre-COVID19 signature
No
Yes

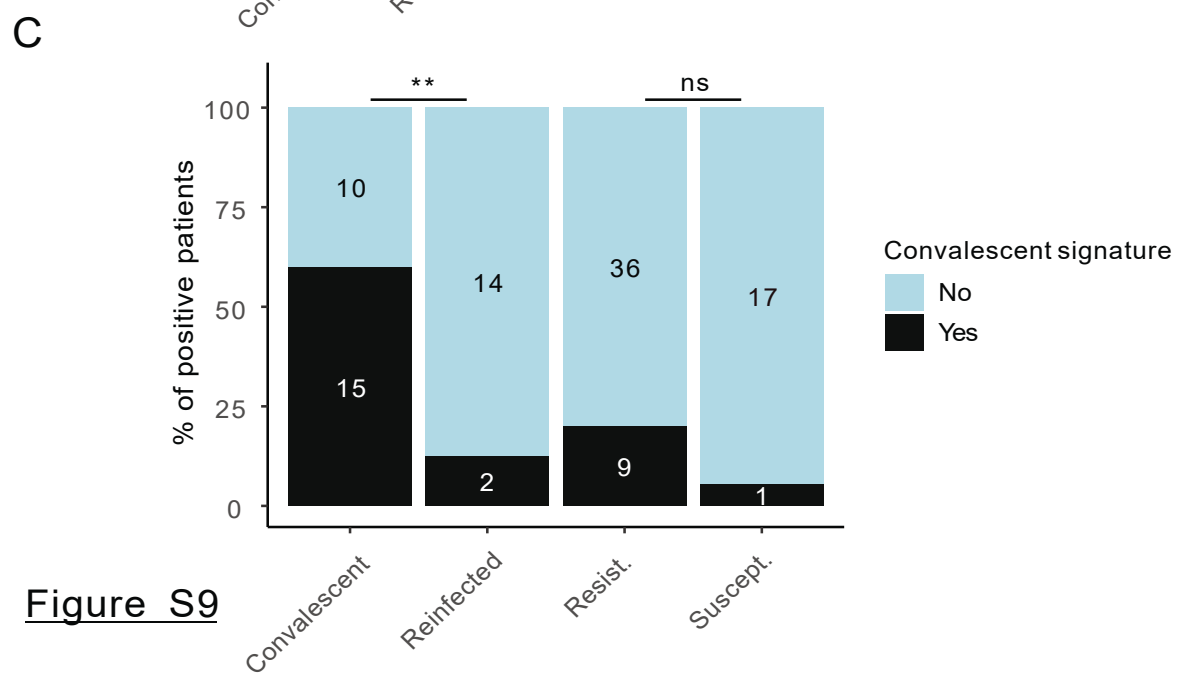
C
**
ns
100
75
50
25
0
% of positive patients
10
14
36
17
15
2
9
1
Convalescent
Reinfected
Resist.
Suscept.
Convalescent signature
No
Yes

Figure S9

Table S1. Consort diagram

510 patients eligible in ONCOVID trial

158 patients eligible in PROTECT-CoV trial

71 patients from the Pre-COVID-19 era

739 patients assessed for eligibility

7 patients excluded
- Decline to participate

732 patients eligible

303 patients excluded
- Not enough PBMCs available to perform cross-presentation assay or peptide based assay

429 patients' samples available for translational research analysis

320 allocated to control group

No detection of SARS-CoV-2 by:
- RT-qPCR
- Serology

320 allocated to control group
- Healthy individuals (n=63)
- Cancer patients (n=257)

109 allocated to COVID-19 group

Detection of SARS-CoV-2 by:
- RT-qPCR (n=109)
- Serology (n=107)

40 Acute COVID-19
- Cancer patients (n=40)

69 Convalescent
- Healthy individuals (n=29)
- Cancer patients (n=40)

Pre-COVID-19 era (from 2000 to 2018)
- Healthy individuals (n=41)
- Cancer patients (n=30)

67 analyzed by cross-presentation assay

23 analyzed by peptide-based assay

Contemporary (from 2020 to 2021)
- Healthy individuals (n=22)
- Cancer patients (n=227)

237 analyzed by cross-presentation assay

123 analyzed by peptide-based assay

Contemporary (from 2020 to 2021)
- Cancer patients (n=40)

24 analyzed by cross-presentation assay

Contemporary (from 2020 to 2021)
- Healthy individuals (n=29)
- Cancer patients (n=40)

54 analyzed by cross-presentation assay

20 analyzed by peptide-based assay

From cancer patients (n=227)

Phoned (n=229)

Unknown (n=159)

157 analyzed by cross-presentation assay

36 analyzed by peptide-based assay

Resistant (n=48)

41 analyzed by cross-presentation assay

45 analyzed by peptide-based assay

Susceptible (n=22)
- Controls (n=20)
- Convalescent (n=2)

19 analyzed by cross-presentation assay

18 analyzed by peptide-based assay

29 patients from the IHU trial

29 patients eligible

1 patient excluded
- Not enough PBMCs available to perform peptide-based assay

28 patients' samples available for translational research analysis

Re-infected (n=17)

4 analyzed by cross-presentation assay

16 analyzed by peptide-based assay

Multi-exposed (n=12)

12 analyzed by cross-presentation assay

0 analyzed by peptide-based assay

Table S2. Characteristics of cancer patients and healthy individuals.

		Controls (n=320)		Acute COVID-19 (n=40)		P.value*	Convalescent (n=69)		P.value #
		n	%	n	%		n	%	
Years	2000 - Nov. 2002	7	2	-	-	< 0.01	-	-	< 0.01
	Nov. 2002 - 2018	61	19	-	-		-	-	
	Unknown	2	1	-	-		-	-	
	2020 - 2021	250	78	40	100		69	100	
Age (years)	Median [Range]	61 [18-89]		63 [20-90]		0.13	56 [21-85]		0.02
Gender	Male	124	45	22	55	0.31	28	41	0.05
	Female	150	55	18	45		41	59	
	Unknown	46	-	-	-		-	-	
Malignancy	Yes	257	80	40	100	< 0.01	40	58	< 0.01
	No	63	20	0	0		29	42	

Refers to available samples described in table S1

* : statistical analyses between controls and acute COVID-19;
# : statistical analyses between controls and convalescent

Table S3. Characteristics of family members during the 2020 lockdown.

		Total		Contact (n=22)		Convalescent (n=29)		P.value
Age (years)	Median [Range]	46 [17-75]		39 [17-75]		49 [20-62]		0.69
		n	**%**	**n**	**%**	**n**	**%**	
Gender	Male	26	51	13	59	13	45	0.40
	Female	25	49	9	41	16	55	
Number of contacts per case within the family								
1-3				5	23	1	3	< 0.01
4-6				14	64	15	52	
7-9				1	5	8	28	
10-12				2	9	0	0	
> 12				0	0	5	17	
Number of SARS-CoV-2 positive individuals in the family								
0				4	18	0	0	< 0.01
1-3				18	82	18	62	
4-6				0	0	5	17	
7-15				0	0	6	21	
Household size								
0				2	9	0	0	< 0.01
1-2				0	0	5	17	
3-5				18	82	16	55	
6-8				2	9	8	28	
Household living space (m^2)								
< 70				7	32	6	21	0.16
70-100				3	14	11	38	
> 100				12	55	12	41	
Number of rooms in the household								
2-3				10	45	7	24	0.22
4-5				6	27	14	48	
6-8				6	27	8	28	
Number of individuals using personal protective equipment				13	59	18	62	1
Number of individuals respecting barriers gestures				16	73	22	76	1

Table S4. Clinical characteristics of all contact cases (susceptible and resistant).

		Resistant (n=48)		Susceptible (n=22)		P.value
Age (years)	Median [Range]	57 [21-77]		54 [23-82]		0.84
		n	**%**	**n**	**%**	
Gender	Male	16	33	11	50	0.20
	Female	32	67	11	50	
Malignancy	Yes	48	100	22	100	1.00
	No	0	0	0	0	

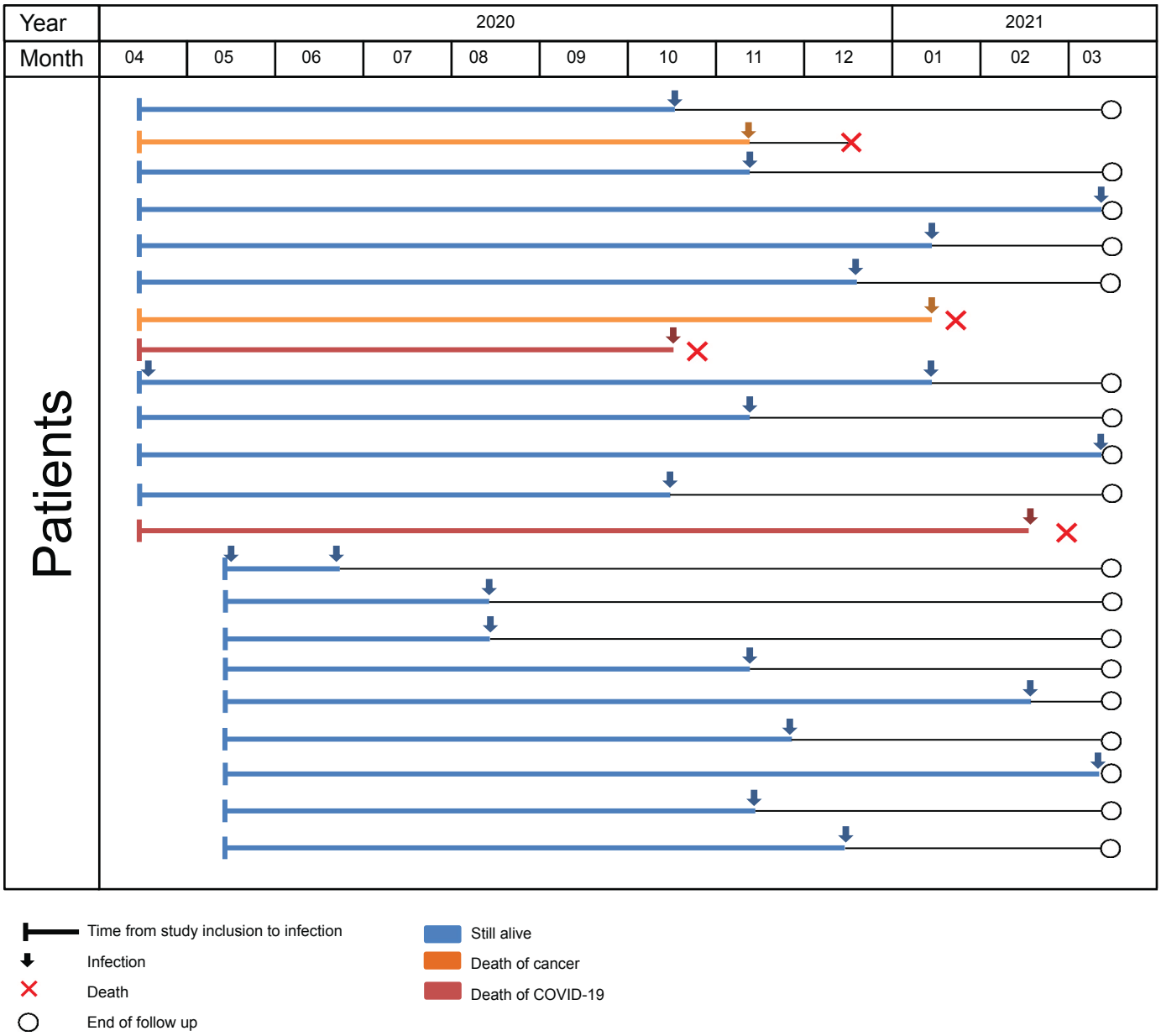

Table S5. Characteristics of multi-exposed and re-infected cancer-free individuals.

		Re-infected (n=17)		Multi-exposed cases (n=12)		P.value
Age (years)	Median [Range]	37 [16-78]		48 [28-69]		0.08
		n	**%**	**n**	**%**	
Gender	Male Female	7 10	41 59	6 6	50 50	0.72
Comorbidities	Yes No Unknown	5 11 1	31 69 -	- - -	- - -	-
Type of comorbidities	Asthma Obesity Type 2 diabetes Cancer HIV* HBP**	3 2 2 1 2	60 40 40 20 20 40	- - - - - -	- - - - - -	-
Time to reinfection (mo.)	< 03 03 - 06 > 06 Unknown	2 7 3 5	17 58 25 -	- - - -	- - - -	-
Second surge variants	B.1.177 B.1.160 B.1.351 B.1.1.7 Unknown	1 6 1 2 7	- - - - -	- - - - -	- - - - -	-

Refers to eligible patients described in table S1

*Human Immunodeficiency Virus
**High Blood Pressure

Table S7. Peptide-specific T cell polarisation determined by IL-5 or IFNγ quantification.

SARS-CoV-2 protein		n	IL-5$^-$/IFNγ$^-$	IL-5$^+$/IFNγ$^-$	IL-5$^-$/IFNγ$^+$	IL-5$^+$/IFNγ$^+$	P.value
Membrane	Resistant	35	20	3	1	1	0.76
	Susceptible		10	0	0	0	
Nucleocapsid	Resistant	42	17	3	7	3	0.58
	Susceptible		9	0	3	0	
S1	Resistant	36	15	0	9	4	0.34
	Susceptible		7	0	1	0	
S1-RBD	Resistant	36	15	3	10	0	0.06
	Susceptible		8	0	0	0	
S2	Resistant	23	8	0	7	1	0.75
	Susceptible		5	0	2	0	
ORF8	Resistant	22	11	0	5	0	1.00
	Susceptible		4	0	2	0	
ORF10	Resistant	23	15	0	1	0	0.53
	Susceptible		6	0	1	0	
ORF3a	Resistant	22	14	0	1	0	1.00
	Susceptible		7	0	0	0	

The numbers correspond to the enumeration of patients who were positive for at least one of the epitopes of each protein listed in Table S6.

Table S10. Characteristics of vaccinated healthcare workers.

		Controls (n=70)		Convalescent (n=14)		P.value
Age (years)	Median [Range]	49 [21-76]		48 [28-69]		0.71
		n	**%**	**n**	**%**	
Gender	Male	18	26	2	14	0.50
	Female	52	74	12	86	

TableS6. SARS-CoV-1 and CoV-2 orfeome peptide list: sequences and positions.

Peptide name	Peptide sequence	Virus	Protein	Similar sequence in SARS-CoV-2	SARS-CoV-2 Ref seq ID	Reference	SARS-CoV-2 first position	SARS-CoV-2 last position	SARS-CoV-1 Refseq ID	SARS-CoV-1 first position	SARS-CoV-1 last position
Spike1	MFVFLVLLPLVSSQC	SARS-CoV-2	Spike		QHD43416.1		1	15			
Spike2	VNLTTRTQLPPAYTN	SARS-CoV-2	Spike		QHD43416.1		16	30			
Spike3	SFTRGVYYPDKVFRS	SARS-CoV-2	Spike		QHD43416.1		31	45			
Spike4	SVLHSTQDLFLPFFS	SARS-CoV-2	Spike		QHD43416.1		46	60			
Spike5	NVTWFHAIHVSGTNG	SARS-CoV-2	Spike		QHD43416.1		61	75			
Spike6	TKRFDNPVLPFNDGV	SARS-CoV-2	Spike		QHD43416.1		76	90			
Spike7	YFASTEKSNIIRGWI	SARS-CoV-2	Spike		QHD43416.1		91	105			
Spike8	FGTTLDSKTQSLLIV	SARS-CoV-2	Spike		QHD43416.1		106	120			
Spike9	NNATNVVIKVCEFQF	SARS-CoV-2	Spike		QHD43416.1		121	135			
Spike10	CNDPFLGVYYHKNNK	SARS-CoV-2	Spike		QHD43416.1		136	150			
Spike11	SWMESEFRVYSSANN	SARS-CoV-2	Spike		QHD43416.1		151	165			
Spike12	CTFEYVSQPFLMDLE	SARS-CoV-2	Spike		QHD43416.1		166	180			
Spike13	GKQGNFKNLREFVFK	SARS-CoV-2	Spike		QHD43416.1		181	195			
Spike14	NIDGYFKIYSKHTPI	SARS-CoV-2	Spike		QHD43416.1		196	210			
Spike15	NLVRDLPQGFSALEP	SARS-CoV-2	Spike		QHD43416.1		211	225			
Spike16	LVDLPIGINITRFQT	SARS-CoV-2	Spike		QHD43416.1		226	240			
Spike17	LLALHRSYLTPGDSS	SARS-CoV-2	Spike		QHD43416.1		241	255			
Spike18	SGWTAGAAAYYVGYL	SARS-CoV-2	Spike		QHD43416.1		256	270			
Spike19	QPRTFLLKYNENGTI	SARS-CoV-2	Spike		QHD43416.1		271	285			
Spike20	TDAVDCALDPLSETK	SARS-CoV-2	Spike		QHD43416.1		286	300			
Spike21	CTLKSFTVEKGIYQT	SARS-CoV-2	Spike		QHD43416.1		301	315			
Spike22	SNFRVQPTESIVRFP	SARS-CoV-2	Spike		QHD43416.1		316	330			
Spike23	NITNLCPFGEVFNAT	SARS-CoV-1 +SARS-CoV-2	Spike		QHD43416.1		331	345	AAP41037.1	318	332
Spike24	RFASVYAWNRKRISN	SARS-CoV-2	Spike		QHD43416.1		346	360			
Spike25	CVADYSVLYNSASFS	SARS-CoV-2	Spike		QHD43416.1		361	375			
Spike26	TFKCYGVSPTKLNDL	SARS-CoV-2	Spike		QHD43416.1		376	390			
Spike27	CFTNVYADSFVIRGD	SARS-CoV-2	Spike		QHD43416.1		391	405			
Spike28	EVRQIAPGQTGKIAD	SARS-CoV-2	Spike		QHD43416.1		406	420			
Spike29	YNYKLPDDFTGCVIA	SARS-CoV-2	Spike		QHD43416.1		421	435			
Spike30	WNSNNLDSKVGGNYN	SARS-CoV-2	Spike		QHD43416.1		436	450			
Spike31	YLYRLFRKSNLKPFE	SARS-CoV-2	Spike		QHD43416.1		451	465			
Spike32	RDISTEIYQAGSTPC	SARS-CoV-2	Spike		QHD43416.1		466	480			
Spike33	NGVEGFNCYFPLQSY	SARS-CoV-2	Spike		QHD43416.1		481	495			
Spike34	GFQPTNGVGYQPYRV	SARS-CoV-2	Spike		QHD43416.1		496	510			
Spike35	VVLSFELLHAPATVC	SARS-CoV-2	Spike		QHD43416.1		511	525			
Spike36	GPKKSTNLVKNKCVN	SARS-CoV-2	Spike		QHD43416.1		526	540			
Spike37	FNFNGLTGTGVLTES	SARS-CoV-2	Spike		QHD43416.1		541	555			
Spike38	NKKFLPFQQFGRDIA	SARS-CoV-2	Spike		QHD43416.1		556	570			
Spike39	DTTDAVRDPQTLEIL	SARS-CoV-2	Spike		QHD43416.1		571	585			
Spike40	DITPCSFGGVSVITP	SARS-CoV-2	Spike		QHD43416.1		586	600			
Spike41	GTNTSNQVAVLYQDV	SARS-CoV-2	Spike		QHD43416.1		601	615			
Spike42	NCTEVPVAIHADQLT	SARS-CoV-2	Spike		QHD43416.1		616	630			
Spike43	PTWRVYSTGSNVFQT	SARS-CoV-2	Spike		QHD43416.1		631	645			
Spike44	RAGCLIGAEHVNNSY	SARS-CoV-2	Spike		QHD43416.1		646	660			
Spike45	ECDIPIGAGICASYQ	SARS-CoV-2	Spike		QHD43416.1		661	675			
Spike46	TQTNSPRRARSVASQ	SARS-CoV-2	Spike		QHD43416.1		676	690			
Spike47	SIIAYTMSLGAENSV	SARS-CoV-2	Spike		QHD43416.1		691	705			
Spike48	AYSNNSIAIPTNFTI	SARS-CoV-2	Spike		QHD43416.1		706	720			
Spike49	SVTTEILPVSMTKTS	SARS-CoV-2	Spike		QHD43416.1		721	735			
Spike50	VDCTMYICGDSTECS	SARS-CoV-2	Spike		QHD43416.1		736	750			
Spike51	NLLLQYGSFCTQLNR	SARS-CoV-1 +SARS-CoV-2	Spike		QHD43416.1		751	765	AAP41037.1	733	747
Spike52	ALTGIAVEQDKNTQE	SARS-CoV-2	Spike		QHD43416.1		766	780			
Spike53	VFAQVKQIYKTPPIK	SARS-CoV-2	Spike		QHD43416.1		781	795			
Spike54	DFGGFNFSQILPDPS	SARS-CoV-2	Spike		QHD43416.1		796	810			
Spike55	KPSKRSFIEDLLFNK	SARS-CoV-2	Spike		QHD43416.1		811	825			
Spike56	VTLADAGFIKQYGDC	SARS-CoV-2	Spike		QHD43416.1		826	840			
Spike57	LGDIAARDLICAQKF	SARS-CoV-2	Spike		QHD43416.1		841	855			
Spike58	NGLTVLPPLLTDEMI	SARS-CoV-2	Spike		QHD43416.1		856	870			
Spike59	AQYTSALLAGTITSG	SARS-CoV-2	Spike		QHD43416.1		871	885			
Spike60	WTFGAGAALQIPFAM	SARS-CoV-1 +SARS-CoV-2	Spike		QHD43416.1		886	900	AAP41037.1	868	882
Spike61	QMAYRFNGIGVTQNV	SARS-CoV-1 +SARS-CoV-2	Spike		QHD43416.1		901	915	AAP41037.1	883	897
Spike62	LYENQKLIANQFNSA	SARS-CoV-2	Spike		QHD43416.1		916	930			
Spike63	IGKIQDSLSSTASAL	SARS-CoV-2	Spike		QHD43416.1		931	945			
Spike64	GKLQDVVNQNAQALN	SARS-CoV-1 +SARS-CoV-2	Spike		QHD43416.1		946	960	AAP41037.1	928	942
Spike65	TLVKQLSSNFGAISS	SARS-CoV-1 +SARS-CoV-2	Spike		QHD43416.1		961	975	AAP41037.1	943	957
Spike66	VLNDILSRLDKVEAE	SARS-CoV-1 +SARS-CoV-2	Spike		QHD43416.1		976	990	AAP41037.1	958	972
Spike67	VQIDRLITGRLQSLQ	SARS-CoV-1 +SARS-CoV-2	Spike		QHD43416.1		991	1005	AAP41037.1	973	987
Spike68	TYVTQQLIRAAEIRA	SARS-CoV-1 +SARS-CoV-2	Spike		QHD43416.1		1006	1020	AAP41037.1	988	1002
Spike69	SANLAATKMSECVLG	SARS-CoV-1 +SARS-CoV-2	Spike		QHD43416.1		1021	1035	AAP41037.1	1003	1017
Spike70	QSKRVDFCGKGYHLM	SARS-CoV-1 +SARS-CoV-2	Spike		QHD43416.1		1036	1050	AAP41037.1	1018	1032
Spike71	SFPQSAPHGVVFLHV	SARS-CoV-2	Spike		QHD43416.1		1051	1065			
Spike72	TYVPAQEKNFTTAPA	SARS-CoV-2	Spike		QHD43416.1		1066	1080			
Spike73	ICHDGKAHFPREGVF	SARS-CoV-2	Spike		QHD43416.1		1081	1095			
Spike74	VSNGTHWFVTQRNFY	SARS-CoV-2	Spike		QHD43416.1		1096	1110			
Spike75	EPQIITTDNTFVSGN	SARS-CoV-2	Spike		QHD43416.1		1111	1125			
Spike76	CDVVIGIVNNTVYDP	SARS-CoV-2	Spike		QHD43416.1		1126	1140			
Spike77	LQPELDSFKEELDKY	SARS-CoV-1 +SARS-CoV-2	Spike		QHD43416.1		1141	1155	AAP41037.1	1123	1137
Spike78	FKNHTSPDVDLGDIS	SARS-CoV-1 +SARS-CoV-2	Spike		QHD43416.1		1156	1170	AAP41037.1	1138	1152
Spike79	GINASVVNIQKEIDR	SARS-CoV-1 +SARS-CoV-2	Spike		QHD43416.1		1171	1185	AAP41037.1	1153	1167
Spike80	LNEVAKNLNESLIDL	SARS-CoV-1 +SARS-CoV-2	Spike		QHD43416.1		1186	1200	AAP41037.1	1168	1182
Spike81	QELGKYEQYIKWPWY	SARS-CoV-1 +SARS-CoV-2	Spike		QHD43416.1		1201	1215	AAP41037.1	1183	1197
Spike82	IWLGFIAGLIAIVMV	SARS-CoV-2	Spike		QHD43416.1		1216	1230			
Spike83	TIMLCCMTSCCSCLK	SARS-CoV-2	Spike		QHD43416.1		1231	1245			
Spike84	GCCSCGSCCKFDEDD	SARS-CoV-2	Spike		QHD43416.1		1246	1260			
Spike85	SEPVLKGVKLHYT	SARS-CoV-1 +SARS-CoV-2	Spike		QHD43416.1		1261	1273	AAP41037.1	1243	1255
Nucleocapsid_1	MSDNGPQNQRNAPRI	SARS-CoV-2	Nucleocapsid		QHD43423.2		1	15			
Nucleocapsid_2	TFGGPSDSTGSNQNG	SARS-CoV-2	Nucleocapsid		QHD43423.2		16	30			
Nucleocapsid_3	ERSGARSKQRRPQGL	SARS-CoV-2	Nucleocapsid		QHD43423.2		31	45			
Nucleocapsid_4	PNNTASWFTALTQHG	SARS-CoV-1 +SARS-CoV-2	Nucleocapsid		QHD43423.2		46	60	AAP41047.1	47	61
Nucleocapsid_5	KEDLKFPRGQGVPIN	SARS-CoV-2	Nucleocapsid		QHD43423.2		61	75			
Nucleocapsid_6	TNSSPDDQIGYYRRA	SARS-CoV-2	Nucleocapsid		QHD43423.2		76	90			
Nucleocapsid_7	TRRIRGGDGKMKDLS	SARS-CoV-2	Nucleocapsid		QHD43423.2		91	105			
Nucleocapsid_8	PRWYFYYLGTGPEAG	SARS-CoV-2	Nucleocapsid		QHD43423.2		106	120			
Nucleocapsid_9	LPYGANKDGIIWVAT	SARS-CoV-2	Nucleocapsid		QHD43423.2		121	135			
Nucleocapsid_10	EGALNTPKDHIGTRN	SARS-CoV-1 +SARS-CoV-2	Nucleocapsid		QHD43423.2		136	150	AAP41047.1	137	151
Nucleocapsid_11	PANNAAIVLQLPQGT	SARS-CoV-2	Nucleocapsid		QHD43423.2		151	165			
Nucleocapsid_12	TLPKGFYAEGSRGGS	SARS-CoV-1 +SARS-CoV-2	Nucleocapsid		QHD43423.2		166	180	AAP41047.1	167	181
Nucleocapsid_13	QASSRSSSRSRNSSR	SARS-CoV-2	Nucleocapsid		QHD43423.2		181	195			
Nucleocapsid_14	NSTPGSSRGTSPARM	SARS-CoV-2	Nucleocapsid		QHD43423.2		196	210			
Nucleocapsid_15	AGNGGDAALALLLLD	SARS-CoV-2	Nucleocapsid		QHD43423.2		211	225			
Nucleocapsid_16	RLNQLESKMSGKGQQ	SARS-CoV-2	Nucleocapsid		QHD43423.2		226	240			
Nucleocapsid_17	QQGQTVTKKSAAEAS	SARS-CoV-1 +SARS-CoV-2	Nucleocapsid		QHD43423.2		241	255	AAP41047.1	242	256
Nucleocapsid_18	KKPRQKRTATKAYNV	SARS-CoV-2	Nucleocapsid		QHD43423.2		256	270			
Nucleocapsid_19	TQAFGRRGPEQTQGN	SARS-CoV-1 +SARS-CoV-2	Nucleocapsid		QHD43423.2		271	285	AAP41047.1	272	286
Nucleocapsid_20	FGDQELIRQGTDYKH	SARS-CoV-2	Nucleocapsid		QHD43423.2		286	300			
Nucleocapsid_21	WPQIAQFAPSASAFF	SARS-CoV-1 +SARS-CoV-2	Nucleocapsid		QHD43423.2		301	315	AAP41047.1	302	316
Nucleocapsid_22	GMSRIGMEVTPSGTW	SARS-CoV-1 +SARS-CoV-2	Nucleocapsid		QHD43423.2		316	330	AAP41047.1	317	331
Nucleocapsid_23	LTYTGAIKLDDKDPN	SARS-CoV-2	Nucleocapsid		QHD43423.2		331	345			
Nucleocapsid_24	FKDQVILLNKHIDAY	SARS-CoV-2	Nucleocapsid		QHD43423.2		346	360			
Nucleocapsid_25	KTFPPTEPKKDKKKK	SARS-CoV-1 +SARS-CoV-2	Nucleocapsid		QHD43423.2		361	375	AAP41047.1	362	376
Nucleocapsid_26	ADETQALPQRQKKQQ	SARS-CoV-2	Nucleocapsid		QHD43423.2		376	390			
Nucleocapsid_27	TVTLLPAADLDDFSK	SARS-CoV-2	Nucleocapsid		QHD43423.2		391	405			
Nucleocapsid_28	QLQQSMSSADSTQA	SARS-CoV-2	Nucleocapsid		QHD43423.2		406	419			
Membrane_1	MADSNGTITVEELKK	SARS-CoV-2	Membrane		QHD43419.1		1	15			
Membrane_2	ITVEELKKLLEQWNL	SARS-CoV-2	Membrane		QHD43419.1		8	22			
Membrane_3	KKLLEQWNLVIGFLF	SARS-CoV-2	Membrane		QHD43419.1		15	29			
Membrane_4	EQWNLVIGFLFLTWI	SARS-CoV-2	Membrane		QHD43419.1		22	36			
Membrane_5	LLESELVIGAVILRG	SARS-CoV-2	Membrane		QHD43419.1		133	147			
Membrane_6	IGAVILRGHLRIAGH	SARS-CoV-2	Membrane		QHD43419.1		140	154			
Membrane_7	HLRIAGHHLGRCDIK	SARS-CoV-2	Membrane		QHD43419.1		148	162			
SARS_2016.05.006	LLNKHIDAYKTFP	SARS-CoV-1 +SARS-CoV-2	Nucleocapsid		QHD43423.2	https://dx.doi.org/10.1016/j.immuni.2016.05.006	352	364	AAP41047.1	353	365
SARS_10.1128_1	PLQASLPFGWLVIGV	SARS-CoV-1	ORF3a	PIQASLPFGWLIVGV	QHD43417.1	https://dx.doi.org/10.4049/jimmunol.181.8.5490	36	50	AYV99776.1	36	50
SARS_10.1128_2	NYNYKYRYLRGKLRPF	SARS-CoV-1	Spike	NYNYLYRLFRKSNLKPF	QHD43416.1	https://dx.doi.org/10.4049/jimmunol.181.8.5490	448	464	AAP41037.1	435	451
SARS_10.1128_3	AGCLIGAEHVDTSYECDI	SARS-CoV-1	Spike	AGCLIGAEHVNNSYECDI	QHD43416.1	https://dx.doi.org/10.4049/jimmunol.181.8.5490	647	664	AAP41037.1	633	650
SARS_10.1128_4	GETALALLLLDRLNQ	SARS-CoV-1	Nucleocapsid	GDAALALLLLDRLNQ	QHD43423.2	https://dx.doi.org/10.4049/jimmunol.181.8.5490	215	229	AAP41047.1	216	230
SARS_10.1128_5	GHLRMAGHSLGRCDI	SARS-CoV-1	Membrane	GHLRIAGHHLGRCDI	QHD43419.1	https://dx.doi.org/10.4049/jimmunol.181.8.5490	147	162	AAP41041.1	146	161
SARS_10.1128_6	NFNGLTGTGVLTPSSKRF	SARS-CoV-1	Spike	NFNGLTGTGVLTESNKKF	QHD43416.1	https://dx.doi.org/10.4049/jimmunol.181.8.5490	542	559	AAP41037.1	528	545
SARS_10.1128_7	DIPIGAGICASYHTVSLL	SARS-CoV-1	Spike	DIPIGAGICASYQTQTNS	QHD43416.1	https://dx.doi.org/10.4049/jimmunol.181.8.5490	663	680	AAP41037.1	649	666
SARS_10.1128_8	SWFITQRNFFSPQII	SARS-CoV-1	Spike	HWFVTQRNFYEPQII	QHD43416.1	https://dx.doi.org/10.4049/jimmunol.181.8.5490	1101	1115	AAP41037.1	1083	1097
SARS_HLA-A*02:01_1	FIAGLIAIV	SARS-CoV-1 +SARS-CoV-2	Spike		QHD43416.1	https://dx.doi.org/10.1038/emi.2012.26	1220	1228	AAP41037.1	1202	1210
SARS_HLA-A*02:01_2	LITGRLQSL	SARS-CoV-1 +SARS-CoV-2	Spike		QHD43416.1	https://dx.doi.org/10.1038/emi.2012.26	996	1004	AAP41037.1	978	988
SARS_HLA-A*02:01_3	RLNEVAKNL	SARS-CoV-1 +SARS-CoV-2	Spike		QHD43416.1	https://dx.doi.org/10.1038/emi.2012.26	1185	1193	AAP41037.1	1167	1175
SARS_HLA-A*02:01_4	ILPDPLKPT	SARS-CoV-1	Spike	ILPDPSKPS	QHD43416.1	https://dx.doi.org/10.1038/emi.2012.26	805	813	AAP41037.1	787	795
SARS_HLA-A*02:01_5	VVFLHVTYV	SARS-CoV-1 +SARS-CoV-2	Spike		QHD43416.1	https://dx.doi.org/10.1038/emi.2012.26	1060	1068	AAP41037.1	1042	1050
SARS_HLA-A*02:01_6	KLPDDFMGCV	SARS-CoV-1	Spike	KLPDDFTGCV	QHD43416.1	https://dx.doi.org/10.1038/emi.2012.26	424	433	AAP41037.1	411	420
SARS_HLA-A*02:01_7	VLNDILSRL	SARS-CoV-1 +SARS-CoV-2	Spike		QHD43416.1	https://dx.doi.org/10.1038/emi.2012.26	976	984	AAP41037.1	958	966
SARS_HLA-A*02:01_8	LLLDRLNQL	SARS-CoV-1 +SARS-CoV-2	Nucleocapsid		QHD43423.2	https://dx.doi.org/10.1038/emi.2012.26	222	230	AAP41047.1	223	231
SARS_HLA-A*02:01_9	RLNQLESKV	SARS-CoV-1	Nucleocapsid	RLNQLESKM	QHD43423.2	https://dx.doi.org/10.1038/emi.2012.26	226	234	AAP41047.1	227	235
SARS_HLA-A*02:01_10	GMSRIGMEV	SARS-CoV-1 +SARS-CoV-2	Nucleocapsid		QHD43423.2	https://dx.doi.org/10.1038/emi.2012.26	316	324	AAP41047.1	317	325
SARS_HLA-A*02:01_11	WLTYHGAIKLDDKDPQF	SARS-CoV-1	Nucleocapsid	WLTYTGAIKLDDKDPNF	QHD43423.2	https://dx.doi.org/10.1038/emi.2012.26	330	346	AAP41047.1	331	347
SARS_HLA-A*02:01_12	QFKDNVILLNKHIDAYK	SARS-CoV-1	Nucleocapsid	NFKDQVILLNKHIDAYK	QHD43423.2	https://dx.doi.org/10.1038/emi.2012.26	345	361	AAP41047.1	346	362
SARS_HLA-A*02:01_13	MASGGGETALALLLLDRLNQLESKV	SARS-CoV-1	Nucleocapsid	MAGNGGDAALALLLLDRLNQLESKM	QHD43423.2	https://dx.doi.org/10.1038/emi.2012.26	210	234	AAP41047.1	211	235
SARS_HLA-A*02:01_14	TWLTYHGAIKLDDKDPQFKDNVILL	SARS-CoV-1	Nucleocapsid	TWLTYTGAIKLDDKDPNFKDQVILL	QHD43423.2	https://dx.doi.org/10.1038/emi.2012.26	329	353	AAP41047.1	330	354
SARS_HLA-A*02:01_15	GETALALLL	SARS-CoV-1	Nucleocapsid	GDAALALLLL	QHD43423.2	https://dx.doi.org/10.1038/emi.2012.26	215	224	AAP41047.1	216	225
SARS_HLA-A*02:01_16	LVIGFLFLAWIMLLQFAYSNRNRF	SARS-CoV-1	Membrane	LVIGFLFLTWICLLQFAYANRNRF	QHD43419.1	https://dx.doi.org/10.1038/emi.2012.26	22	45	AAP41041.1	21	44
SARS_HLA-A*02:01_17	VLAAVYRINWVTGGIAIAMACIVGLMW	SARS-CoV-1	Membrane	VLAAVYRINWITGGIAIAMACLVGLMW	QHD43419.1	https://dx.doi.org/10.1038/emi.2012.26	66	92	AAP41041.1	65	91
SARS_HLA-A*02:01_18	ILLNVPLRGTIVTRPLMESELVIG	SARS-CoV-1	Membrane	ILLNVPLHGTILTRPLLESELVIG	QHD43419.1	https://dx.doi.org/10.1038/emi.2012.26	116	141	AAP41041.1	117	140
SARS_HLA-A*02:01_19	IGNYKLNTDHAGSNDNIALLV	SARS-CoV-1	Membrane	IGNYKLNTDHSSSSDNIALLV	QHD43419.1	https://dx.doi.org/10.1038/emi.2012.26	199	221	AAP41041.1	200	220
SARS_HLA-A*02:01_20	GHLRMAGHPLGRCDI	SARS-CoV-1	Membrane	GHLRIAGHHLGRCDI	QHD43419.1	https://dx.doi.org/10.1038/emi.2012.26	145	161	AYV99779.1	146	160
SARS_HLA-A*02:01_21	PLQASLPFGWLVIGV	SARS-CoV-1	ORF3a	PIQASLPFGWLIVGV	QHD43417.1	https://dx.doi.org/10.1038/emi.2012.26	36	50	AYV99776.1	36	50
SARS_01026-X	DVNCTDVSTAIHADQLTPAWR	SARS-CoV-1	Spike	DVNCTEVPVAIHADQLTPTWR	QHD43416.1	https://dx.doi.org/10.1016/S1672-0229(03)01026-X	614	634	AYV99775.1	600	620
SARS_01025-8_1	KDKKKKTDEAQPLPQRQKKQ	SARS-CoV-1	Nucleocapsid	KDKKKKADETQALPQRQKKQ	QHD43423.2	https://dx.doi.org/10.1016/S1672-0229(03)01025-8	370	389	AAP41047.1	371	390
SARS_01025-8_2	QRQKKQPTVTLLPAADMDDFSRQ	SARS-CoV-1	Nucleocapsid	QRQKKQQTVTLLPAADLDDFSKQ	QHD43423.2	https://dx.doi.org/10.1016/S1672-0229(03)01025-8	384	406	AAP41047.1	385	407
SARS_HLA-DR0401_1	NAFNCTFEYISDAFSLDV	SARS-CoV-1	Spike			https://doi.org/10.1093/intimm/dxn124			AAP41037.1	155	172
SARS_HLA-DR0401_2	YISDAFSLDVSEKSGNFK	SARS-CoV-1	Spike			https://doi.org/10.1093/intimm/dxn124			AAP41037.1	163	180
SARS_HLA-DR0401_3	YLRHGKLRPFERDISNVP	SARS-CoV-1	Spike			https://doi.org/10.1093/intimm/dxn124			AAP41037.1	442	459
SARS_HLA-DR0401_4	RPFERDISNVPFSPDGK	SARS-CoV-1	Spike			https://doi.org/10.1093/intimm/dxn124			AAP41037.1	449	465
SARS_3726.2005_1	MADNGTITVEELKQLLEQWNLVIGFLFLAWI	SARS-CoV-1	Membrane	MADSNGTITVEELKKLLEQWNLVIGFLFLTWI	QHD43419.1	https://doi.org/10.1128/jcm.43.8.3718-3726.2005	1	32	AAP41041.1	1	31
SARS_3726.2005_2	LMESELVIGAVIIRGHLRMAGHPLGRCDIK	SARS-CoV-1	Membrane	LLESELVIGAVILRGHLRIAGHHLGRCDIK	QHD43419.1	https://doi.org/10.1128/jcm.43.8.3718-3726.2005	133	162	AYV99779.1	132	161
SARS_5314.2004_1	NNNAATVLQLPQGTTLPKGFYAEGSR	SARS-CoV-1	Nucleocapsid	ANNAAIVLQLPQGTTLPKGFYAEGSR	QHD43423.2	https://doi.org/10.1128/jcm.42.11.5309-5314.2004	152	175	AAP41047.1	153	176
SARS_5314.2004_2	KTFPPTEPKKDKKKKTDEAQPLPQRQKKQPTVTLLPAADMDDFSRQLQNSM	SARS-CoV-1	Nucleocapsid	KTFPPTEPKKDKKKKADETQALPQRQKKQQTVTLLPAADLDDFSKQLQQSM	QHD43423.2	https://doi.org/10.1128/jcm.42.11.5309-5314.2004	361	411	AAP41047.1	362	412
ORF8_1	MKFLVFLGIITTVAA	SARS-CoV-2	ORF8		QHD43422.1		1	15			
ORF8_2	GIITTVAAFHQECSL	SARS-CoV-2	ORF8		QHD43422.1		8	22			
ORF8_3	AFHQECSLQSCTQHQ	SARS-CoV-2	ORF8		QHD43422.1		15	29			
ORF8_4	LQSCTQHQPYVVDDP	SARS-CoV-2	ORF8		QHD43422.1		22	36			
ORF8_5	QPYVVDDPCPIHFYS	SARS-CoV-2	ORF8		QHD43422.1		29	43			
ORF8_6	PCPIHFYSKWYIRVG	SARS-CoV-2	ORF8		QHD43422.1		36	50			
ORF8_7	SKWYIRVGARKSAPL	SARS-CoV-2	ORF8		QHD43422.1		43	57			
ORF8_8	GARKSAPLIELCVDE	SARS-CoV-2	ORF8		QHD43422.1		50	64			
ORF8_9	LIELCVDEAGSKSPI	SARS-CoV-2	ORF8		QHD43422.1		57	71			
ORF8_10	EAGSKSPIQYIDIGN	SARS-CoV-2	ORF8		QHD43422.1		64	78			
ORF8_11	IQYIDIGNYTVSCLP	SARS-CoV-2	ORF8		QHD43422.1		71	85			
ORF8_12	NYTVSCLPFTINCQE	SARS-CoV-2	ORF8		QHD43422.1		78	92			
ORF8_13	PFTINCQEPKLGSLV	SARS-CoV-2	ORF8		QHD43422.1		85	99			
ORF8_14	EPKLGSLVVRCSFYE	SARS-CoV-2	ORF8		QHD43422.1		92	106			
ORF8_15	VVRCSFYEDFLEYHD	SARS-CoV-2	ORF8		QHD43422.1		99	113			
ORF8_16	EDFLEYHDVRVVLDF	SARS-CoV-2	ORF8		QHD43422.1		106	120			
ORF8_17	DVRVVLDFI	SARS-CoV-2	ORF8		QHD43422.1		113	121			
ORF10_1	MGYINVFAFPFTIYS	SARS-CoV-2	ORF10		QHI42199.1		1	15			
ORF10_2	AFPFTIYSLLLCRMN	SARS-CoV-2	ORF10		QHI42199.1		8	22			
ORF10_3	SLLLCRMNSRNYIAQ	SARS-CoV-2	ORF10		QHI42199.1		15	29			
ORF10_4	NSRNYIAQVDVVNFN	SARS-CoV-2	ORF10		QHI42199.1		22	36			
ORF10_5	QVDVVNFNLT	SARS-CoV-2	ORF10		QHI42199.1		29	38			
ORF8_A	GNYTVSCSPFTINCQ	SARS-CoV-2	ORF8		QHN73801.1	https://doi.org/10.1016/j.ijid.2020.07.016	77	91			
ORF8_BC	GNYTVSCLPFTINCQ	SARS-CoV-2	ORF8		QHD43422.1	https://doi.org/10.1016/j.ijid.2020.07.016	77	91			
ORF3a_AB	VQIHTIDGSSGVVNP	SARS-CoV-2	ORF3a		QHD43417.1	https://doi.org/10.1016/j.ijid.2020.07.016	244	258			
ORF3a_C	VQIHTIDVSSGVVNP	SARS-CoV-2	ORF3a		QHZ00380.1	https://doi.org/10.1016/j.ijid.2020.07.016	244	258			

LEGEND:	
(yellow)	SARS-CoV-2
(salmon)	SARS-CoV-1 +SARS-CoV-2
(blue)	SARS-CoV-1

Table S8a. HLA phenotyping and genotyping of susceptible and resistant individuals (class I).

HLA-A alleles

Peptide sequence	Mutated and WT peptide name	HLA-A02:01	HLA-A03:01	HLA-A01:01	HLA-A24:02	HLA-A11:01	HLA-A26:01	HLA-A23:01	HLA-A29:02	HLA-A32:01	HLA-A68:01	HLA-A25:01	HLA-A68:02	HLA-A02:05	HLA-A31:01	HLA-A30:01	HLA-A30:02	HLA-A33:01	HLA-A29:01	HLA-A02:02	HLA-A33:03	HLA-A01:02	HLA-A01:03	HLA-A02:03	HLA-A02:06	HLA-A02:07	HLA-A02:08	HLA-A02:11	HLA-A03:02	HLA-A24:03	HLA-A26:08	HLA-A30:04	HLA-A34:02	HLA-A36:01	HLA-A66:01	HLA-A66:02	HLA-A69:01	HLA-A74:01	HLA-A74:03
	Allele freq.(%)	25.8	11.7	9.5	8.53	7.36	3.73	3.52	2.99	2.77	2.03	2.03	2.03	1.71	1.6	1.39	1.39	1.39	<1	<1	<1	<1	<1	<1	<1	<1	<1	<1	<1	<1	<1	<1	<1	<1	<1	<1	<1	<1	<1
RFASVYAWNRKRISN	Spike24wt	0	1	0	1	2	0	1	0	1	2	0	0	0	2	1	0	2	0	0	2	0	0	0	0	0	0	0	1	1	0	0	2	0	2	2	0	2	2
CVADYSVLYNSASFS	Spike25wt	0	1	2	1	1	2	1	2	2	1	2	0	0	0	0	2	0	2	0	0	2	2	0	0	0	0	0	1	1	2	2	2	2	2	2	0	0	0
CVADYSFLYNSASFS	Spike25_V367F	1	1	2	2	2	2	2	2	2	1	2	0	1	0	0	2	0	2	1	0	2	2	2	1	0	0	1	1	2	2	2	2	2	2	2	0	1	1
TFKCYGVSPTKLNDL	Spike26wt	0	1	0	1	0	0	1	0	0	0	0	0	0	0	1	0	0	0	0	0	0	0	0	0	0	0	0	1	2	0	0	0	0	0	0	0	1	1
CFTNVYADSFVIRGD	Spike27wt	0	0	2	2	1	1	2	1	1	2	2	2	2	1	0	0	2	1	1	2	1	2	1	1	1	2	1	1	1	2	1	2	1	2	2	2	1	1
EVRQIAPGQTGKIAD	Spike28wt	0	2	0	0	1	0	0	0	0	1	0	0	0	0	1	0	0	0	0	0	0	0	0	0	0	0	0	2	0	0	0	2	0	1	1	0	1	1
EVRQIAPGQTGNIAD	Spike28_K417N	0	0	0	0	0	0	0	0	0	0	0	0	0	0	0	0	0	0	0	0	0	0	0	0	0	0	0	0	0	0	0	0	0	1	1	0	0	0
EVRQIAPGQTGPIAD	Spike28_K417P	0	0	0	0	0	0	0	0	0	0	0	1	0	0	0	0	0	0	0	0	0	0	0	0	0	0	0	0	0	0	0	0	0	1	1	0	0	0
YNYKLPDDFTGCVIA	Spike29wt	1	0	0	0	0	0	0	0	0	0	0	0	2	0	0	0	0	0	2	0	0	0	2	2	2	2	1	0	0	0	0	0	0	0	0	0	0	0
WNSNNLDSKVGGNYN	Spike30wt	0	0	2	0	0	0	0	0	0	0	0	0	0	0	0	1	0	0	0	0	2	2	0	0	0	0	0	0	0	1	0	0	2	0	0	0	0	0
WNSKNLDSKVGGNYN	Spike30_N439K	0	0	2	0	0	0	0	0	0	0	0	0	0	0	0	1	0	0	0	0	2	2	0	0	0	0	0	0	0	1	0	0	2	0	0	0	0	0
WNSNKLDSKVGGNYN	Spike30_N440K	0	1	2	0	0	0	0	0	0	0	0	0	0	0	0	2	0	0	0	0	1	2	0	0	0	0	0	0	0	0	1	0	2	0	0	0	0	0
YLYRLFRKSNLKPFE	Spike31wt	0	2	0	1	2	0	1	0	2	1	0	0	0	2	2	0	0	0	0	0	0	0	0	0	0	0	0	2	1	0	1	2	0	0	0	0	2	2
YRYRLFRKSNLKPFE	Spike31_L452R	0	2	0	1	2	0	1	0	2	1	0	0	0	2	2	0	0	0	0	0	0	0	0	0	0	0	0	2	1	0	1	2	0	0	0	0	2	2
RDISTEIYQVGSTPC	Spike32_A475V	0	0	0	0	0	0	0	0	0	0	0	1	0	0	0	0	0	0	0	0	0	0	0	0	0	0	0	0	0	0	0	0	0	0	0	2	0	0
RDISTEIYQAGSTPC	Spike32wt	0	0	0	0	0	0	0	0	0	0	0	0	0	0	0	0	0	0	0	0	0	0	0	0	0	0	0	0	0	0	0	0	0	0	0	0	0	0
RDISTEIYQAGNTPC	Spike32_S477N	0	0	0	0	0	0	0	0	0	0	0	0	0	0	0	0	0	0	0	0	0	0	0	0	0	0	0	0	0	0	0	0	0	0	0	0	0	0
RDISTEIYQAGSKPC	Spike32_T478K	0	1	0	0	2	0	0	0	0	1	0	0	0	0	0	0	0	0	0	0	0	0	0	0	0	0	0	1	0	0	0	2	0	1	2	0	0	0
NGVEGFNCYFPLQSY	Spike33wt	0	0	1	0	0	1	0	2	0	0	0	1	0	0	0	1	0	2	0	0	2	1	0	0	0	0	0	0	0	1	1	0	1	0	0	1	0	0
NGVKGFNCYFPLQSY	Spike33_E484K	0	0	1	1	0	1	1	2	2	0	1	0	0	1	1	1	0	2	0	0	2	1	0	1	1	0	0	0	1	1	2	0	1	0	0	0	1	1
NGVQGFNCYFPLQSY	Spike33_E484Q	1	0	1	0	0	1	1	2	1	0	0	0	1	0	0	1	0	2	0	0	2	1	0	1	1	1	0	0	0	1	1	0	1	0	0	1	0	0
NGVEGFNCYFPLRSY	Spike33_Q493R	0	0	1	0	0	1	0	2	0	2	0	1	0	2	0	1	2	2	0	2	2	1	0	0	0	0	0	0	0	1	1	1	1	0	0	1	1	1
NGAEGFNCYFPLQSY	Spike33_V483A	0	0	1	0	0	1	0	2	0	0	0	1	0	0	0	1	0	2	0	0	2	1	0	0	0	0	0	0	0	1	1	0	1	0	0	1	0	0
GFQPTNGVGYQPYRV	Spike34wt	0	0	1	0	0	1	0	1	0	1	0	0	0	0	0	2	1	1	0	1	2	1	0	0	0	0	0	0	0	1	1	0	1	0	0	0	0	0
GFQPTYGVGYQPYRV	Spike34_N501Y	0	0	1	0	0	1	0	2	0	1	1	0	0	1	0	1	2	2	0	2	1	1	0	0	0	0	0	0	1	1	1	0	1	0	0	0	0	0
VVLSFELLHAPATVC	Spike35wt	2	1	0	0	1	0	0	1	0	0	0	1	1	0	0	0	0	1	2	0	0	0	2	2	2	1	2	0	0	0	0	0	0	0	0	2	0	0

LEGEND:

0	= **no** binding
1	= **weak** binding(contains atleastone8-11mer weak binder)
2	= **strong** binding(contains atleastone8-11mer strongbinder)

HLA-B alleles

Peptide sequence	Mutated and WT peptide name	HLA-B07:02	HLA-B08:01	HLA-B18:01	HLA-B44:02	HLA-B51:01	HLA-B35:01	HLA-B44:03	HLA-B15:01	HLA-B14:02	HLA-B13:02	HLA-B27:05	HLA-B38:01	HLA-B49:01	HLA-B35:03	HLA-B40:02	HLA-B40:01	HLA-B57:01	HLA-B50:01	HLA-B55:01	HLA-B14:01	HLA-B35:02	HLA-B53:01	HLA-B37:01	HLA-B52:01	HLA-B58:01	HLA-B35:08	HLA-B15:02	HLA-B15:03	HLA-B15:10	HLA-B15:17	HLA-B27:02	HLA-B27:03	HLA-B46:01	HLA-B56:01	HLA-B57:03
	Allele freq.(%)	11.43	7.48	7.16	6.73	5.98	5.24	4.81	4.49	3.95	2.35	2.35	2.46	2.14	2.03	2.03	1.92	1.92	1.71	1.6	1.5	1.39	1.18	1.18	1.07	1.07	<1	<1	<1	<1	<1	<1	<1	<1	<1	<1
RFASVYAWNRKRISN	Spike24wt	0	1	0	0	1	0	0	0	0	0	0	0	0	0	0	0	1	0	0	0	0	0	0	0	1	0	0	0	0	0	1	0	0	0	0
CVADYSVLYNSASFS	Spike25wt	0	0	0	0	0	2	0	2	0	0	0	0	0	1	0	0	1	1	0	0	1	1	1	1	1	2	2	2	0	2	0	0	2	0	2
CVADYSFLYNSASFS	Spike25_V367F	0	0	1	0	0	2	0	2	1	0	0	0	0	1	1	0	1	1	0	1	1	2	1	2	2	2	2	2	1	2	0	0	2	1	2
TFKCYGVSPTKLNDL	Spike26wt	1	0	0	0	0	0	0	0	0	0	0	0	0	0	0	0	0	0	0	0	0	0	0	0	0	0	0	0	0	0	0	0	0	0	0
CFTNVYADSFVIRGD	Spike27wt	0	0	0	0	1	2	0	1	1	2	0	1	0	1	0	0	0	0	0	1	1	1	0	2	1	2	1	1	1	2	0	0	2	0	1
EVRQIAPGQTGKIAD	Spike28wt	1	0	0	0	1	0	0	1	0	2	1	0	1	0	0	0	0	1	1	0	0	0	0	1	0	0	0	1	0	0	0	1	0	1	0
EVRQIAPGQTGNIAD	Spike28_K417N	1	0	0	0	1	0	0	1	0	2	0	0	1	0	0	0	0	1	2	0	0	0	0	2	0	0	0	1	0	0	0	0	0	1	0
EVRQIAPGQTGPIAD	Spike28_K417P	1	0	0	0	1	0	0	1	0	2	0	0	1	0	0	1	0	1	2	0	0	0	0	2	0	0	0	1	0	0	0	0	0	2	0
YNYKLPDDFTGCVIA	Spike29wt	1	0	0	0	2	1	0	0	0	0	0	0	0	2	0	0	0	0	1	0	2	2	0	0	0	2	0	0	0	0	0	0	0	2	0
WNSNNLDSKVGGNYN	Spike30wt	0	0	0	0	0	0	0	0	0	0	0	0	0	0	0	0	0	0	0	0	0	0	0	0	0	0	1	0	0	0	0	0	0	0	0
WNSKNLDSKVGGNYN	Spike30_N439K	0	0	0	0	0	0	0	0	0	0	0	0	0	0	0	0	0	0	0	0	0	0	0	0	0	0	1	0	0	0	0	0	0	0	0
WNSNKLDSKVGGNYN	Spike30_N440K	0	0	0	0	0	0	0	1	0	0	0	0	0	0	0	0	0	0	0	0	0	0	0	0	0	0	0	0	0	0	0	0	0	0	0
YLYRLFRKSNLKPFE	Spike31wt	0	2	0	0	0	0	0	1	2	0	2	0	0	0	0	0	0	0	0	2	0	0	0	0	0	0	1	1	1	0	1	2	0	0	0
YRYRLFRKSNLKPFE	Spike31_L452R	0	2	0	0	0	0	0	1	2	0	2	0	0	0	0	0	0	0	0	2	0	0	0	0	0	0	1	1	1	0	2	2	0	0	0
RDISTEIYQVGSTPC	Spike32_A475V	0	0	1	0	0	0	0	0	0	1	0	0	1	0	1	0	0	2	0	0	0	0	1	0	0	0	0	0	0	0	0	0	0	0	0
RDISTEIYQAGSTPC	Spike32wt	0	0	0	0	0	0	0	0	0	0	0	0	1	0	0	0	0	2	0	0	0	0	0	0	0	0	0	0	0	0	0	0	0	0	0
RDISTEIYQAGNTPC	Spike32_S477N	0	0	0	0	0	0	0	0	0	0	0	0	1	0	0	0	0	2	0	0	0	0	0	0	0	0	0	0	0	0	0	0	0	0	0
RDISTEIYQAGSKPC	Spike32_T478K	0	0	0	0	0	0	0	0	0	0	0	0	1	0	0	0	0	1	0	0	0	0	0	0	0	0	0	0	0	0	0	0	0	0	0
NGVEGFNCYFPLQSY	Spike33wt	0	1	1	1	1	1	1	1	1	0	0	0	1	1	2	2	0	1	0	1	1	0	2	1	0	1	2	1	0	0	0	0	1	0	0
NGVKGFNCYFPLQSY	Spike33_E484K	0	0	0	0	0	1	0	1	0	1	0	0	0	0	0	0	0	0	0	0	0	0	1	2	1	1	2	1	0	0	0	0	1	0	1
NGVQGFNCYFPLQSY	Spike33_E484Q	0	0	0	0	0	1	0	1	1	2	0	1	0	1	1	1	0	0	0	1	1	0	1	2	0	1	2	1	0	0	0	0	1	0	0
NGVEGFNCYFPLRSY	Spike33_Q493R	0	1	1	1	1	1	1	0	1	0	0	0	1	1	2	2	0	1	0	1	1	0	2	1	0	1	1	1	0	0	0	0	1	0	0
NGAEGFNCYFPLQSY	Spike33_V483A	0	1	1	2	1	1	2	1	1	1	0	0	2	1	2	2	0	1	0	1	1	0	2	1	0	1	2	1	0	0	0	0	1	0	0
GFQPTNGVGYQPYRV	Spike34wt	0	0	0	0	0	1	0	1	0	0	0	0	0	0	0	0	0	0	0	0	0	0	0	1	0	1	1	1	0	0	0	0	1	0	0
GFQPTYGVGYQPYRV	Spike34_N501Y	0	0	1	0	0	1	0	1	0	0	0	0	0	0	0	0	0	0	0	0	0	0	0	1	0	1	1	2	0	0	0	0	1	1	0
VVLSFELLHAPATVC	Spike35wt	0	0	2	0	0	0	0	0	0	1	0	0	2	0	2	1	0	2	1	0	0	0	2	1	0	0	0	0	0	0	0	0	0	1	0

Peptide sequence	Mutated and WT peptide name	HLA-B39:01	HLA-B40:06	HLA-B41:01	HLA-B42:01	HLA-B45:01	HLA-B07:05	HLA-B07:06	HLA-B13:01	HLA-B15:16	HLA-B15:18	HLA-B18:03	HLA-B27:04	HLA-B27:05	HLA-B35:04	HLA-B35:05	HLA-B35:43	HLA-B39:10	HLA-B41:02	HLA-B44:05	HLA-B47:01	HLA-B50:02	HLA-B51:02	HLA-B58:02	HLA-B78:01	HLA-B81:01	HLA-B38:02	HLA-B39:05	HLA-B39:24	HLA-B40:16	HLA-B44:04	HLA-B51:08	HLA-B54:01	HLA-B73:01	HLA-B82:01
	Allele freq.(%)	<1	<1	<1	<1	<1	<1	<1	<1	<1	<1	<1	<1	<1	<1	<1	<1	<1	<1	<1	<1	<1	<1	<1	<1	<1	<1	<1	<1	<1	<1	<1	<1	<1	<1
RFASVYAWNRKRISN	Spike24wt	0	0	0	0	0	0	0	0	0	0	0	0	0	0	0	0	0	0	0	0	0	1	1	0	0	0	0	0	0	0	1	0	0	0
CVADYSVLYNSASFS	Spike25wt	0	1	1	0	1	0	0	1	2	1	0	0	0	1	2	2	0	0	0	0	1	0	1	0	0	0	0	0	0	0	0	0	0	1
CVADYSFLYNSASFS	Spike25_V367F	0	1	1	0	1	0	0	1	2	2	1	0	0	1	2	2	0	0	0	1	1	1	2	1	0	0	0	0	0	1	0	1	0	1
TFKCYGVSPTKLNDL	Spike26wt	0	0	0	1	0	1	1	0	0	0	0	0	0	0	0	0	0	0	0	0	0	0	0	0	0	0	0	1	0	0	0	0	0	0
CFTNVYADSFVIRGD	Spike27wt	1	0	0	0	0	0	0	1	2	1	0	0	0	1	2	2	1	0	0	0	0	1	1	1	0	0	1	1	0	0	1	0	0	0
EVRQIAPGQTGKIAD	Spike28wt	0	0	0	1	0	1	1	2	0	0	0	0	1	0	0	0	0	0	0	1	0	1	0	0	0	0	0	0	1	0	0	0	0	1
EVRQIAPGQTGNIAD	Spike28_K417N	0	0	0	1	0	1	1	2	0	0	0	0	0	0	0	0	1	0	0	1	0	1	0	0	0	0	0	0	1	0	0	1	0	1
EVRQIAPGQTGPIAD	Spike28_K417P	0	0	0	1	0	1	1	2	0	0	0	1	0	0	0	0	1	0	0	1	0	1	0	1	0	0	0	0	1	0	0	1	0	1
YNYKLPDDFTGCVIA	Spike29wt	0	0	0	1	0	1	1	0	0	0	1	0	0	2	0	0	2	0	0	0	0	2	0	1	1	0	0	0	0	0	2	2	0	2
WNSNNLDSKVGGNYN	Spike30wt	0	0	0	0	0	0	0	0	0	0	0	0	0	0	0	0	0	0	0	0	0	0	0	0	0	0	0	0	0	0	0	0	0	0
WNSKNLDSKVGGNYN	Spike30_N439K	0	0	0	0	0	0	0	0	0	0	0	0	0	0	0	0	0	0	0	0	0	0	0	0	0	0	0	0	0	0	0	0	0	0
WNSNKLDSKVGGNYN	Spike30_N440K	0	0	0	0	0	0	0	0	0	0	0	0	0	0	0	0	0	0	0	0	0	0	0	0	0	0	0	0	0	0	0	0	0	0
YLYRLFRKSNLKPFE	Spike31wt	1	0	0	0	0	0	0	1	0	2	0	2	2	0	0	0	0	0	0	0	0	0	0	0	0	1	0	2	0	0	0	0	1	0
YRYRLFRKSNLKPFE	Spike31_L452R	1	0	0	0	0	0	0	1	0	2	0	2	2	0	0	0	0	0	0	0	0	0	0	0	0	1	0	2	0	0	0	0	2	0
RDISTEIYQVGSTPC	Spike32_A475V	0	1	1	0	1	0	0	0	0	0	1	0	0	0	0	0	0	0	0	0	2	0	0	0	0	0	0	0	0	0	1	0	0	0
RDISTEIYQAGSTPC	Spike32wt	0	1	1	0	1	0	0	0	0	0	0	0	0	0	0	0	0	0	0	0	2	0	0	0	0	0	0	0	0	0	0	0	0	0
RDISTEIYQAGNTPC	Spike32_S477N	0	1	1	0	1	0	0	0	0	0	0	0	0	0	0	0	0	0	0	0	2	0	0	0	0	0	0	0	0	0	0	0	0	0
RDISTEIYQAGSKPC	Spike32_T478K	0	1	1	0	1	0	0	0	0	0	0	0	0	0	0	0	0	0	0	0	1	0	0	0	0	0	0	0	0	0	0	0	0	0
NGVEGFNCYFPLQSY	Spike33wt	1	2	1	0	1	0	0	1	0	0	1	0	0	1	1	1	1	2	2	2	1	1	0	1	1	0	1	1	2	1	1	0	0	1
NGVKGFNCYFPLQSY	Spike33_E484K	0	0	0	0	0	0	0	1	0	0	1	0	0	0	1	1	0	0	0	1	0	0	1	0	1	0	0	1	0	0	0	0	0	0
NGVQGFNCYFPLQSY	Spike33_E484Q	1	0	0	0	0	0	0	2	0	0	1	1	0	1	1	1	1	0	0	2	0	0	1	1	1	1	1	1	0	0	0	0	0	1
NGVEGFNCYFPLRSY	Spike33_Q493R	1	2	1	0	1	0	0	1	0	0	1	0	0	1	1	1	1	2	2	2	1	1	0	1	1	0	1	1	2	1	1	0	0	1
NGAEGFNCYFPLQSY	Spike33_V483A	1	2	2	0	2	0	0	2	0	0	1	0	0	1	1	1	1	2	2	2	2	1	0	1	1	0	1	1	2	2	1	0	0	1
GFQPTNGVGYQPYRV	Spike34wt	0	0	0	0	0	0	0	0	0	2	0	0	0	0	1	1	0	0	0	0	0	0	0	0	0	0	0	0	0	0	0	0	0	0
GFQPTYGVGYQPYRV	Spike34_N501Y	0	0	0	0	0	0	0	0	0	2	0	0	0	0	1	1	0	0	0	1	0	0	0	0	0	0	0	0	0	0	0	1	0	0
VVLSFELLHAPATVC	Spike35wt	0	2	2	0	2	0	0	1	0	0	2	0	0	0	0	0	0	2	1	1	2	0	0	1	0	0	1	0	1	0	0	1	1	0

HLA-C alleles

Peptide sequence	Mutated and WT peptide name	HLA-C07:01	HLA-C07:02	HLA-C04:01	HLA-C06:02	HLA-C05:01	HLA-C12:03	HLA-C02:02	HLA-C08:02	HLA-C16:01	HLA-C03:03	HLA-C03:04	HLA-C01:02	HLA-C15:02	HLA-C14:02	HLA-C12:02	HLA-C02:10	HLA-C03:02	HLA-C07:04	HLA-C08:01	HLA-C17:01	HLA-C04:03	HLA-C07:18	HLA-C08:04	HLA-C15:04	HLA-C15:05	HLA-C15:06	HLA-C15:09	HLA-C16:02	HLA-C16:04	HLA-C17:03	HLA-C18:01
	Allele freq.(%)	14.16	12.23	12.02	7.94	7.4	5.47	5.47	5.04	4.51	4.08	4.08	3.33	2.9	1.61	1.5	<1	<1	<1	<1	<1	<1	<1	<1	<1	<1	<1	<1	<1	<1	<1	<1
RFASVYAWNRKRISN	Spike24wt	0	1	0	1	0	1	0	0	0	0	0	0	0	1	0	0	0	1	0	0	0	0	0	0	0	0	0	0	0	0	0
CVADYSVLYNSASFS	Spike25wt	1	1	0	0	1	1	2	1	2	2	2	1	0	1	2	2	2	0	1	1	1	1	1	2	1	1	2	1	2	1	0
CVADYSFLYNSASFS	Spike25_V367F	2	2	1	0	1	2	2	1	2	2	2	1	1	2	2	2	2	1	2	1	1	2	2	2	1	1	2	2	2	1	1
TFKCYGVSPTKLNDL	Spike26wt	0	1	0	0	0	0	0	0	0	0	0	2	0	1	0	0	0	1	0	0	0	0	0	0	0	0	0	0	0	0	1
CFTNVYADSFVIRGD	Spike27wt	1	1	1	0	1	2	2	1	2	2	2	0	1	1	2	2	2	1	2	1	2	1	2	2	1	1	2	2	2	1	1
EVRQIAPGQTGKIAD	Spike28wt	0	0	0	0	0	1	0	0	0	0	0	2	0	0	0	0	0	0	0	1	0	0	0	0	0	0	0	0	0	1	0
EVRQIAPGQTGNIAD	Spike28_K417N	0	0	0	1	0	1	0	0	0	0	0	2	0	0	0	0	0	0	0	1	0	0	0	0	0	0	0	0	0	1	0
EVRQIAPGQTGPIAD	Spike28_K417P	0	0	0	0	0	1	0	0	1	1	1	2	0	0	0	0	0	0	1	1	0	0	1	0	0	0	0	0	1	1	0
YNYKLPDDFTGCVIA	Spike29wt	0	0	1	0	1	0	0	1	0	0	0	1	0	0	0	0	0	0	1	0	1	0	0	0	0	0	0	0	0	0	1
WNSNNLDSKVGGNYN	Spike30wt	0	0	0	0	0	0	0	0	0	0	0	0	0	0	0	0	0	0	0	0	0	0	0	0	0	0	0	0	0	0	0
WNSKNLDSKVGGNYN	Spike30_N439K	0	0	0	0	0	0	0	0	0	0	0	0	0	0	0	0	0	0	0	0	0	0	0	0	0	0	0	0	0	0	0
WNSNKLDSKVGGNYN	Spike30_N440K	0	0	0	0	0	0	0	0	0	0	0	0	0	0	0	0	0	0	0	0	0	0	0	0	0	0	0	0	0	0	0
YLYRLFRKSNLKPFE	Spike31wt	2	2	0	2	0	1	0	0	0	0	0	0	0	1	1	0	0	2	0	0	0	2	0	0	0	0	0	0	0	0	1
YRYRLFRKSNLKPFE	Spike31_L452R	2	2	0	2	0	1	0	0	0	0	0	0	0	1	1	0	0	2	0	0	0	2	0	0	0	0	0	0	0	0	1
RDISTEIYQVGSTPC	Spike32_A475V	0	0	0	0	0	0	0	0	0	0	0	0	0	1	0	0	0	0	0	0	0	0	0	0	0	0	0	0	0	0	0
RDISTEIYQAGSTPC	Spike32wt	0	0	0	0	0	0	0	0	0	0	0	0	0	1	0	0	0	0	0	0	0	0	0	0	0	0	0	0	0	0	0
RDISTEIYQAGNTPC	Spike32_S477N	0	0	0	0	0	0	0	0	0	0	0	0	0	1	0	0	0	0	0	0	0	0	0	0	0	0	0	0	0	0	0
RDISTEIYQAGSKPC	Spike32_T478K	0	0	0	0	0	0	0	0	0	0	0	0	0	1	0	0	0	0	0	0	0	0	0	0	0	0	0	0	0	0	0
NGVEGFNCYFPLQSY	Spike33wt	1	1	0	0	1	1	1	1	1	0	0	0	0	2	1	1	1	0	1	0	1	1	0	1	0	0	1	0	1	0	0
NGVKGFNCYFPLQSY	Spike33_E484K	1	1	1	0	0	1	1	0	1	0	0	1	1	2	1	1	1	0	1	1	0	1	1	1	0	0	1	1	1	1	0
NGVQGFNCYFPLQSY	Spike33_E484Q	1	1	1	0	0	1	1	0	1	1	1	0	0	2	1	1	1	0	1	0	0	1	1	1	0	0	1	0	1	0	0
NGVEGFNCYFPLRSY	Spike33_Q493R	1	1	0	0	1	1	1	1	1	0	0	0	0	2	1	1	1	0	1	0	1	1	0	1	0	0	1	0	1	0	0
NGAEGFNCYFPLQSY	Spike33_V483A	1	1	1	0	2	1	1	1	1	0	0	0	0	2	1	1	1	0	1	0	1	1	1	1	0	0	1	0	1	0	0
GFQPTNGVGYQPYRV	Spike34wt	0	2	0	0	0	0	1	0	0	0	0	0	0	1	1	1	1	0	0	0	0	0	0	0	0	0	0	0	0	0	0
GFQPTYGVGYQPYRV	Spike34_N501Y	1	2	0	0	0	1	1	0	0	0	0	0	0	2	1	1	1	0	0	0	0	1	0	0	0	0	0	0	0	0	0
VVLSFELLHAPATVC	Spike35wt	0	0	0	0	0	0	0	0	0	0	0	0	0	0	0	0	0	0	0	0	0	0	0	0	0	0	0	0	0	0	0

Table S8b. HLA phenotyping and genotyping of susceptible and resistant individuals (class II).

LEGEND :

0	= **no** binding
1	= **weak** binding
2	= **strong** binding

HLA-DP alleles

Peptide sequence	Mutated and WT peptide name	DPA10103-DPB10401	DPA10103-DPB10201	DPA10103-DPB10402	DPA10103-DPB10301	DPA10201-DPB10101	DPA10202-DPB10501	DPA10201-DPB10501	DPA10201-DPB11701	DPA10201-DPB11301	DPA10201-DPB11101	DPA10201-DPB11001	DPA10201-DPB11401	DPA10103-DPB10601
	Allele freq. (%)	34.32	13.11	11.44	8.23	6.43	5.27		2.96	2.96	2.06	1.8	1.67	1.67
RFASVYAWNRKRISN	**Spike24**wt	0	0	0	1	0	1	1	1	0	0	0	1	1
CVADYSVLYNSASFS	**Spike25**wt	0	0	0	0	0	0	0	0	0	0	0	0	0
CVADYSFLYNSASFS	**Spike25**_V367F	0	0	0	0	0	0	0	0	0	0	0	0	0
TFKCYGVSPTKLNDL	**Spike26**wt	0	0	0	0	0	0	0	0	0	0	0	0	0
CFTNVYADSFVIRGD	**Spike27**wt	0	0	0	0	0	0	0	0	0	0	0	0	0
EVRQIAPGQTGKIAD	**Spike28**wt	0	0	0	0	0	0	0	0	0	0	0	0	0
EVRQIAPGQTGNIAD	**Spike28**_K417N	0	0	0	0	0	0	0	0	0	0	0	0	0
EVRQIAPGQTGPIAD	**Spike28**_K417P	0	0	0	0	0	0	0	0	0	0	0	0	0
YNYKLPDDFTGCVIA	**Spike29**wt	0	0	0	0	0	0	0	0	0	0	0	0	0
WNSNNLDSKVGGNYN	**Spike30**wt	0	0	0	0	0	0	0	0	0	0	0	0	0
WNSKNLDSKVGGNYN	**Spike30**_N439K	0	0	0	0	0	0	0	0	0	0	0	0	0
WNSNKLDSKVGGNYN	**Spike30**_N440K	0	0	0	0	0	0	0	0	0	0	0	0	0
YLYRLFRKSNLKPFE	**Spike31**wt	1	1	1	0	0	2	2	1	0	0	1	1	1
YRYRLFRKSNLKPFE	**Spike31**_L452R	1	1	1	0	0	2	2	1	0	1	1	1	1
RDISTEIYQVGSTPC	**Spike32**_A475V	0	0	0	0	0	0	0	0	0	0	0	0	0
RDISTEIYQAGSTPC	**Spike32**wt	0	0	0	0	0	0	0	0	0	0	0	0	0
RDISTEIYQAGNTPC	**Spike32**_S477N	0	0	0	0	0	0	0	0	0	0	0	0	0
RDISTEIYQAGSKPC	**Spike32**_T478K	0	0	0	0	0	0	0	0	0	0	0	0	0
NGVEGFNCYFPLQSY	**Spike33**wt	0	0	0	0	0	0	0	0	0	0	0	0	0
NGVKGFNCYFPLQSY	**Spike33**_E484K	0	0	0	0	0	0	0	0	0	0	0	0	0
NGVQGFNCYFPLQSY	**Spike33**_E484Q	0	0	0	0	0	0	0	0	0	0	0	0	0
NGVEGFNCYFPLRSY	**Spike33**_Q493R	0	0	0	0	0	0	0	0	0	0	0	0	0
NGAEGFNCYFPLQSY	**Spike33**_V483A	0	0	0	0	0	0	0	0	0	0	0	0	0
GFQPTNGVGYQPYRV	**Spike34**wt	0	0	0	0	0	0	0	0	0	0	0	0	0
GFQPTYGVGYQPYRV	**Spike34**_N501Y	0	0	0	0	0	0	0	0	0	0	0	0	0
VVLSFELLHAPATVC	**Spike35**wt	0	0	0	0	0	0	0	0	0	0	0	0	0

HLA-DQ alleles

Peptide sequence	Mutated and WT peptide name	DQA10501-DQB10301	DQA10505-DQB10301	DQA10301-DQB10301	DQA10401-DQB10301	DQA10101-DQB10501	DQA10102-DQB10501	DQA10102-DQB10602	DQA10201-DQB10202	DQA10501-DQB10201	DQA10201-DQB10201	DQA10301-DQB10302	DQA10103-DQB10603	DQA10101-DQB10503	DQA10104-DQB10503	DQA10102-DQB10502	DQA10102-DQB10604	DQA10401-DQB10402	DQA10201-DQB10303	DQA10301-DQB10303
	Allele freq. (%)	21.80				11.64		11.30	11.07	10.96		7.88	4.79	4.11		3.08	2.51	2.40	2.28	
RFASVYAWNRKRISN	**Spike24**wt	0	0	0	0	0	0	0	0	0	0	0	0	0	0	0	0	0	0	0
CVADYSVLYNSASFS	**Spike25**wt	0	0	0	0	0	0	0	0	0	0	0	0	0	0	0	0	0	0	0
CVADYSFLYNSASFS	**Spike25**_V367F	0	0	0	0	0	0	0	0	0	0	0	0	0	0	0	0	0	0	0
TFKCYGVSPTKLNDL	**Spike26**wt	0	0	0	0	0	0	0	0	0	0	0	0	0	0	0	0	0	0	0
CFTNVYADSFVIRGD	**Spike27**wt	0	0	0	0	1	0	0	0	0	0	0	0	0	0	1	0	0	0	0
EVRQIAPGQTGKIAD	**Spike28**wt	1	1	0	0	0	0	0	0	0	0	0	0	0	0	0	0	0	0	0
EVRQIAPGQTGNIAD	**Spike28**_K417N	0	0	0	0	0	0	0	0	0	0	0	0	0	0	0	0	0	0	0
EVRQIAPGQTGPIAD	**Spike28**_K417P	1	1	0	0	0	0	0	0	0	0	0	0	0	0	0	0	0	0	0
YNYKLPDDFTGCVIA	**Spike29**wt	0	0	0	0	0	0	0	0	0	0	0	0	0	0	0	0	0	0	0
WNSNNLDSKVGGNYN	**Spike30**wt	0	0	0	0	0	0	0	0	0	0	0	0	0	0	0	0	0	0	0
WNSKNLDSKVGGNYN	**Spike30**_N439K	0	0	0	0	0	0	0	0	0	0	0	0	0	0	0	0	0	0	0
WNSNKLDSKVGGNYN	**Spike30**_N440K	0	0	0	0	0	0	0	0	0	0	0	0	0	0	0	0	0	0	0
YLYRLFRKSNLKPFE	**Spike31**wt	0	0	0	0	0	0	0	0	0	0	0	0	0	0	0	0	0	0	0
YRYRLFRKSNLKPFE	**Spike31**_L452R	0	0	0	0	0	0	0	0	0	0	0	0	0	0	0	0	0	0	0
RDISTEIYQVGSTPC	**Spike32**_A475V	0	0	0	0	0	0	0	0	0	0	0	0	0	0	0	0	0	0	0
RDISTEIYQAGSTPC	**Spike32**wt	0	0	0	0	0	0	0	0	0	0	0	0	0	0	0	0	0	0	0
RDISTEIYQAGNTPC	**Spike32**_S477N	0	0	0	0	0	0	0	0	0	0	0	0	0	0	0	0	0	0	0
RDISTEIYQAGSKPC	**Spike32**_T478K	0	0	0	0	0	0	0	0	0	0	0	0	0	0	0	0	0	0	0
NGVEGFNCYFPLQSY	**Spike33**wt	0	0	0	0	1	0	0	0	0	0	0	0	1	1	1	0	0	0	0
NGVKGFNCYFPLQSY	**Spike33**_E484K	0	0	0	0	1	0	0	0	0	0	0	0	1	1	1	0	0	0	0
NGVQGFNCYFPLQSY	**Spike33**_E484Q	0	0	0	0	1	0	0	0	0	0	0	0	1	1	1	0	0	0	0
NGVEGFNCYFPLRSY	**Spike33**_Q493R	0	0	0	0	0	0	0	0	0	0	0	0	1	1	1	0	0	0	0
NGAEGFNCYFPLQSY	**Spike33**_V483A	0	0	0	0	1	0	0	0	0	0	0	0	1	1	1	0	0	0	0
GFQPTNGVGYQPYRV	**Spike34**wt	0	0	0	0	0	0	0	0	0	0	0	0	0	0	0	0	0	0	0
GFQPTYGVGYQPYRV	**Spike34**_N501Y	0	0	0	0	0	0	0	0	0	0	0	0	0	0	0	0	0	0	0
VVLSFELLHAPATVC	**Spike35**wt	0	0	0	0	0	1	0	0	0	0	0	0	1	1	0	0	0	0	0

HLA-DR alleles

Peptide sequence	Mutated and WT peptide name	DRB1_0701	DRB1_1501	DRB1_0301	DRB1_1101	DRB1_0101	DRB1_0401	DRB1_1301	DRB1_1302	DRB1_1104	DRB1_0102	DRB1_0404	DRB1_0405	DRB1_1454	DRB1_1601	DRB1_0801	DRB1_1401	DRB1_1303	DRB1_1001	DRB1_1201	DRB1_1502	DRB1_0804	DRB1_0901
	Allele freq. (%)	12.58	10.89	9.83	8.46	6.24	5.71	5.29	4.65	4.55	3.17	2.33	1.9	1.9	1.9	1.8	1.8	1.7	1.48	1.48	1.37	1.06	1.06
RFASVYAWNRKRISN	**Spike24**wt	0	1	0	2	0	0	2	0	1	0	0	0	1	2	1	1	2	0	0	0	1	0
CVADYSVLYNSASFS	**Spike25**wt	0	0	0	0	1	2	0	1	0	0	1	2	0	1	0	0	0	2	0	1	0	0
CVADYSFLYNSASFS	**Spike25**_V367F	0	0	0	0	1	2	0	1	0	0	1	2	0	1	0	0	1	2	0	1	0	1
TFKCYGVSPTKLNDL	**Spike26**wt	1	0	0	0	0	0	0	0	0	0	0	0	0	0	0	0	0	0	0	0	0	1
CFTNVYADSFVIRGD	**Spike27**wt	1	0	1	0	0	0	0	0	0	0	0	0	0	0	0	0	0	0	0	0	0	0
EVRQIAPGQTGKIAD	**Spike28**wt	0	0	0	0	0	0	0	0	0	0	0	0	0	0	0	0	0	0	0	0	0	0
EVRQIAPGQTGNIAD	**Spike28**_K417N	0	0	0	0	0	0	0	0	0	0	0	0	0	0	0	0	0	0	0	0	0	0
EVRQIAPGQTGPIAD	**Spike28**_K417P	0	0	0	0	0	0	0	0	0	0	0	0	0	0	0	0	0	0	0	0	0	0
YNYKLPDDFTGCVIA	**Spike29**wt	0	0	0	0	0	0	0	0	0	0	0	0	0	0	0	0	0	0	0	0	0	0
WNSNNLDSKVGGNYN	**Spike30**wt	0	0	0	0	0	0	0	0	0	0	0	0	0	0	0	0	0	0	0	0	0	0
WNSKNLDSKVGGNYN	**Spike30**_N439K	0	0	0	0	0	0	0	0	0	0	0	0	0	0	0	0	0	0	0	0	0	0
WNSNKLDSKVGGNYN	**Spike30**_N440K	0	0	0	0	0	0	0	0	0	0	0	0	0	0	0	0	0	0	0	0	0	0
YLYRLFRKSNLKPFE	**Spike31**wt	1	1	0	2	0	0	2	1	2	0	0	1	2	2	2	2	2	0	1	1	1	1
YRYRLFRKSNLKPFE	**Spike31**_L452R	1	1	0	2	0	0	2	1	2	0	0	1	2	2	2	2	2	0	1	1	1	1
RDISTEIYQVGSTPC	**Spike32**_A475V	0	0	0	0	0	0	0	0	0	0	0	0	0	0	0	0	0	0	0	0	0	0
RDISTEIYQAGSTPC	**Spike32**wt	0	0	0	0	0	0	0	0	0	0	0	0	0	0	0	0	0	0	0	0	0	0
RDISTEIYQAGNTPC	**Spike32**_S477N	0	0	0	0	0	0	0	0	0	0	0	0	0	0	0	0	0	0	0	0	0	0
RDISTEIYQAGSKPC	**Spike32**_T478K	0	0	0	0	0	0	0	0	0	0	0	0	0	0	0	0	0	0	0	0	0	0
NGVEGFNCYFPLQSY	**Spike33**wt	0	0	0	0	0	0	0	0	0	0	0	0	0	0	0	0	0	0	0	0	0	0
NGVKGFNCYFPLQSY	**Spike33**_E484K	0	0	0	0	0	0	0	0	0	0	0	0	0	0	0	0	0	0	0	0	0	0
NGVQGFNCYFPLQSY	**Spike33**_E484Q	0	0	0	0	0	0	0	0	0	0	0	0	0	0	0	0	0	0	0	0	0	0
NGVEGFNCYFPLRSY	**Spike33**_Q493R	0	0	0	0	0	0	0	0	0	0	0	0	0	0	0	0	0	0	0	0	0	0
NGAEGFNCYFPLQSY	**Spike33**_V483A	0	0	0	0	0	0	0	0	0	0	0	0	0	0	0	0	0	0	0	0	0	0
GFQPTNGVGYQPYRV	**Spike34**wt	0	0	0	0	0	0	0	0	0	0	0	0	0	0	0	0	0	0	0	0	0	0
GFQPTYGVGYQPYRV	**Spike34**_N501Y	0	0	0	0	0	0	0	0	0	0	0	0	0	0	0	0	0	0	0	0	0	0
VVLSFELLHAPATVC	**Spike35**wt	0	0	0	0	2	1	0	0	0	2	1	1	0	2	0	0	0	2	0	0	0	1

Peptide sequence	Mutated and WT peptide name	DRB1_0403	DRB1_1102	DRB1_0402	DRB1_1202	DRB1_1503	DRB1_0103	DRB1_0407	DRB1_1103	DRB1_0302	DRB1_1602	DRB1_0406	DRB1_0803	DRB1_1304	DRB1_1305	DRB1_1404	DRB1_0408	DRB1_1402	DRB3_0101	DRB3_0202	DRB4_0101	DRB5_0101	DRB5_0202
	Allele freq. (%)	<1	<1	<1	<1	<1	<1	<1	<1	<1	<1	<1	<1	<1	<1	<1	<1	<1	n/a	n/a	n/a	n/a	n/a
RFASVYAWNRKRISN	**Spike24**wt	0	2	1	1	1	1	0	2	1	1	0	0	2	2	0	0	1	0	1	0	2	2
CVADYSVLYNSASFS	**Spike25**wt	1	0	0	0	0	0	1	0	1	1	1	0	0	0	0	2	1	0	1	0	0	0
CVADYSFLYNSASFS	**Spike25**_V367F	1	0	0	0	0	1	2	0	1	1	1	1	0	0	0	2	1	1	2	0	0	0
TFKCYGVSPTKLNDL	**Spike26**wt	0	0	0	0	0	0	0	0	0	0	0	0	0	0	0	0	0	0	0	0	0	0
CFTNVYADSFVIRGD	**Spike27**wt	0	0	0	0	0	0	0	0	1	0	0	0	0	0	0	0	0	1	0	0	0	0
EVRQIAPGQTGKIAD	**Spike28**wt	0	0	0	0	0	0	0	0	0	0	0	0	0	0	0	0	0	0	0	0	0	0
EVRQIAPGQTGNIAD	**Spike28**_K417N	0	0	0	0	0	0	0	0	0	0	0	0	0	0	0	0	0	0	0	0	0	0
EVRQIAPGQTGPIAD	**Spike28**_K417P	0	0	0	0	0	0	0	0	0	0	0	0	0	0	0	0	0	0	0	0	0	0
YNYKLPDDFTGCVIA	**Spike29**wt	0	0	0	0	0	0	0	0	0	0	0	0	0	0	0	0	0	0	0	0	0	0
WNSNNLDSKVGGNYN	**Spike30**wt	0	0	0	0	0	0	0	0	0	0	0	0	0	0	0	0	0	0	0	0	0	0
WNSKNLDSKVGGNYN	**Spike30**_N439K	0	0	0	0	0	0	0	0	0	0	0	0	0	0	0	0	0	0	0	0	0	0
WNSNKLDSKVGGNYN	**Spike30**_N440K	0	0	0	0	0	0	0	0	0	0	0	0	0	0	0	0	0	0	0	0	0	0
YLYRLFRKSNLKPFE	**Spike31**wt	0	2	1	2	2	2	0	2	1	1	0	2	2	2	2	0	1	0	1	1	1	1
YRYRLFRKSNLKPFE	**Spike31**_L452R	0	2	1	2	2	2	0	2	1	2	0	2	2	2	2	0	1	0	1	1	2	1
RDISTEIYQVGSTPC	**Spike32**_A475V	0	0	0	0	0	0	0	0	0	0	0	0	0	0	0	0	0	0	0	0	0	0
RDISTEIYQAGSTPC	**Spike32**wt	0	0	0	0	0	0	0	0	0	0	0	0	0	0	0	0	0	0	0	0	0	0
RDISTEIYQAGNTPC	**Spike32**_S477N	0	0	0	0	0	0	0	0	0	0	0	0	0	0	0	0	0	0	0	0	0	0
RDISTEIYQAGSKPC	**Spike32**_T478K	0	0	0	0	0	0	0	0	0	0	0	0	0	0	0	0	0	0	0	0	0	0
NGVEGFNCYFPLQSY	**Spike33**wt	0	0	0	0	0	0	0	0	0	0	0	0	0	0	0	0	0	0	0	0	0	0
NGVKGFNCYFPLQSY	**Spike33**_E484K	0	0	0	0	0	0	0	0	0	0	0	0	0	0	0	0	0	0	0	0	0	0
NGVQGFNCYFPLQSY	**Spike33**_E484Q	0	0	0	0	0	0	0	0	0	0	0	0	0	0	0	0	0	0	0	0	0	0
NGVEGFNCYFPLRSY	**Spike33**_Q493R	0	0	0	0	0	0	0	0	0	0	0	0	0	0	0	0	0	0	0	0	0	0
NGAEGFNCYFPLQSY	**Spike33**_V483A	0	0	0	0	0	0	0	0	0	0	0	0	0	0	0	0	0	0	0	0	0	0
GFQPTNGVGYQPYRV	**Spike34**wt	0	0	0	0	0	0	0	0	0	0	0	0	0	0	0	0	0	0	0	0	0	0
GFQPTYGVGYQPYRV	**Spike34**_N501Y	0	0	0	0	0	0	0	0	0	0	0	0	0	0	0	0	0	0	0	0	0	0
VVLSFELLHAPATVC	**Spike35**wt	1	0	0	0	1	2	1	0	0	2	1	0	0	0	0	1	0	0	0	0	0	0

Table S9. Mutational hotspots in the peptide residues.

Peptide name	Peptide sequence	Mutated peptide sequence	Mutation	B.1.526 (New York)	B.1.526.2 (USA)	B.1.427 (California/WestCoast)	B.1.429 (California/WestCoast)	P.1 (Brazilian (Manaus))	P.2 Brazilian (Rio de Janeiro)	B.1.525 (UK)	B.1.1.7 (UK)	B.1.351 (South Africa)	B.1.526.1 (USA)	B.1.617.1 (India)	B.1.617.2 (India)	B.1.526.3 (India)	Gaebleretal. (Nature, 2021)
Spike1	MFVFLVLLPLVSSQC	MFVF*VLLPLVSSQC	L5F	x	x												
Spike1	MFVFLVLLPLVSSQC	MFVFLVLLPLVS*QC	S13I			x	x										
Spike2	VNLTTRTQLPPAYTN	VN*TTRTQLPPAYTN	L18F					x									
Spike2	VNLTTRTQLPPAYTN	VNL*TRTQLPPAYTN	T19R												x	x	
Spike2	VNLTTRTQLPPAYTN	VNLT*RTQLPPAYTN	T20N					x									
Spike2	VNLTTRTQLPPAYTN	VNLTTRTQLP*AYTN	P26S					x									
Spike4	SVLHSTQDLFLPFFS	SVLHST*DLFLPFFS	Q52R							x							
Spike5	NVTWFHAIHVSGTNG	NVTWFH*IHVSGTNG	A67V							x							
Spike5	NVTWFHAIHVSGTNG	NVTWFHAI*SGTNG	HV69-70del							x	x						
Spike6	TKRFDNPVLPFNDGV	TKRF*NPVLPFNDGV	D80A									x					
Spike6	TKRFDNPVLPFNDGV	TKRF*NPVLPFNDGV	D80G										x				
Spike7	YFASTEKSNIIRGWI	YFAS*EKSNIIRGWI	T95I	x	x												
Spike10	CNDPFLGVYYHKNNK	CN*PFLGVYYHKNNK	D138Y					x									
Spike10	CNDPFLGVYYHKNNK	CNDPFLGV*YHKNNK	Y144del							x	x		x				
Spike11	SWMESEFRVYSSANN	S*MESEFRVYSSANN	W152C			x	x										
Spike11	SWMESEFRVYSSANN	SWMESE*RVYSSANN	F157S										x				
Spike11	SWMESEFRVYSSANN	SWMESE*VYSSANN	FR157-158del												x		
Spike13	GKQGNFKNLREFVFK	GKQGNFKNL*EFVFK	R190S					x									
Spike15	NLVRDLPQGFSALEP	NLVR*LPQGFSALEP	D215G									x					
Spike17	LLALHRSYLTPGDSS	LHRSYLTPGDSS	LLA241-243del		x							x					
Spike17	LLALHRSYLTPGDSS	LLALHRSYLTPG*SS	D253G	x	x												
Spike24	RFASVYAWNRKRISN	R*ASVYAWNRKRISN	R346S														x
Spike25	CVADYSVLYNSASFS	CVADYS*LYNSASFS	V367F	a													x
Spike28	EVRQIAPGQTGKIAD	EVRQIAPGQTG*IAD	K417N									x					
Spike28	EVRQIAPGQTGKIAD	EVRQIAPGQTG*IAD	K417T					x									
Spike30	WNSNNLDSKVGGNYNWNSN*NLDSKVGGNYNN439K																x
Spike30	WNSNNLDSKVGGNYNWNSN*LDSKVGGNYNN440K																x
Spike31	YLYRLFRKSNLKPFE	Y*YRLFRKSNLKPFE	L452R			x	x						x	x	x	x	
Spike32	RDISTEIYQAGSTPC	RDISTEIYQ*GSTPC	A475V														x
Spike32	RDISTEIYQAGSTPC	RDISTEIYQAG*TPC	S477N		x												x
Spike32	RDISTEIYQAGSTPC	RDISTEIYQAGS*PC	T478K												x		
Spike33	NGVEGFNCYFPLQSY	NG*EGFNCYFPLQSY	V483A														x
Spike33	NGVEGFNCYFPLQSY	NGVEGFNCYFPLQSY	E484K	x				x	x	x		x					x
Spike33	NGVEGFNCYFPLQSY	NGV*GFNCYFPLQSYE484Q												x		x	
Spike33	NGVEGFNCYFPLQSY	NGVEGFNCYFPL*SY	Q493R														x
Spike34	GFQPTNGVGYQPYRV	GFQPT*GVGYQPYRV	N501Y					x			x	x					
Spike38	NKKFLPFQQFGRDIA	NKKFLPFQQFGRDI	A570D								x						
Spike41	GTNTSNQVAVLYQDV	GTNTSNQVAVLYQ*V	D614G	x	x	x	x	x	x	x	x	x	x	x	x	x	
Spike44	RAGCLIGAEHVNNSY	RAGCLIGAE*VNNSY	H655Y					x									
Spike46	TQTNSPRRARSVASQ	T*TNSPRRARSVASQ	Q677H							x							
Spike46	TQTNSPRRARSVASQ	TQTNS*RRARSVASQ	P681H								x						
Spike46	TQTNSPRRARSVASQ	TQTNS*RRARSVASQ	P681R											x	x	x	
Spike47	SIIAYTMSLGAENSV	SIIAYTMSLG*ENSV	A701V	x								x					
Spike48	AYSNNSIAIPTNFTI	AYSNNSIAIP*NFTI	T716I								x						
Spike58	NGLTVLPPLLTDEMI	NGL*VLPPLLTDEMI	T859V										x				
Spike60	WTFGAGAALQIPFAM	WT*GAGAALQIPFAM	F888L							x							
Spike64	GKLQDVVNQNAQALN	GKLQD*VVNQNAQALN	D950H										x				
Spike64	GKLQDVVNQNAQALN	GKLQD*VVNQNAQALN	D950N												x		
Spike64	GKLQDVVNQNAQALN	GKLQDVVNQNA*ALN	Q957R		x												
Spike66	VLNDILSRLDKVEAE	VLNDIL*RLDKVEAE	S982A								x						
Spike69	SANLAATKMSECVLG	SANLAA*KMSECVLG	T1027I					x									
Spike75	EPQIITTDNTFVSGN	EPQIITT*NTFVSGN	D1118H								x						
Spike79	GINASVVNIQKEIDR	GINAS*VNIQKEIDR	V1176F					x	x								
Nucleocapsid_1	MSDNGPQNQRNAPRIMS	MSD*NGPQNQRNAPRI	D3L								x						
Nucleocapsid_1	MSDNGPQNQRNAPRIMS	MSD*NGPQNQRNAPRI	D3del							x							
Nucleocapsid_1	MSDNGPQNQRNAPRIMS	MSDNGPQNQRN*PRIA12G								x							
Nucleocapsid_1	MSDNGPQNQRNAPRIMS	MSDNGPQNQRNA*RI	P13L		x												
Nucleocapsid_5	KEDLKFPRQGQVPIN	KE*LKFPRQGQVPIN	D63G												x		
Nucleocapsid_5	KEDLKFPRQGQVPIN	KEDLKF*RQGQVPIN	P67S													x	
Nucleocapsid_6	TNSSPDDQIGYYRRA	TNSS*DDQIGYYRRA	P80R					x									
Nucleocapsid_8	PRWYFYYLGTGPEAG	PRWYFYYLGTGPE*G	A119S						x								
Nucleocapsid_14	NSTPGSSRGTSPARMN	NST*GSSRGTSPARM	P199L	x													
Nucleocapsid_14	NSTPGSSRGTSPARMN	NSTPGS*RGTSPARMS202R			x												
Nucleocapsid_14	NSTPGSSRGTSPARMN	NSTPGSS*GTSPARM	R203K					x	x		x						
Nucleocapsid_14	NSTPGSSRGTSPARMN	NSTPGSSRG*TSPARMR203M												x	x	x	
Nucleocapsid_14	NSTPGSSRGTSPARMN	NSTPGSSR*TSPARM	G204R					x	x		x						
Nucleocapsid_14	NSTPGSSRGTSPARMN	NSTPGSSRG*SPARM	T205I			x	x			x		x	x				
Nucleocapsid_16	RLNQLESKMSGKGQQ	RLNQLESK*SGKGQQ	M234I	x					x				x				
Nucleocapsid_16	RLNQLESKMSGKGQQ	RLNQLESKM*GKGQQS235F									x						
Nucleocapsid_26	ADETQALPQRQKKQQ	A*ETQALPQRQKKQQ	D377Y											x	x	x	
SARS_HLA-A*02:01_7VLNDILSRL		VLNDIL*RL	S982A								x						
ORF8_1	MKFLVFLGIITTVAA	MKFLVFLGII*TVAA	T11I	x	x								x				
ORF8_3	AFHQECSLQSCTQHQ	AFHQECSLQSC*QHQ	T26I													x	
ORF8_3	AFHQECSLQSCTQHQ	AFHQECSLQSCT*HQ	Q27X								x						
ORF8_4	LQSCTQHQPYVVDDP	LQSCTQH*QPYVVDDP	T26I													x	
ORF8_4	LQSCTQHQPYVVDDP	LQSCTQH*HQPYVVDDP	Q27X								x						
ORF8_7	SKWYIRVGARKSAPL	SKWYIRVG*RKSAPL	A51S										x				
ORF8_7	SKWYIRVGARKSAPL	SKWYIRVGA*KSAPL	R52I								x						
ORF8_8	GARKSAPLIELCVDE	G*RKSAPLIELCVDE	A51S										x				
ORF8_8	GARKSAPLIELCVDE	GA*KSAPLIELCVDE	R52I								x						
ORF8_10	EAGSKSPIQYIDIGN	EAGSKSPIQ*IDIGN	Y73C								x						
ORF8_11	IQYIDIGNYTVSCLP	IQ*IDIGNYTVSCLP	Y73C								x						
ORF8_13	PFTINCQEPKLGSLV	PFTINCQ*PKLGSLV	E92K					x									
ORF8_14	EPKLGSLVVRCSFYE	K*PKLGSLVVRCSFYE	E92K					x									
ORF3a_AB	VQIHTIDGSSGVVNP	VQIHTIDGS*GVVNP	S253P					x									
ORF3a_C	VQIHTIDVSSGVVNP	VQIHTIDVS*GVVNP	S253P					x									